

Functional Analyses of Abiotic Stress-Induced
Adaptive Responses and Metabolite Changes in
Japanese Bunching Onion (*Allium fistulosum* L.)

(ネギにおける非生物学的ストレス誘発適応応答および代謝物変化の機能解析)

Tetsuya Nakajima

Graduate School of Sciences and Technology for Innovation

YAMAGUCHI UNIVERSITY

March 2025

TABLE OF CONTENTS

Chapter 1: GENERAL INTRODUCTION	1
Chapter 2: Effects of Drought Stress on Abscisic Acid Content and Its Related Transcripts in <i>Allium fistulosum</i> — <i>A. cepa</i> Monosomic Addition Lines.....	6
Introduction	6
Material and Methods	9
Results	16
Discussion	25
Chapter 3: Metabolite Profiling and Association Analysis of Leaf Tipburn in Heat-Tolerant Bunching Onion Varieties	29
Introduction	29
Materials and Methods	32
Results	44
Discussion	61
Chapter 4: Metabolome Profiling and Predictive Modeling of Dark Green Trait in Heat- Tolerant Bunching Onion Varieties	67
Introduction	67
Materials and Methods	70
Results	79
Discussion	95
Chapter 5: GENERAL DISCUSSION	102
LITERATURE CITED	109
SUMMARY	124
JAPANESE SUMMARY	128
LIST OF PAPERS RELATED TO THE THESIS	132
ACKNOWLEDGEMENT	133

Chapter 1: GENERAL INTRODUCTION

The genus *Allium* is one of the largest genera in the family of Amaryllidaceae. It is comprised of more than 1000 species, and the number is still increasing (Friesen et al., 2020). The plant genus *Allium* contains a variety of vegetable species famous for their pungent, spicy properties, usually consumed raw in salads or cooked (Khandagale et al., 2020). *Allium* species produce a diverse array of secondary metabolites, encompassing polyphenols, organosulfur compounds, saponins, polysaccharides, and tannins (Zolfaghari et al., 2016), which are widely utilized as functional components. The genus *Allium* holds significant economic importance due to several essential vegetable crops, such as onion (*A. cepa* L.; $2n = 2x = 16$), shallot (*A. cepa* L. Aggregatum Group; $2n = 2x = 16$), garlic (*A. sativum* L.; $2n = 2x = 16$), leek (*A. ampeloprasum* L.; $2n = 4x = 32$), bunching onion (*A. fistulosum* L.; $2n = 2x = 16$), Chinese chive (*A. tuberosum* Rottler ex Spreng; $2n = 2x = 16$, occasionally $3x$ or $4x$), and others (Galmarini, 2018; McCallum et al., 2012; Yao et al., 2024). The total production value of *Allium* crops in 2022 was US\$89,699 million, with “onions and shallots, dry,” “garlic, green,” “onions and shallots, green,” and “leeks and other alliaceous vegetables” contributing 56.0%, 38.2%, 3.0%, and 2.7%, respectively (Food and agriculture Organization of the United Nations, 2022).

The bunching onion, also known as the Welsh onion, green onion, spring onion, or scallion, is widely distributed from Siberia to tropical Asia,

particularly in East Asia, where numerous varieties have adapted to diverse local environmental conditions (Yamasaki and Tsukazaki, 2022). In Japan, the cultivation area of the bunching onion was 21,500 ha, ranking sixth among vegetables in 2023 (e-Stat, 2023). The classification of the bunching onion is based on morphological characteristics such as tillering, dormancy, and utilization, and includes varieties such as ‘Kaga,’ ‘Senju,’ ‘Kujo,’ and ‘Yagura-Negi’ (Inden and Asahira, 1990). The bunching onions used in this study belong to the ‘Kujo’ category and are consumed for their leaf blades. Their leaf blades are highly sought after as garnishes due to their aromatic quality, vibrant color, and ease of use in raw dishes, maintaining consistent demand throughout the year.

In Japan, while the production of F₁ hybrid varieties of leaf onions is increasing, region-specific traditional varieties continue to be cultivated. In Yamaguchi Prefecture, a traditional variety from Shimonoseki City, characterized by its deep green color, is gaining attention as a unique local specialty. The deep green color is a trait of high commercial value and a key characteristic for producers. At the Yamaguchi Prefectural Agriculture and Forestry General Technology Center, a selected and stabilized variety derived from this traditional strain has been registered as ‘YSG1go’ (Registered Variety Number: 24596). Efforts are underway to develop heat-tolerant F₁ hybrid varieties that retain the deep green color and exhibit robust growth in the summer. In general, the dark green color is considered to be attributed to chlorophyll; however, it is actually not caused by a single pigment but rather arises from interactions among various pigment compounds (Cheng et al.,

2018). To date, studies on pigment compounds in bunching onions have reported on chlorophylls and carotenoids (Kopsell et al., 2010), but no reports exist on other pigment compounds. Understanding the mechanisms behind the dark green coloration would enable the efficient development of new varieties through breeding. Furthermore, chlorophyll and carotenoids, which are associated with dark green coloration, are known as photosynthetic pigments that not only facilitate the efficient utilization of light energy but also play a role in environmental stress responses (Li et al., 2024a; Egea et al., 2022). Therefore, provided that these pigment compounds can be easily measured, it would be possible to monitor plant stress responses and implement appropriate measures at the right time.

Climate change has had a significant impact on the growth and quality of crops, including bunching onions. Abiotic stresses such as high temperatures and drought are major factors leading to reduced yields and quality deterioration due to poor crop growth. According to some reports, the projection of these stresses significantly affects growth and productivity by reducing crop yield and overall crop production by 70% and 50%, respectively (Kaur et al., 2008; Mantri et al., 2012). In bunching onions, a physiological disorder known as “leaf tipburn” is particularly problematic, as it significantly reduces the commercial value of the crop. While calcium deficiency has generally been considered the cause of leaf tipburn, multiple factors are involved, and the detailed mechanisms remain unclear (Kuronuma et al., 2019; Su et al., 2019; Wang et al., 2019a). Identifying compounds associated with leaf tipburn could provide clues for its prevention.

Furthermore, there have been no reports on pigment compounds and functional components related to the incidence of leaf tipburn and quality during the summer season. Organizing information related to the growth period and timing is crucial for analyzing their relationships with leaf tipburn. The plant hormone abscisic acid (ABA) plays an important role in maintaining crop water status by closing stomata under drought stress (Bharath et al., 2021). High accumulation of ABA has been reported to enhance stress tolerance, raising expectations for the development of abiotic stress-tolerant varieties (Zhang et al., 2012; Wei et al., 2015).

Here, we focus on recent advances in genomic technologies. The improvement in precision and reduction in costs of next-generation sequencing technologies have led to the publication of draft genomes for *Allium* species such as the onion, bunching onion, and garlic (Liao, 2022; Hao, 2023). These advancements are expected to enable genome-based interspecific hybridization as an effective strategy for enhancing the genetic diversity of *Allium* species for desirable agricultural traits (Liao, 2022). Indeed, attempts at genome editing using CRISPR/Cas9 technology have been reported for the onion (Mainkar, 2023). However, there have been no reports of significant progress in the application of genetic modification or genome-editing technologies for bunching onions.

Nevertheless, anticipating future practical applications for these technologies, it is crucial at this stage to systematically and comprehensively accumulate phenotypic data and genetic information using diverse lines with distinctive traits. These data will serve as a foundation for designing efficient

and effective breeding strategies for *Allium* species.

Thus, this study aimed to improve the dark green coloration and abiotic stress adaptability of bunching onions. The objectives of this research were as follows: (1) to elucidate the mechanisms of ABA accumulation under drought conditions, (2) to identify metabolites associated with leaf tipburn, and (3) to identify metabolites related to dark green coloration.

This chapter is the first of five that comprise this dissertation. Chapter 2 addresses Objective (1), Chapter 3 focuses on Objective (2), Chapter 4 explores Objective (3), and Chapter 5 provides a general discussion. This dissertation compiles the results of studies conducted by the author at the Laboratory of Vegetable Crop Science, Division of Life Science, Graduate School of Sciences and Technology for Innovation, Yamaguchi University, Yamaguchi, with the objectives outlined above, during the period from 2022 to 2025.

Chapter 2: Effects of Drought Stress on Abscisic Acid Content and Its Related Transcripts in *Allium fistulosum*— *A. cepa* Monosomic Addition Lines

Introduction

The Japanese bunching onion (*A. fistulosum* L., FF), also named the Welsh onion, spring onion, and scallion, is widely distributed from Siberia to tropical Asia, especially in east Asia, with many varieties adapted to local environmental conditions (Kumazawa, 1965; FORD-LLOYD and ARMSTRONG, 1993; Liu et al., 2021). FF is relatively tolerant to heat, cold, and drought conditions, but it is susceptible to waterlogging (Yiu et al., 2008). However, in recent summer production, high levels of light and drought have retarded growth, resulting in lower yields (Liting et al., 2015). Additionally, the process of withholding irrigation just before harvest has caused the wilting of leaf tips, resulting in the loss of product value. With global warming and desertification becoming problems due to climate variation, drought-resistant traits are required for the stable production of FF. Plants have unique ways of responding to various external environmental stresses; among them, the plant hormone abscisic acid (ABA) plays a role in plant dormancy and drought response (Rai et al., 2024). Studies on the drought response of ABA have been conducted in a variety of plants. For example,

exogenous ABA treatment (Kumazawa, 1965) can regulate the processes of metabolizing energy, amino acids, and lipids; promote the accumulation of flavonoids, betaine, and other substances; improve enzymatic and non-enzymatic antioxidant regulation systems; and enhance the photosynthetic performance and relative water content of plants to promote plant growth and improve drought resistance of diverse crops, including maize (*Zea mays*), wheat (*Triticum aestivum*), sweet potatoes (*Ipomoea batatas*), and pearl millet (*Pennisetum glaucum*) (Zhang et al., 2012; Wei et al., 2015; Awan et al., 2021; Huan et al., 2020). Additionally, plants exposed to abiotic stress swiftly activate the ABA signaling cascade, leading to the activation of ABA-responsive transcription factors and genes, promoting stomatal closure, modifying root architecture, and affecting the expression of stress-responsive genes and physiological responses (Bharath et al., 2021). Once stress tolerance is achieved, it is essential to terminate or attenuate the ABA pathway. This balance is maintained through the selective degradation of specific components of the ABA signaling pathway, marked for decay by ubiquitination (Sirko et al., 2021). Furthermore, an additional layer of complexity is introduced by the extensive crosstalk between ABA and other phytohormones, such as cytokinin, ethylene, jasmonic acid, and gibberellins, to maintain the balance between stress adaptation and growth (Abdelrahman et al., 2021). These mechanisms collectively underscore the importance of ABA in enhancing plant resilience to drought stress. By elucidating the role of ABA and its associated pathways, we aim to contribute to the development of drought-tolerant crops, which is vital for agricultural sustainability in the face

of climate change (Şimşek et al., 2024). The shallot (*Allium cepa* L. Aggregatum Group, AA) is a species of subtropical origin that has been recognized as a potential genetic resource for improving *Allium* crops because of its adaptability to environmental stresses (Currah, 2002; Abdelrahman et al., 2015b). Alien monosomic addition lines (AMALs) are valuable for elucidating genome structure and transferring useful genes and traits in plant breeding. AMALs were used in breeding programs of rice (*Oryza sativa* L.), oilseed rape (*Brassica napus* L.), and wheat (Multani et al., 2003; Reamon-Ramos and Wricke, 1992; Chevre et al., 1996; Fu et al., 2013). Shigyo et al. (Shigyo et al., 1996) have generated a series of AMALs in FF strains by introducing shallot chromosomes. These lines have been investigated to study the morphological features, primary metabolites, secondary metabolites, and other biochemical characteristics influenced by each shallot chromosome addition. Furthermore, the bunching onion line FF + 1A, with an added shallot, has shown high resistance to rust disease, while FF + 2A exhibits resistance to onion yellow dwarf virus, as has been reported (Wako et al., 2015; Vu et al., 2012). The impacts of AMALs on the biotic factor have become evident. Therefore, this study aims to investigate the impact of drought stress on ABA and its precursor, β -carotene, using a complete set of AMALs of *A. fistulosum* with extra chromosomes from shallot. We analyze the expression levels of genes related to ABA biosynthesis, catabolism, and drought stress signal transduction in AMALs, particularly FF + 1A and FF + 6A, which show characteristic variation in ABA accumulation. By examining both ABA and β -carotene, we aim to provide a comprehensive

understanding of the biosynthetic pathway and the role of ABA in drought stress tolerance in FF.

Material and Methods

Plant Materials and Drought Treatment

The plant materials—eight different AMALs ($2n = 2x + 1 = 17$; FF + 1A, FF + 2A, FF + 3A, FF + 4A, FF + 5A, FF + 6A, FF + 7A, FF + 8A) (Shigyo et al., 1996) and *A. fistulosum* (FF)—were grown in 6-inch clay pots filled with sand. Each pot contained one plant, and all of the plant genotypes were vegetatively propagated in the greenhouse of Yamaguchi University (34° N, 131° E). Pots were randomly arranged on a rack, watered every two days, and fertilized with 1000× HYPONeX solution (Hyponex Japan, Osaka, Japan) once a week until the drought test. Watering was accomplished by slowly filling the pot until the water overflowed the top (approximately 300 mL/pot). In January 2019, the drought treatment was implemented by stopping irrigation for 30 days, while the control condition was implemented by irrigating every 2 days. Plants were collected from each line separately in biological replicates ($n = 5$) for each condition. Leaf tips, excluding the yellowed parts, were collected at approximately 10 cm and were frozen in liquid nitrogen. The frozen samples were powdered using a mortar and pestle; samples were then dried using a freeze dryer (TAITEC VD-250R freeze dryer coupled with a vacuum pump, TAITEC, Saitama, Japan). These

dried samples were used for measuring β -carotene, violaxanthin, neoxanthin, and ABA, as well as quantitative qRT-PCR (qPCR) of genes involved in ABA biosynthesis and catabolism and drought stress signal transduction.

β -Carotene, Violaxanthin, and Neoxanthin Measurement

Briefly, 4 mg of dried sample was accurately weighed and transferred to a 1.5 mL tube, to which 500 μ L of cold 100% acetone was added. The solution was vortexed for 2 min and ultrasonicated for 20 min in a cool condition. The extract was centrifuged at 5000 rpm for 5 min at 10 °C, and the supernatant was collected. Again, 100% cold acetone was added to the remaining residue of the lower layer, and the same operation was performed twice to obtain the supernatant. All supernatants obtained were filtered through filter tubes (Nanosep® centrifugal devices, Pall Corporation, New York, NY, USA) and used as sample solutions for HPLC. The sample solution was stored at -20 °C in a freezer and used for measurement within 3 days. The extracts were analyzed by HPLC equipped with a UV-Vis detector (HITACHI L7420, Hitachi, Tokyo, Japan) operating at 435 nm to detect the carotenoids. The carotenoids were separated on LiChroCART 250-4.0 Lichrospher 100RP-18 5 μ m (KANTO CHEMICAL, Tokyo, Japan). The separation was achieved by gradient elution with (A) 80% MeOH solution (mixing 400 mL of methanol (HPLC-grade)), 50 mL of ultrapure water, and 50 mL of 100 μ M HEPES (pH 7.5) and (B) ethyl acetate. The modified gradient elution program was run as follows: (i) the initial conditions were

100 % (A), (ii) a 20 min linear gradient to 50% (A) and 50% (B), and (iii) 50% (A) and 50% (B) for 30 min, and the flow rate was 1 mL/minute. The column temperature was set to 30 °C, and the injection volume was 20 µL.

ABA Measurement

Briefly, 2 mg of each dried sample was accurately weighed and transferred to a 1.5 mL tube, to which 250 µL of 80% methanol and 25 µL of 1 ppm d6ABA (Toronto Research Chemicals, Toronto, ON, Canada) were added as an internal standard. The solution was vortexed and incubated overnight at room temperature under light protection. The extract was then centrifuged at 15,000 rpm for 5 min at 4 °C, and the supernatant was filtered through filter tubes (Nanosep® centrifugal devices, Pall Corporation, New York, USA) and used as a sample solution for LC-MS/MS. The samples were analyzed by a Prominence Modular HPLC (SHIMADZU, Kyoto, Japan) equipped with Mightysil RP-18 GP (II) 150-2.0, 5 µm (KANTO CHEMICAL, Tokyo, Japan), eluted with a 0.2 mL/min binary gradient containing the mobile phases (A) 0.1% formic acid solution (LCMS-grade) dissolved in ultrapure water and (B) 0.1% formic acid solution (LCMS-grade) dissolved in acetonitrile (LCMS-grade). The modified gradient elution program was performed as follows: (i) the initial conditions were 80% (A) and 20% (B) for 5 min, (ii) a 15 min linear gradient to 10% (A) and 90% (B), (iii) 10 % (A) and 90% (B) for 10 min, and (iv) a 5 min linear gradient to 80% (A) and 20%. The column temperature was set at 40 °C, and the injection volume was 4 µL.

Mass spectrometric analysis was carried out on a triple-quadrupole 3200 QTrap mass spectrometer (SCIEX, Framingham, MA, USA) equipped with negative electrospray ionization (ESI).

qPCR

Total RNA was extracted using an RNeasy Plant Mini Kit (QIAGEN Sciences, Hilden, Germany). RNA quality was assessed using a NanoDrop (Thermo Fisher, Waltham, MA, USA). The cDNA library was constructed using ReverTra Ace qPCR RT Master Mix with gDNA Remover (TOYOBO, Osaka, Japan) in accordance with the manufacturer's instructions. qPCR was used to measure transcript abundance for *β-carotene hydroxylase1 (BCH1)*, *zeaxanthin epoxidase (ABA1)*, *nine-cis-epoxycarotenoid dioxygenase 3 (NCED3)*, *xanthoxin dehydrogenase (ABA2)*, *abscisic-aldehyde oxidase (AAO3)*, and *molybdenum cofactor sulfurase (ABA3)* as ABA biosynthesis genes, *ABA 8'-hydroxylase (CYP707A1, CYP707A3)* as ABA catabolism genes, *transducin*, and *late embryogenesis abundant (LEA4-5)* genes as drought stress signal transduction genes in drought (Figure 1) conditions and control conditions. qPCR was performed using THUNDERBIRD SYBR qPCR Mix (QPS-201, TOYOBO, Osaka, Japan) on a QuantStudio 1 instrument. Amplification was performed using the following cycling parameters: 1 cycle of 94 °C for 1 s, 40 cycles of 95 °C for 15 s, 60 °C for 60 s, and 95 °C for 1 s. Fluorescence was acquired at 60 °C. The relative transcript levels were calculated using the comparative C_t (Threshold Cycle)

method, with the *β-actin* gene as an internal control. Results were obtained by excluding the highest C_t value and the lowest C_t value and calculating the mean for three replicates.

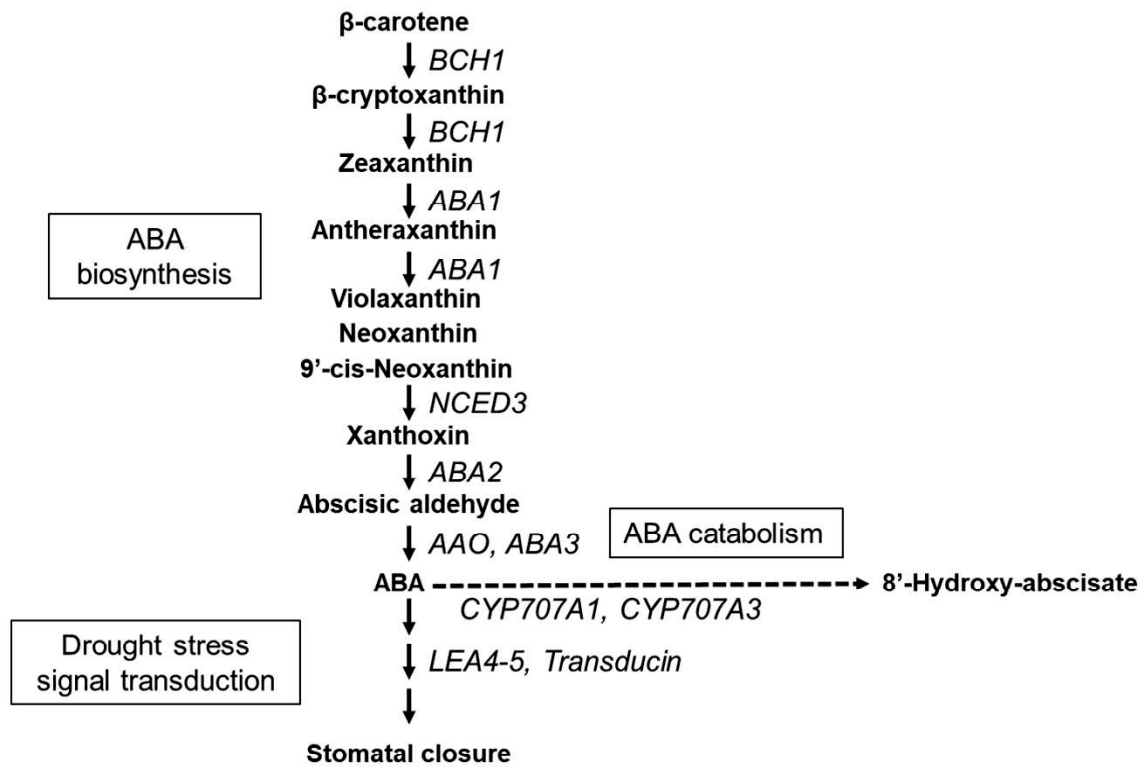


Figure 1. catabolism, and drought stress signal transduction.

BCH1: *β-carotene hydroxylase1*; *ABA1*: *zeaxanthin epoxidase*;

NCED3: *nine-cis-epoxycarotenoid dioxygenase 3*;

ABA2: *xanthoxin dehydrogenase*; *AAO*: *abscisic-aldehyde oxidase*;

ABA3: *Molybdenum cofactor sulfurase*; *CYP707A1*: *ABA 8'-hydroxylase1*;

CYP707A3: *ABA 8'-hydroxylase3*; *LEA4-5*: *late embryogenesis abundant*.

Primer Design

The genes involved in ABA biosynthesis, catabolism, and signal

transduction in the *Allium* genus were investigated using the *Allium* genus transcriptome database known as *Allium* TDB (AlliumTDB, 2017). Specifically, gene searches were conducted through keyword searches in *Allium* TDB, and Unified Genes from a DHA (doubled-haploid of shallot) bulb (Endang et al., 1997), with similarity to genes in the *Arabidopsis* Information Resource (TAIR) database (TAIR, 1999), were obtained. Subsequently, primers for qPCR were designed using the obtained Unified Genes' information from FF that matched the identified DHA bulb genes (Table 1).

Table 1. Primer list for genes used in this study as shown in Figure 1.

Arabidopsis Genome Initiative code	Gene Name	Homologs			Primer sequence based on <i>A. flosiliosum</i> Unigenes				
		<i>A. cepza</i> Unigene (bp)	Identity to Arabidopsis Gene (%)	Chromosomal location	<i>A. flosiliosum</i> Unigene (bp)	Identity to <i>A. cepza</i> UniGene (%)	Chromosomal location	Forward (5' to 3')	Reverse (5' to 3')
AT4G25700.1	<i>BCH1</i>	CL831.Contig1_DHA_Bulb (1169)	73.4	8A	Unigene22611_FFStem (339)	97.9	1F, 7F	AGGCAAAAACGAAAGCAGCAG	TCCGGCAACCAATAAAGTG
AT5G67030.2	<i>AB41</i>	Unigene26642_DHA_Bulb (687)	82.9	4A, 5A	CL2970.Contig3_FFStem (1321)	100.0	4F, 5F	TCCTCTTTCAGCAGAGGTG	AAGAGGTCATGAGTCTGGC
AT3G14440.1	<i>NCE13</i>	Unigene2060_DHA_Bulb (237)	59.2	7A	Unigene33308_FF_3AStem (510)	86.8	1F	GTTGGTTCACCGGTGCAAAAG	ACATATTCCAACAAGCTGCAGC
AT1G52340.1	<i>AB42</i>	CL2419.Contig1_DHA_Bulb (799)	62.9	4A	CL736.Contig4_FFStem (960)	97.7	6F	TGGTCTCTGAGAACAAAG	GAGCGTTGATGACCTCAATAGC
AT2G27150.2	<i>A4O</i>	CL1978.Contig1_DHA_Bulb (423)	70.1	3A, 5A, 8A	Unigene26780_FFStem (865)	89.5	2F, 3F, 5F, 7F, 8F	TCCACAAAACCTCTCCAAC	CATGCCAAGCCCTCAATTTAC
AT1G16540.1	<i>AB43</i>	Unigene33397_DHA_Bulb	48.9	4A, 5A, 8A	Unigene34756_FFStem (260)	97.7	6F	TGGTCTCTGAGAACAAAG	GAGCGTTGATGACCTCAATAGC
A14G19230.1	<i>CYP707A1</i>	CL2918.Contig1_DHA_Bulb (1782)	72.0	5A, 8A	CL5541.Contig1_FFStem (249)	99.2	7F	TGTGGTCAGGTGATGAAAGC	GCACAAAGCCAAACACTTTC
A15G45340.2	<i>CYP707A3</i>	Unigene28686_DHA_Bulb (437)	76.6	4A	Unigene30555_FFStem (440)	99.3	4F	ACCTTTACCTCCAGGCTCTAIG	GGCAACCCTCAAGATGTGAGHTTTG
AT1G49450.1	<i>Transducin</i>	Unigene7829_DHA_Bulb (423)	45.5	1A	Unigene31313_FFStem (590)	97.8	1F	TGTGCCACGGCGAATTTAC	AATGTCGGTCTGTTCACC
AT1G01470.1	<i>LE44-5</i>	CL838.Contig2_DHA_Bulb (610)	53.7	3A, 4A, 6A	Unigene30105_FFStem (491)	95.7	2F, 5F, 6F, 7F, 8F	TTTCTGGTCACATGGAAGCG	TGGTGCCAAATGAAAAGTGGAC
AT3G53750.1	<i>β-actin</i>	CL575.Contig2_DHA_Bulb (454)	99.3	-	CL1482.Contig7_FFStem (351)	98.0	-	GTTGGTATGGGGCAAAAAGA	AGCCTTTGGATTGAGTGGTG

Ascorbic Acid Measurement

The ascorbic acid content was measured monthly from April 2005 to March 2006 using fresh leaf blades of FF, 1A, and 6A as plant materials to obtain a comprehensive and detailed understanding of the seasonal variations in ascorbic acid levels. This year-long assessment allowed us to capture any fluctuations due to environmental changes over the seasons, providing a robust dataset for analysis. The ascorbic acid content was detected using a previously described method (Yaguchi et al., 2008).

Statistical Analysis

Statistical analyses were performed with *SPSS* Ver28. Each sample was measured once, and the data are expressed as the mean \pm the standard error (SE). Calculations were performed using one-way ANOVA and Dunnett's multiple comparison test or Student's *t*-test. Dunnett's multiple comparison test was designed for comparing the difference the mean value of each line, and Student's *t*-test was designed for comparing the difference of the two conditions; $p < 0.05$ was considered as statistically significant.

Results

β -Carotenoid and ABA Content in AMALs under Drought Conditions

As a result of the drought treatment, all 45 individuals (FF and AMALs with five replicates each) survived (Figure 2). Measurements of β -carotene

under both control and drought conditions revealed significantly higher β -carotene content in FF + 1A compared with FF and other AMALs (Figure 3A). On the other hand, β -carotene content decreased significantly ($p < 0.05$) under drought versus control conditions in all investigated AMALs, except for FF and FF + 5A, which did not show any significant changes (Figure 3A). Similarly, ABA content increased significantly in all investigated AMALs under drought versus control conditions, with FF + 1A exhibiting the highest ABA accumulation (Figure 3B). On the other hand, only the FF + 6A line showed the highest ABA accumulation under control conditions compared to FF and the other AMALs (Figure 3B). Additionally, a moderate positive correlation was observed between β -carotene and ABA contents under drought conditions (Figure 4). Additionally, when comparing the amount of violaxanthin and neoxanthin for FF, FF + 1A, and FF + 6A, no significant differences were observed between the control and drought conditions (Figure 5A, 5B). However, under drought conditions for FF + 6A, the peaks of violaxanthin and neoxanthin were not detected.

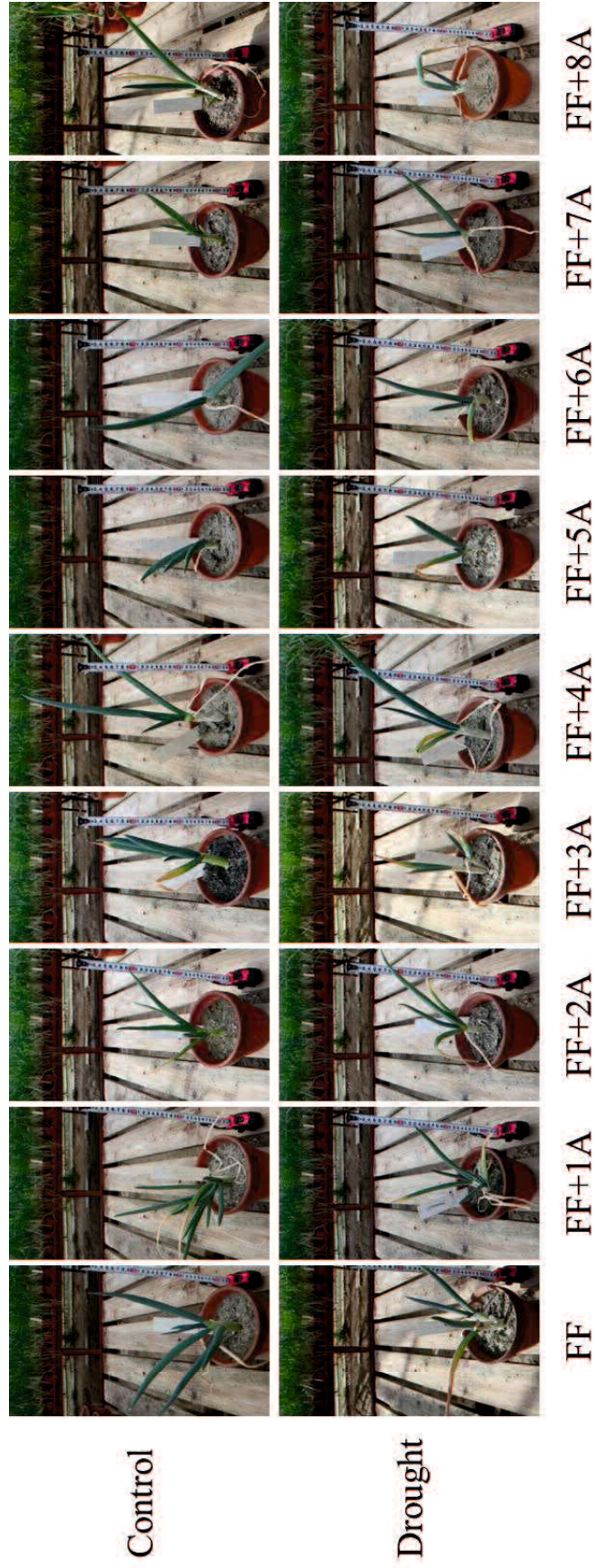


Figure 2. Example of plants (*Allium fistulosum* [FF] and different monosomic addition lines [AMALs: 1A, 2A, 3A, 4A, 5A, 6A, 7A, and 8A]) under control and drought conditions.

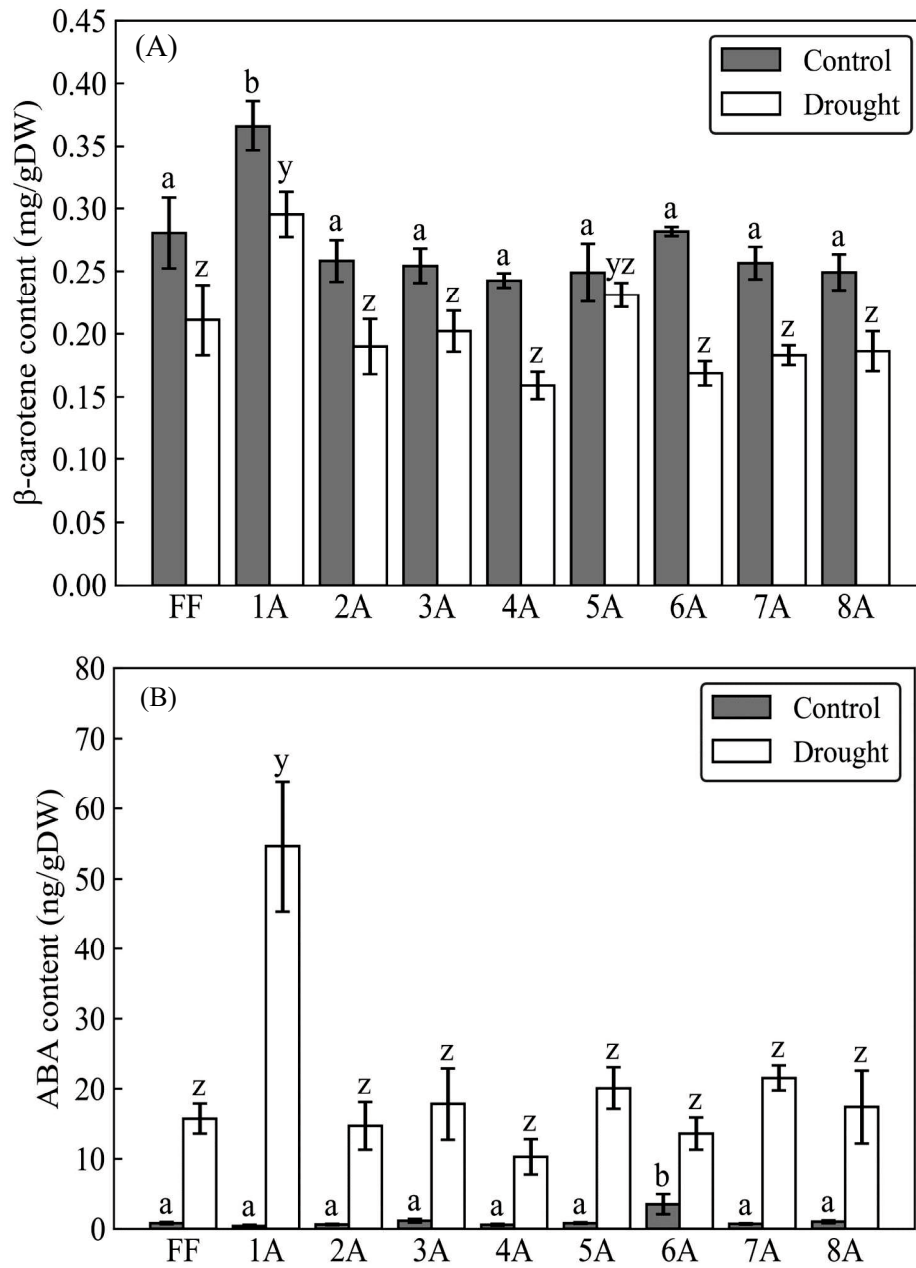


Figure 3. Comparison of (A) β -carotene and (B) abscisic acid (ABA) contents in different monosomic addition lines (AMALs, 1A, 2A, 3A, 4A, 5A, 6A, 7A, and 8A) and *Allium fistulosum* (FF) under control and drought stress conditions. Different letters (a, b for control conditions and y, z for drought conditions) indicate significant differences at $p < 0.05$. Asterisks *, **, and *** represent significant differences at $p < 0.05$, $p < 0.01$, and $p < 0.001$, respectively, as determined by Student's *t*-test. NS indicates not significant at $p < 0.05$.

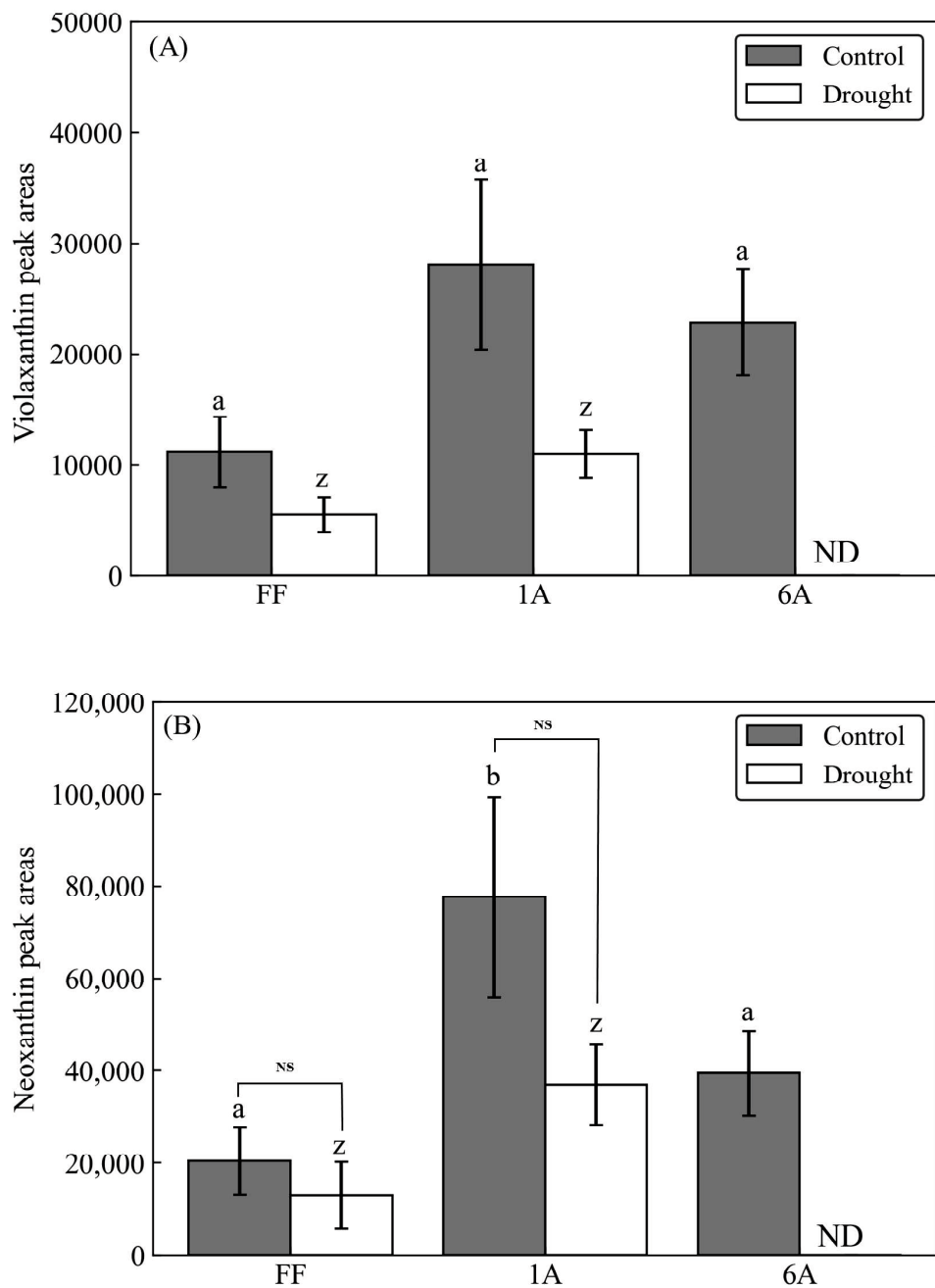


Figure 5. Comparison of (A) violaxanthin and (B) neoxanthin peak areas in FF, FF + 1A, and FF + 6A under control and drought conditions. Different letters (a, b for control conditions and z for drought conditions) indicate significant differences at $p < 0.05$. NS indicates not significant at $p < 0.05$ by Student's t -test.

Expression Analysis of ABA-Related Genes in the Monosomic Addition Lines and *A. fistulosum* under Drought Conditions

Under control conditions, FF + 1A showed an approximately twofold increase in the expression of genes involved in biosynthesis, catabolism, and drought stress signal transduction as compared to FF. In FF + 6A, genes related to biosynthesis (except *NCED3* and *ABA3*) and catabolism showed a decrease, with catabolism-related genes exhibiting a reduction of more than twofold. Genes associated with signaling transduction did not show changes as compared to FF (Figure 6). Conversely, under drought conditions, FF and FF + 6A showed similar trends in gene expression, characterized by a substantial upregulation of genes associated with biosynthesis and a downregulation of genes related to catabolism as compared to the FF control. Particularly noteworthy were the substantial elevations observed in *BCH1* and *NCED3*, while *ABA1* remained unaltered. Regarding signaling, *LEA4-5* displayed an approximately onefold decrease, whereas *transducin* showed an increase.

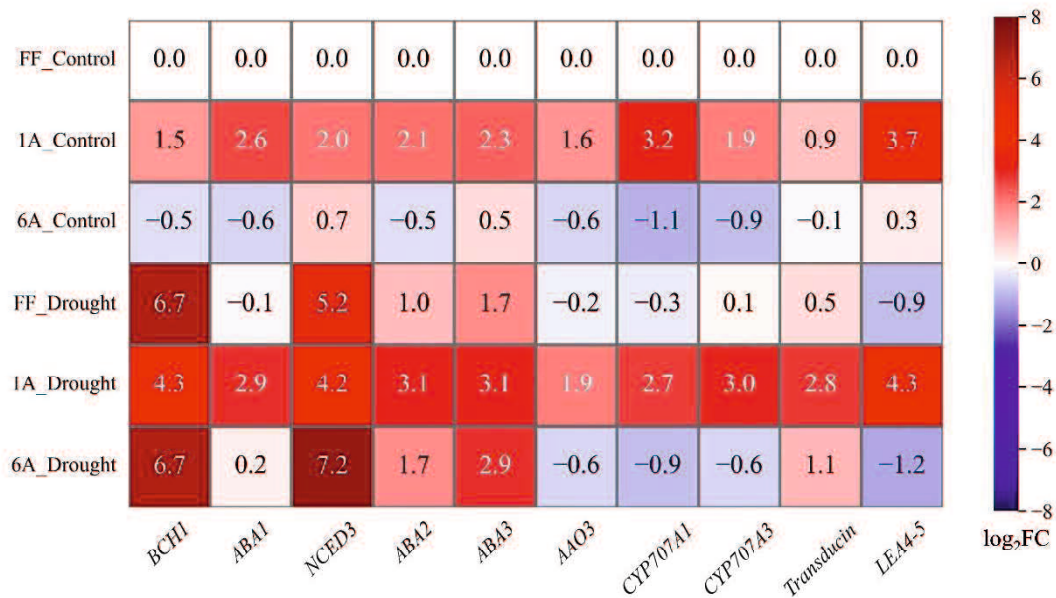


Figure 6. Heatmap of log₂ transformed average gene expression changes in abscisic acid (ABA) biosynthesis and catabolism-related genes under control and drought conditions in FF, FF + 1A, and FF + 6A.

BCH1: β -carotene hydroxylase1; *ABA1*: zeaxanthin epoxidase;

NCED3: nine-cis-epoxycarotenoid dioxygenase 3; *ABA2*: xanthoxin dehydrogenase;

AAO: abscisic-aldehyde oxidase; *ABA3*: Molybdenum cofactor sulfurase;

CYP707A1: ABA 8'-hydroxylase1; *CYP707A3*: ABA 8'-hydroxylase3;

LEA4-5: late embryogenesis abundant.

Determination of Ascorbic Acid Content in FF, FF + 1A, and FF + 6A

The results of Dunnett's multiple comparison test comparing the annual average levels of ascorbic acid content for FF, FF + 1A, and FF + 6A showed that FF + 1A exhibited significantly higher values as compared to FF (Figure 7).

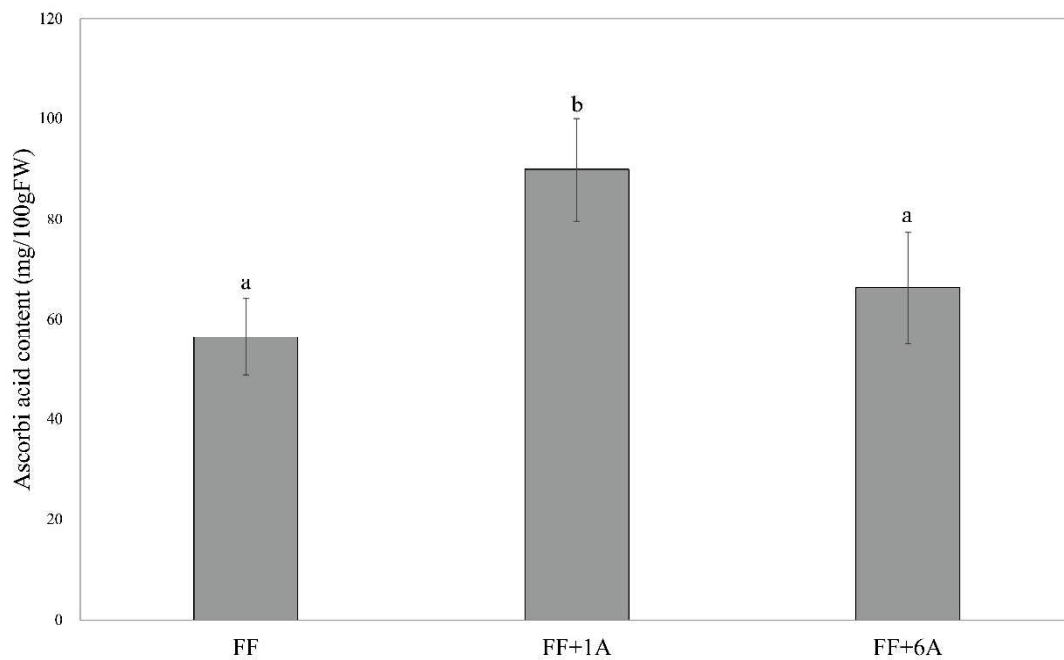


Figure 7. Annual average ascorbic acid content in FF, FF + 1A, and FF + 6A Dunnett's multiple comparison test was used to compare each line with FF as a control. Values are the means \pm SE ($n = 12$). Different small letters (a and b) refer to significant differences ($p < 0.05$).

Discussion

Our results showed three patterns: (i) the addition of chromosome 1A into the FF genome increased the expression of ABA-related genes under control conditions without changes in ABA levels; (ii) FF + 6A under control conditions decreased gene expression, but there was no accumulation of ABA; (iii) FF + 1A under drought conditions increased both gene expression and ABA accumulation (Figure 3B, Figure 6). It has been argued that ABA levels are maintained by a balance between its biosynthesis and catabolism, rather than solely by biosynthesis (Kushiro et al., 2004). Therefore, these patterns can be explained by the balance of the expression levels of genes for biosynthesis and catabolism. Expression analysis in FF + 1A showed higher expression levels of all genes related to biosynthesis, catabolism, and drought stress signal transduction as compared to FF; in particular, higher expression levels were shown in drought conditions. The genomic sequence information of bunching onions and onions that have similarity to shallots was reported by Liao et al. (Liao et al., 2022) and Fei Hao et al. (Hao et al., 2023). This information revealed that ABA biosynthesis genes *BCH1*, *NCED3*, and *transducin* were located on the first chromosome of the bunching onion (Table 1). On the other hand, genes involved in ABA biosynthesis and catabolism were not located on the first chromosome of the shallot. Therefore, the characteristic expression of genes involved in ABA biosynthesis and catabolism in 1A is likely to be the result of the interaction between the additional first chromosome of the shallot and the chromosomes of *A.*

fistulosum. Previous study for the sugar beet monosomic addition line M14, derived from a cross between *Beta vulgaris* L. and *B. coloriflora* Zoss, have reported that the addition of the chromosome affects the gene expression of the recipient chromosome (Ma et al., 2011). Additionally, FF + 1A exhibited high expression of the drought stress signal transduction *LEA4-5*, not only in drought conditions, but also in the control condition, where ABA did not accumulate. LEA proteins are known to confer resistance to drought, low temperature, and high salt concentrations; increased expression of *LEA4* has been shown to enhance resistance to drought, salt, and heavy metal stress in rice (Hu et al., 2016) and Arabidopsis (Jia et al., 2020). Therefore, the high expression of *LEA4-5* in FF + 1A during both control and drought conditions suggests the potential for stress resistance to drought and various abiotic stresses.

ABA1 was highly expressed only in FF + 1A, while no increase was observed in FF and FF + 6A under drought conditions, and ABA accumulation did not progress. Under drought stress, ABA1 increased in the roots, but not in the leaves of *Nicotiana plumbaginifolia* var *Viviani* (*ABA2/NpZEP*) and tomato (*Solanum lycopersicum*) (*LeZEP1*) (Audran et al., 1998; Thompson et al., 2000). In Arabidopsis, drought stress has been reported to lead to an increase in ZEP protein in roots and the degradation of ZEP protein in leaves (Schwarz et al., 2015), which is consistent with the results of FF and FF + 6A in this study. *ABA1* encodes zeaxanthin epoxidase, which converts zeaxanthin to antheraxanthin and violaxanthin, which is related to the xanthophyll cycle, the thermal dissipation system protecting against photoinhibition in plants.

Under drought conditions, reduced CO₂ uptake from stomatal closure decreases dark reaction activity. As a result, the light reaction is higher than the dark reaction, leading to the accumulation of NADPH. Singlet oxygen (¹O₂) is generated in photosystem II, while hydrogen peroxide (H₂O₂) is generated in photosystem I. Defense mechanisms against such situations include the thermal dissipation system and the scavenging systems of reactive oxygen species. In FF and FF + 6A, the xanthophyll cycle is thought to de-epoxidize, lowering the light-harvesting efficiency and converting excess light energy into heat to prevent photoinhibition. In FF + 1A with a high accumulation of ABA, the scavenging system of reactive oxygen species is likely involved. In plants, antioxidants such as β-carotene and ascorbic acid remove singlet oxygen and hydrogen peroxide, respectively (Ramel et al., 2012) (Ramel et al., 2012; Pospíšil and Prasad, 2014). Furthermore, ascorbic acid also plays a role in oxidizing NADPH through the glutathione–ascorbic acid cycle. Ascorbic acid plays a role in increasing stress tolerance in Common bean (*Phaseolus vulgaris* L.), maize, flax (*Linum usitatissimum* L.), wheat, and broccoli (*Brassica oleracea* var. *italica*) (Dolatabadian et al., 2010; Gaafar et al., 2020; Sh, 2014; Hafez and Gharib, 2016). FF + 1A was found to have significantly higher β-carotene content under drought conditions, and it was also confirmed that ascorbic acid tends to be higher throughout the year, indicating a high capacity to remove reactive oxygen species and NADPH, making it less susceptible to photoinhibition. Therefore, the epoxidation of the xanthophyll cycle and ABA biosynthesis likely progressed in FF + 1A under drought conditions. Accordingly, *A.*

fistulosum with the extra first chromosome of shallots could be less susceptible to photoinhibition, potentially making it capable of maintaining closed stomata and capable of addressing dryness issues during the summer season. This study highlights the role of ABA in enhancing drought tolerance in *A. fistulosum* through the addition of a shallot chromosome. Our results show that the FF + 1A line exhibits increased ABA-related gene expression and higher ABA accumulation under drought conditions, compared with the FF or FF + 6A line. This suggests a beneficial genetic interaction enhancing the plant drought response mechanisms. Additionally, the high levels of β -carotene and ascorbic acid in FF + 1A under drought conditions indicate a robust reactive oxygen species-scavenging system, reducing photoinhibition and oxidative stress. This adaptation allows the FF + 1A line to maintain efficient photosynthesis during water scarcity. Our findings demonstrate the potential of using AMALs to introduce beneficial traits from related species to improve crop resilience. Specifically, the addition of the first shallot chromosome enhances ABA biosynthesis and stress response pathways, offering a valuable resource for breeding drought-tolerant *A. fistulosum* varieties. In summary, our study underscores the importance of ABA in drought response and the benefits of genetic additions from stress-tolerant species, contributing to more stable crop production amid climate variability.

Chapter 3: Metabolite Profiling and Association Analysis of Leaf Tipburn in Heat-Tolerant Bunching Onion Varieties

Introduction

The bunching onion (*Allium fistulosum* L.), also known as the Welsh onion, green onion, spring onion, or scallion, is widely distributed from Siberia to tropical Asia, particularly in East Asia, where numerous varieties have adapted to diverse local environmental conditions (Yamasaki and Tsukazaki, 2022). The distinct flavor and vibrant color of bunching onions contribute to the richness of dishes, leading consumers to expect high-quality bunching onions that offer exceptional flavor, color, and beneficial functional components (Kim et al., 2023; Singh and Ramakrishna, 2017). Bunching onions are consumed year-round in Japan, necessitating a stable and consistent supply to meet market demand. In recent years, producers have sought traits such as "heat tolerance" to minimize leaf tipburn and poor growth during summer, as well as "dark green coloration" (Yamasaki and Tsukazaki, 2022; Padula et al., 2022), and Japanese seed companies have developed summer F₁ lines characterized by these traits. The chemical composition of bunching onions has been reported to fluctuate across various growth stages and harvest times (Kołota et al., 2012). Therefore, it is crucial to systematically investigate and understand the variations in pigment

compounds and functional components influenced by growing conditions to ensure consistent quality. Furthermore, recent global warming has led to a decline in both production and quality during the summer, with the occurrence of leaf tipburn becoming particularly severe (Liu et al., 2021).

Tipburn is a physiological disorder that occurs during rapid plant growth and is characterized by necrosis at the leaf apex of young, developing leaves (Maruo and Johkan, 2016). As bunching onions are leafy vegetables, the deterioration of the appearance of the leaf blade significantly reduces the commercial value, posing a major challenge for farmers and distributors (Hutchings, 2011; NILSSON, 2000). Tipburn is generally considered a calcium-related disorder or a calcium deficiency-related disorder (Kuronuma et al., 2019; Su et al., 2019; Wang et al., 2019a). The occurrence of tipburn in bunching onions has been reported to be induced by a combination of factors, including soil dryness, high temperatures, prolonged sunlight exposure, and calcium deficiency (Inden, 1987). Additionally, in onions (*A. cepa*), apart from the effects of pests and diseases, deficiencies in nitrogen, sulfur (Abbey et al., 2002), and boron (Jeyakumar and Balamohan, 2007), as well as exposure to ozone (Ahmad et al., 2013) and salinity (Shannon and Grieve, 1998), can also cause tipburn. Tipburn in onions is often regarded as a general symptom of stress, as it can be triggered by a wide range of biotic and abiotic stress factors (Riaz et al., 2020). Leaf tipburn affects not only the *Allium* genus, including crops such as bunching onions, onions, garlic (*A. sativum*), and chives (*A. tuberosum*), but also other crops, such as lettuce (*Lactuca sativa*), white cabbage (*Brassica oleracea* L. var. *capitata*), Chinese

cabbage (*B. pekinensis* (Lour.) Rupr.), Brussels sprouts (*B. oleracea* var. *gemmifera* DC.), and strawberry (*Fragaria* × *ananassa* Duch.) (Saure, 1998; Uno et al., 2016; Palencia et al., 2010). Therefore, it is crucial to systematically investigate and comprehend the factors contributing to this phenomenon across different species.

Metabolomics serves as a powerful tool for biological discoveries in plants, offering insights into the biochemical status of plant cells at specific developmental stages and in response to environmental conditions (Hirai et al., 2004). Metabolomics has the potential to greatly enhance the study of stress biology in plants and other organisms by identifying various compounds, including stress metabolism by-products, molecules involved in stress signal transduction, plant hormones, and compounds associated with the plant's acclimation response (Shulaev et al., 2008; Mascellani Bergo et al., 2024). In *Allium* species, metabolome analyses have been conducted in various studies focusing on the effects of stress, cultivation conditions, treatment methods, and even the impact of adding alien chromosomes (Saviano et al., 2019; Abdelrahman et al., 2019; Medina-Melchor et al., 2022). Despite extensive research on tipburn in leafy crops such as lettuce (*Lactuca sativa* L.), onion, and cauliflower (*Brassica oleracea* L.), most of these studies have primarily focused on nutritional deficiencies or genotype-related tipburn symptoms (Riaz et al., 2020; Hamidon and Ahamed, 2022; Rosen, 1990). There is limited knowledge of the biochemical and physiological mechanisms underlying this disorder in bunching onions, particularly under combined environmental stresses. This study addresses this

gap through integrating metabolomics with pigment and functional component analyses to uncover the mechanisms of tipburn development and identify strategies for improving tolerance in heat-tolerant F₁ hybrid and purebred varieties.

Materials and Methods

Materials and growth conditions

In this study, we examined the following: two F₁ cultivars from Nakahara Seed Product Co., Ltd.—‘Natsuhiko’ (NATS) and ‘Kaminari’ (KAMI); one Yamaguchi Prefecture purebred variety—‘YSG1go’ (YSG1); and six Yamaguchi Prefecture-bred F₁ hybrid lines— ‘Yamakou01’ (YAM1), ‘Yamakou02’ (YAM2), ‘Yamakou03’ (YAM3), ‘Yamakou04’ (YAM4), ‘Yamakou05’ (YAM5), and ‘Nakayamakou’ (NAKA). These plant materials were grown in the greenhouse of Yamaguchi Prefectural Agriculture and Forestry General Technology Center (34°N, 131°E). We established six distinct growth conditions as follows: (1) sown on May 7, 2019, and harvested on July 18, 2019; (2) sown on May 7, 2019, and harvested on August 22, 2019; (3) sown on May 7, 2019, and harvested on September 18, 2019; (4) sown on June 9, 2019, and harvested on August 22, 2019; (5) sown on June 9, 2019, and harvested on September 18, 2019; (6) sown on July 4, 2019, and harvested on September 18, 2019. In growth conditions (1), (2), and (3), we cultivated eight varieties except YSG1, while in growth conditions (4), (5),

and (6), we cultivated all nine varieties. This experiment aimed to screen for the conditions and cultivars most susceptible to leaf tipburn. To make the most of the limited greenhouse space and resources, we selected nine cultivars with three replications and six growth conditions to reflect diverse genetic and environmental scenarios.

The crops were planted in 6 rows on a 90 cm wide ridge, with an inter-row spacing of 12 cm and a seeding density of 120 seeds per square meter. A total of 1.0 kg of nitrogen per area (kg/a) was applied during the experiment. This nitrogen was divided into two applications: an initial 0.5 kg/a as a basal fertilizer, followed by an additional 0.5 kg/a as a topdressing later in the two-leaf stage. The watering conditions were as follows: on the day of sowing, water was applied at 48 L/m², with a soil water tension value set to 1.5 pF. During germination (0–4 days), irrigation was provided at 24 L/m² per application, maintaining a pF value between 1.5 and 1.6. In the cotyledon stage (4–11 days), 6 L/m² of water was applied every 2–3 days, keeping the pF value between 1.6 and 1.8. At the one-leaf stage (11–18 days), 10 L/m² of water was supplied every 2–3 days, maintaining a pF value between 1.7 and 2.0. During the two-leaf stage (18–28 days), irrigation was increased to 12 L/m² daily, with the pF value maintained between 1.6 and 1.8. During the three-leaf stage (28–38 days), irrigation was performed every 3 days with 6 L/m² to maintain a pF value between 2.0 and 2.3. For the four-leaf stage (38–49 days), water was applied almost daily at 12 L/m², maintaining a pF value of 1.8–2.0. During the five-leaf stage (49–59 days), irrigation was carried out every 3 days with 5 L/m², keeping the pF value between 2.0 and 2.5. At the

six-leaf stage (59 days onward), irrigation was reduced to 0–1 time per week with 4 L/m², maintaining a pF value of 2.3–2.5 until harvest. After harvest, the plants were grouped into bundles of 10, with three bundles used for biological replicates ($n = 3$). The outer leaves were removed, leaving two young leaves for further analysis.

Leaf tipburn Measurement

The samples were arranged on a black background to ensure that the leaves did not overlap, and images were captured. From the obtained images, pixel counts for leaf tipburn areas and healthy (green color) areas were calculated using the free software LIA32 Ver. 0.376 β 1 (Yamamoto, 2004). The training images included ‘Asagi-kujyo harvested on August 18, 2017’ (Figure 8), with 50 training points for each class: leaf tipburn area, healthy area, and background. The percentage of leaf tipburn was calculated as follows: (pixel count of leaf tipburn area/pixel count of total plant area) \times 100.



Figure 8. The plant of Asagi-Kujo harvested on August 18, 2017, used as a training image for supervised learning analysis.

SPAD Value Measurement

The SPAD value was determined by averaging three measurements taken at the center of the leaf using a Soil Plant Analysis Development chlorophyll meter (SPAD-502Plus, KONICA MINOLTA, INC., Tokyo, Japan) (Markwell et al., 1995). For each sample, the overall SPAD value was calculated by averaging the SPAD readings from the first (youngest) and second (second youngest) leaves.

Pigment Compound Measurement

The method for measuring pigment compound was developed with reference to Dissanayake et al. (Dissanayake et al., 2008). Chlorophyll *a*, Chlorophyll *b*, Lutein, β -carotene, violaxanthin, and neoxanthin were measured using high-performance liquid chromatography (HPLC L-7000 series, HITACHI, Tokyo, Japan). The leaf blade of the trimmed sample was cut into approximately 5 mm sections using a kitchen knife, and a portion was weighed to precisely 5.0 g for analysis. The sample was placed into a homogenizer cup, followed by the addition of 0.2 g of basic magnesium carbonate, 0.1 g of butylated hydroxytoluene, and 20 mL of cold 100% acetone. The premix was homogenized at 10,000 rpm for 5 minutes using an Ace HOMOGENIZER AM-7 (Nihon Seiki Co., Ltd., Tokyo, Japan). The suspension was filtered using suction filtration, and the filtrate was collected. The residue was transferred to a mortar, mixed with 10 mL of cold 100% acetone, and ground with a pestle. The resulting mixture was filtered again

using suction filtration to collect the filtrate. This process was repeated three times to maximize filtrate recovery. The combined filtrates were dried by adding 5 g of anhydrous sodium sulfate and left in the dark for 30 minutes. Subsequently, the mixture was passed through a filter (Advantec, Tokyo, Japan) to quantify the volume. Finally, the filtrate was passed through a 0.45 μm filter (Advantec, Tokyo, Japan) and used as the extract for HPLC analysis. The extract was analyzed using HPLC equipped with a UV–Vis detector (HITACHI L7420) set at 435 nm for carotenoid detection. Pigmented compounds were separated using a LiChroCART 250-4.0 Lichrospher 100 RP-18 5 μm column (KANTO CHEMICAL, Tokyo, Japan). The separation was performed using gradient elution with two solvents: (A) 80% methanol solution, prepared by mixing 400 mL of HPLC-grade methanol, 50 mL of ultra-pure water, and 50 mL of 100 μM HEPES buffer (pH 7.5), and (B) a 50:50 mixture of ethyl acetate and 80% methanol. The gradient elution program was as follows: it started with 100% solvent A for 20 minutes; then, a linear gradient was followed to solvent B over 50 minutes. The flow rate was maintained at 1 mL/min, with a column temperature of 30 °C and an injection volume of 20 μL .

70% Ethanol Extraction

The method for extraction was developed with reference to Hang et al. (Hang et al., 2004). The leaf blades of the trimmed sample were cut with a kitchen knife at intervals of approximately 5 mm and weighed out to 5.0 g.

The tissue samples were placed in a conical flask containing 35 mL of ethanol and 10 mL of distilled water (final concentration 70%) and boiled in a water bath for 15 minutes. The mixture was then homogenized at 10,000 rpm for 5 minutes using an Ace HOMOGENIZER AM-7 (Nihon Seiki Co., Ltd., Tokyo, Japan). The resulting suspension was filtered using suction filtration, and the filtrate was collected and quantified. The extract was stored at $-20\text{ }^{\circ}\text{C}$ in a freezer for further analysis.

Total Phenolic Compounds Measurement

The total phenolic compounds content in the 70% ethanol extract was measured using the Folin–Ciocalteu method (Folin and Denis, 1915). The 70% ethanol extraction was diluted 5 times with distilled water. Of the diluted solution, 1 μL was put into test tube, and 1 mL of 1N Folin–Ciocalteu reagent was added. After 3 minutes, 1 mL of 10% sodium carbonate solution was added to the test tube. The mixture was incubated for 1 hour at room temperature in the dark. The absorbance of the reaction mixture was measured at 530 nm with a spectrophotometer (U-2000, Hitachi High-Tech corporation, Tokyo, Japan). Catechol was used as a standard, and the results were expressed as milligrams of catechol equivalent (mg CA) per 100 g fresh weight of plant sample.

Total Flavonoid Compound Measurement

The total flavonoid compound content in the 70% ethanol extract was

measured using the method described previously (Vu et al., 2013). The 70% ethanol extract and n-hexane were put into a test tube with a screw cap at a ratio of 1:1 and stirred to dissolve the chlorophyll, carotenoids, and other pigments into the hexane layer. The ethanol layer was diluted 2 times with 70% ethanol. Three mL of the diluted solution was put into a test tube, and 9 mL of 2% aluminum chloride solution was added. The mixture was incubated for 1 hour at room temperature in the dark. The absorbance of the reaction mixture was measured at 420 nm with a spectrophotometer (U-2000, Hitachi High-Tech Corporation, Tokyo, Japan). Quercetin was used as a standard, and the results were expressed as milligrams of quercetin equivalent (mg quercetin) per 100 g fresh weight of the plant sample.

Fructan Measurement

The fructan content in the 70% ethanol extract was measured using the thiobarbituric acid method (Percheron, 1962), with minor modifications. The 70% ethanol extraction was diluted 5 times with 70% ethanol. Of the diluted solution, 20 μ L was put into a test tube, and 10 μ L of 25 mM ammonium acetate buffer was added. Furthermore, 10 μ L of invertase solution was added and left at room temperature for 5 min to hydrolyze the sucrose in the extract. Measures of 50 μ L of distilled water and 10 μ L of 10 N sodium hydroxide solution were added and heated in boiling water for 10 min to decompose the fructose in the solution. After cooling rapidly in ice water, 1 mL of thiobarbituric acid solution and 1 mL of 12 N hydrochloric acid were added

and heated in boiling water for 6 min. The absorbance of the reaction mixture was measured at 432 nm with a spectrophotometer (U-2000, Hitachi High-Tech Corporation, Tokyo, Japan). Fructan was used as a standard, and the results were expressed as milligrams of quercetin equivalent (mg 1-kestose) per 100 g fresh weight of the plant sample.

Metabolome Analysis

Sample preparation was performed automatically by a liquid-handling system (Microlab STAR Plus, Hamilton, Company, Reno, NV, USA) for dispensing, plate transfer, solvent drying (Ultravap Mistral, Porvair PLC, Norfolk, UK), dissolving, and filtration, as described by Sawada et al. (Sawada et al., 2017). The leaf blades of the trimmed samples were frozen in liquid nitrogen. The frozen samples were dried using a freeze-dryer (TAITEC VD-250R freeze-dryer coupled with a vacuum pump, TAITEC, Saitama, Japan) and then powdered using a mill (KMZ-0401/P, Koizumi Seiki Corporation, Osaka, Japan). The powders were weighed out to 4 mg in a 2 mL tube, and a 5 mm zirconia ball (NIKKATO CORPORATION, Osaka, Japan) was added. One milliliter of extraction solvent (80% methanol and 0.1% formic acid coupled with 8.4 nmol/L lidocaine and 210 nmol/L 10-camphorsulfonic acid as internal standard) was added to a 2 ml tube (resulting in a concentration of 4 mg/ml), and the metabolites were extracted in a multi-bead shaker (Shake Master NEO, Biomedical Science, Tokyo, Japan) at 1000 rpm for 2 min. After centrifugation at 9100 G for 1 minute, the supernatants

were diluted 4 times with an extraction solvent (resulting in a concentration of 1 mg/ml). Of each diluted solution, 25 microliters was transferred to a 96-well plate, dried with nitrogen air, redissolved in 250 μ L of ultra-pure water (LC-MS grade), and filtered using a 0.45 μ m pore size filter plate 384 (Multiscreen HTS 384-Well HV, Merck, Rahway, NJ, USA). One microliter of the solution extract at a final concentration of 100 ng/ μ L was subjected to widely targeted metabolomics using LC-QqQ-MS (UHPLC-Nexera MP/LCMS-8050, SHIMADZU, Tokyo, Japan). The solution extract was separated using a ACQUITY UPLC HSS T3 Column, 100 Å, 1.8 μ m, 1 mm X 50 mm (Waters Corp., Milford, USA). The separation was performed using gradient elution with two solvents: (A) 0.1% (v/v) formic acid in distilled water, and (B) 0.1% (v/v) formic acid in acetonitrile. The flow rate was maintained at 0.24 mL/min, with a column temperature of 30 °C. The setting parameters for LC-QqQ-MS analysis are summarized in Table 2 and 3.

Table 2. Gradient condition for LC-QqQ-MS analysis.

Time(min)	Flow (mL/min)	A solution (%)	B (%)
0	0.24	99.9	0.1
0.25	0.24	99.9	0.1
0.40	0.24	91	9
0.80	0.24	83	17
1.90	0.24	0.1	99.9
2.10	0.24	0.1	99.9
2.11	0.24	99.9	0.1
2.70	stop		

Table 3. Mass spectrometry parameters.

Parameters	Ppolarity Positive	Polarity Negative
Interface voltage (kV)	4.0	3.0
Interface temperature (°C)	300	300
DL temperature (°C)	250	250
Heat block temperature (°C)	400	400
Nebulizer gas flow (L/min)	3.0	3.0
Drying gas flow (L/min)	10.0	10.0
Heating gas flow (L/min)	10.0	10.0
Dwell time (sec)	0.005	0.005
Injection volume (uL)	1.0	1.0

Data Analysis

Statistical Analysis

Data for the SPAD values, pigment compounds (chlorophyll *a*, chlorophyll *b*, lutein, β -carotene, violaxanthin, neoxanthin), and functional components (total phenolic compounds, total flavonoid compounds, fructan), along with leaf tipburn rate, were analyzed using one-way analysis of variance (ANOVA) and Tukey's multiple comparison test for each individual growing condition and across all conditions. A significance level of $p < 0.05$ was applied. An analysis of the secondary metabolite characteristics of the varieties was conducted. The dataset, including chlorophyll *a*, chlorophyll *b*, lutein, β -carotene, violaxanthin, neoxanthin, total phenolic compounds, total flavonoid compounds, and fructan, was first standardized using the StandardScaler function from Scikit-Learn. Subsequently, the standardized data was analyzed using principal component analysis (PCA) with two components (`n_components=2`) and K-means clustering (`n_clusters=4`, `random_state=42`) to assess the variation in metabolite profiles across samples. The analysis was performed using Python 3.9.7 with Pandas 1.3.4, Scikit-Learn 0.24.2, and Matplotlib 3.4.3 libraries.

Estimate Compounds Associated with Leaf Tipburn Using Metabolomics

A total of 472 metabolite intensities were obtained from the metabolome analysis. Missing values were imputed with a value of 10, and the signal intensities for all samples ($n = 3$) were averaged. Metabolites with

signal-to-noise ratios (S/N, defined as the ratio of the average signal intensity to that of the extraction solvent control) of less than 5 across all experimental groups were excluded. Additionally, metabolites with relative standard deviations (RSD) greater than 0.3 in all experimental groups were removed, resulting in a final dataset of 267 metabolites. The data matrix was then normalized to the median and auto-scaled. Initially, partial least squares discriminant analysis (PLS-DA) was performed on all 267 metabolites, and VIP scores were used to assess the overall trends in metabolomic data between the leaf tipburn group (top 5% in leaf tipburn rate) and the control group (bottom 5% in leaf tipburn rate). This method is particularly suitable for high-dimensional metabolomic data as it emphasizes group separation and identifies key metabolites using VIP scores. However, despite limitations such as assumptions of linearity and the risk of overfitting, it remains a valuable tool for exploring group separation in high-dimensional datasets. Additionally, a Student's *t*-test, followed by false discovery rate (FDR) correction using the Benjamini–Hochberg procedure, was conducted to compare metabolites between groups, identifying those with significant differences (FDR < 0.05) and a change of 1.5-fold or more (\log_2 FC [Leaf tipburn/control] ≥ 0.58 or ≤ -0.58). These metabolites were then used to create volcano plots. The preprocessing steps, including missing value imputation, S/N filtering, RSD calculations, and intensity correction via dividing by internal standards, were performed using Python 3.9.7 with Pandas 1.3.4. Data normalization and subsequent analysis were conducted using MetaboAnalyst 6.0.

Machine Learning Methods

A random forest regression model was employed to predict the leaf tipburn rate using 267 metabolite profiles as input features. This method was chosen to address the limitations of PLS-DA, specifically its inability to capture non-linear relationships, and to mitigate the risk of overfitting inherent in single decision tree models. The data, which included all available samples, was first split into training and test sets using a 70–30 split, ensuring a consistent random state=42 to enable reproducibility. The training set was used to fit the random forest model, which was optimized based on the following hyperparameters: `n_estimators=100`, `max_features='log2'`, `min_samples_leaf=2`, `min_samples_split=2`, and `max_depth=None`. To gain insights into the model's predictions, Shapley additive explanations (SHAP) analysis was performed. All analyses and visualizations were conducted using Python 3.9.7. The following libraries were used: Pandas 1.3.4, Scikit-Learn 0.24.2, SHAP 0.46.9, and Matplotlib 3.4.3.

Results

Variation in Pigment Contents and Functional Components Among Different Bunching Onion Varieties and Breeding Lines Across Different Growing Conditions

Images of the plants under each growing condition are shown in Figure 9–14. The varieties KAMI and NATS showed significantly lower SPAD values, whereas YSG1 and YAM1-5 exhibited significantly higher SPAD

values (Figure 15). On the other hand, NAKA variety showed an intermediate SPAD value trend. Pigment compounds associated with SPAD values, including chlorophyll *a* and *b*, lutein, violaxanthin, and neoxanthin, exhibited trends consistent with the SPAD measurements across the investigated varieties. In contrast, β -carotene exhibited only minor variations among the different varieties (Figure 16). Additionally, functional components, including total phenolic compounds and total flavonoid compounds, were significantly lower in KAMI and significantly higher in YSG1, whereas the other varieties displayed intermediate levels, with no significant differences observed (Figure 17).

PCA and K-means clustering were applied to assess the varietal characteristics under different growing conditions, focusing on samples sown on May 7 and harvested on July 18 (1), August 22 (2), and September 18 (3). The data were projected onto two principal components (PC1 and PC2), which together explained 80.13% of the total variance, with PC1 accounting for 62.10% and PC2 for 18.03% (Figure 18A). The loadings of PC1 were primarily associated with pigment compounds (excluding β -carotene), with an increase in pigment levels on the positive side and a decrease on the negative side. The loadings of PC2 were associated with functional components, including β -carotene, showing increases on the positive side and β -carotene on the negative side (Figure 18B). K-means clustering classified all samples into four clusters: cluster 1 included samples with increased β -carotene, cluster 2 included samples with increased pigment compounds, cluster 3 included samples with decreased pigment compounds, and cluster 4

included samples with increased functional components. Focusing on the variety, NAKA, NATS, and KAMI were grouped into clusters 3 and 4, positioned on the negative side of PC1. In contrast, YAM1-5 was classified into clusters 1, 2, and 4, and was situated on the positive side of PC1 (Table 4). Focusing on the growing conditions, samples from May sowing and July harvest (1) were part of clusters 0 or 2 and were positioned on the negative side of the second principal component, while samples harvested in the following months (2) and (3) shifted to the positive side.

Similarly, PCA and K-means clustering were performed using results from May sowing and September harvest (4), June sowing and September harvest (5), and July sowing and September harvest (6). These samples were also projected onto two principal components, accounting for 71.27% of the total variance. PC1 contributed 55.06%, while PC2 contributed 16.21% (Figure 19A). The loadings of PC1 were predominantly associated with pigment compounds, with increased values on the positive side and decreased values on the negative side. PC2 loadings were linked to functional components, including β -carotene, showing an increase on the positive side and a decrease on the negative side (Figure 19B). K-means clustering grouped all samples into four distinct clusters: cluster 1 consisted of samples with elevated levels of both pigment compounds and functional components; cluster 2 included samples with reduced levels of both; cluster 3 contained samples with increased pigment compounds and decreased functional components; cluster 4 was comprised of samples with decreased pigment compounds and increased functional components. YAM1-5 and YSG1 were

classified into clusters 1 and 3, while NAKA, NATS, and KAMI were grouped into clusters 2 and 4 (Table 5).

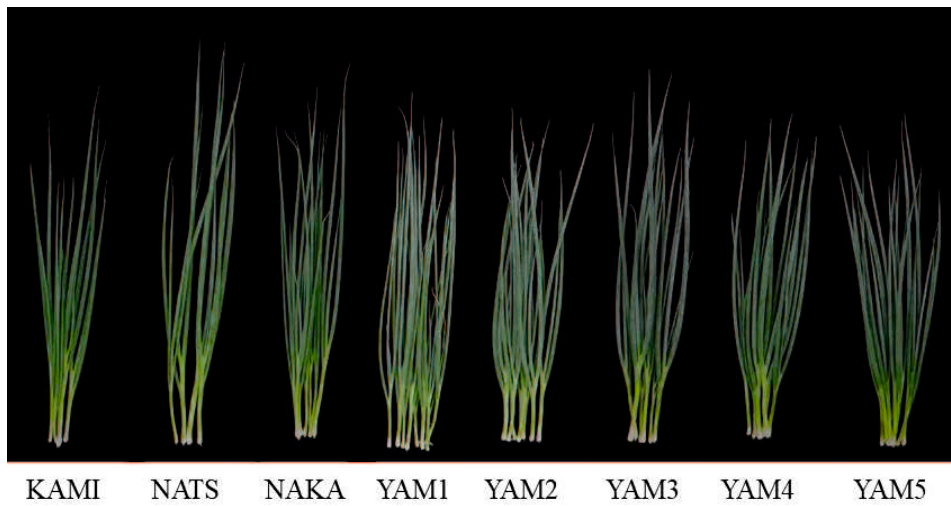


Figure 9. Plants from samples sown in May and harvested in July.

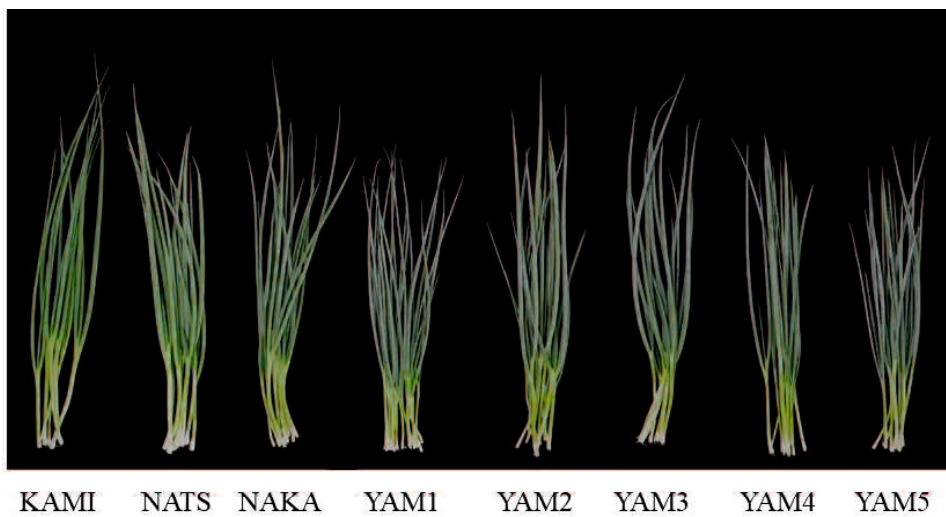
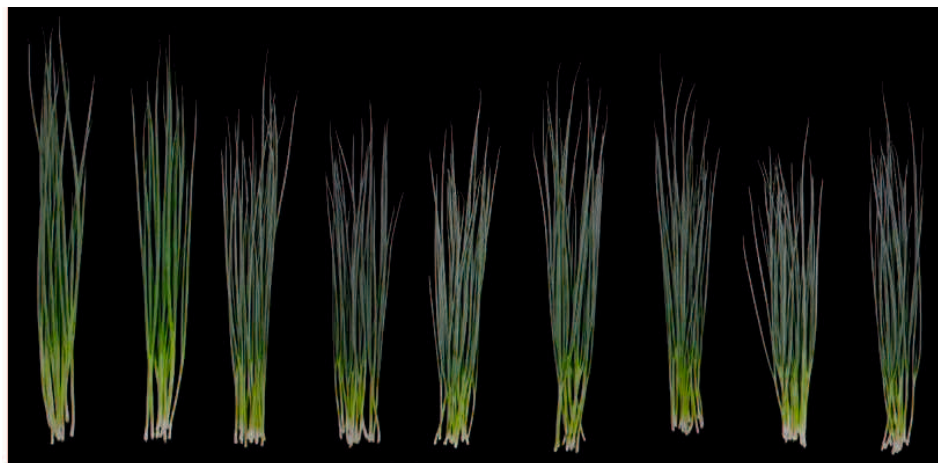


Figure 10. Plants from samples sown in May and harvested in August.



KAMI NATS NAKA YAM1 YAM2 YAM3 YAM4 YAM5

Figure 11. Plants from samples sown in May and harvested in September.



KAMI NATS NAKA YSG1 YAM1 YAM2 YAM3 YAM4 YAM5

Figure 12. Plants from samples sown in June and harvested in August.



KAMI NATS NAKA YSG1 YAM1 YAM2 YAM3 YAM4 YAM5

Figure 13. Plants from samples sown in June and harvested in September.



KAMI NATS NAKA YSG1 YAM1 YAM2 YAM3 YAM4 YAM5

Figure 14. Plants from samples sown in July and harvested in September.

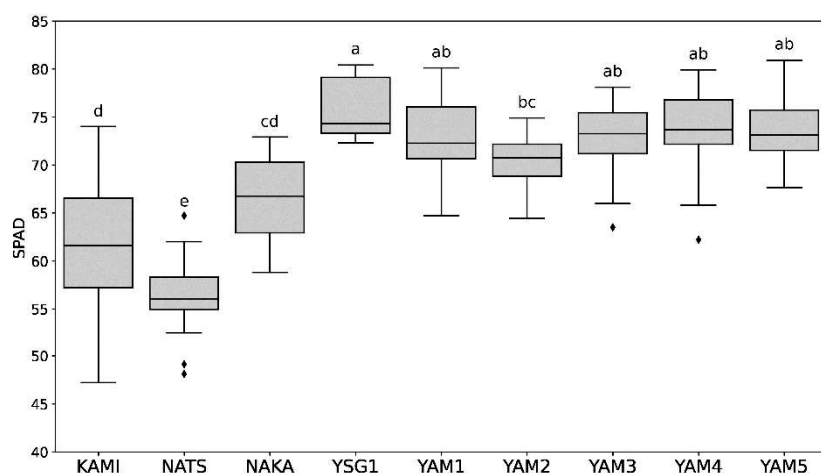


Figure 15. Boxplot of SPAD values by varieties and lines under all growing conditions. The box represents the interquartile range, the horizontal line within the box indicates the median, and dots represent outliers. Different letters indicate significant differences at $p < 0.05$.

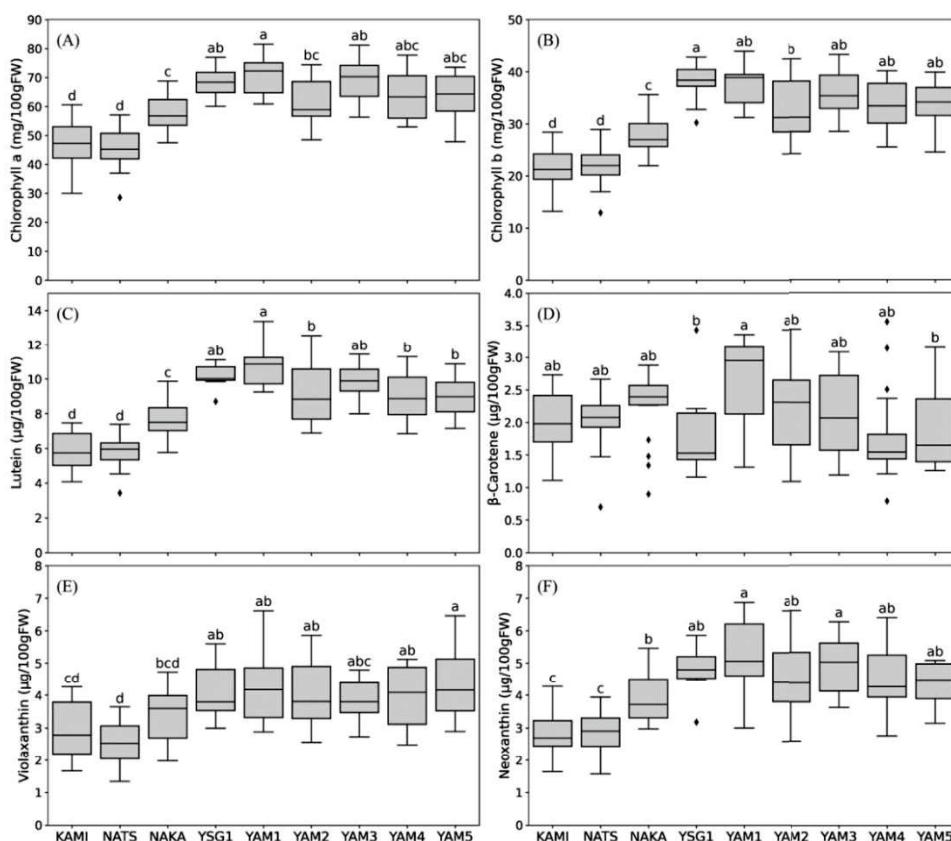


Figure 16. Boxplot of pigment compounds, including chlorophyll *a* (A), chlorophyll *b* (B), lutein (C), β -carotene (D), violaxanthin (E), and neoxanthin (F), across varieties and lines under all growing conditions. Different letters denote significant differences at $p < 0.05$.

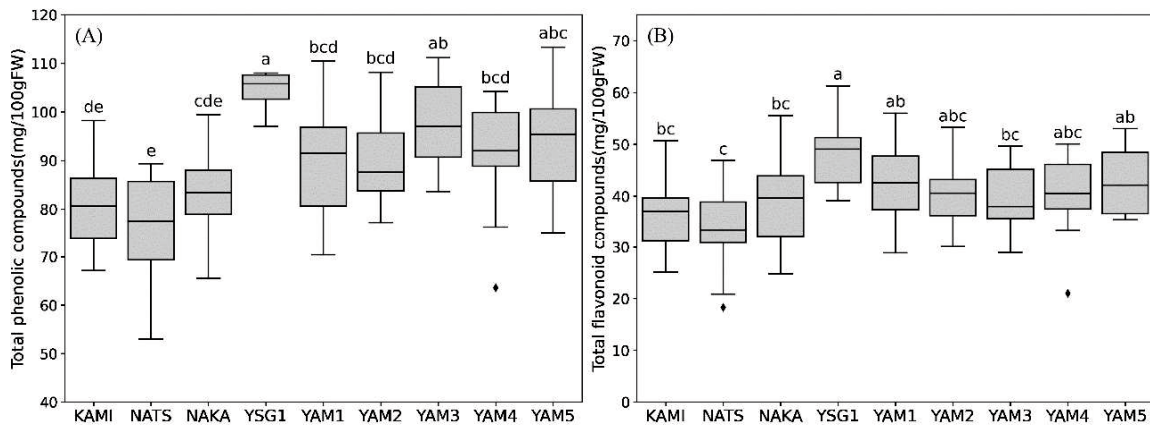


Figure 17. Boxplot of functional components, including total phenolic compounds (A) and total flavonoid compounds (B), across varieties and lines under all growing conditions. Different letters denote significant differences at $p < 0.05$.

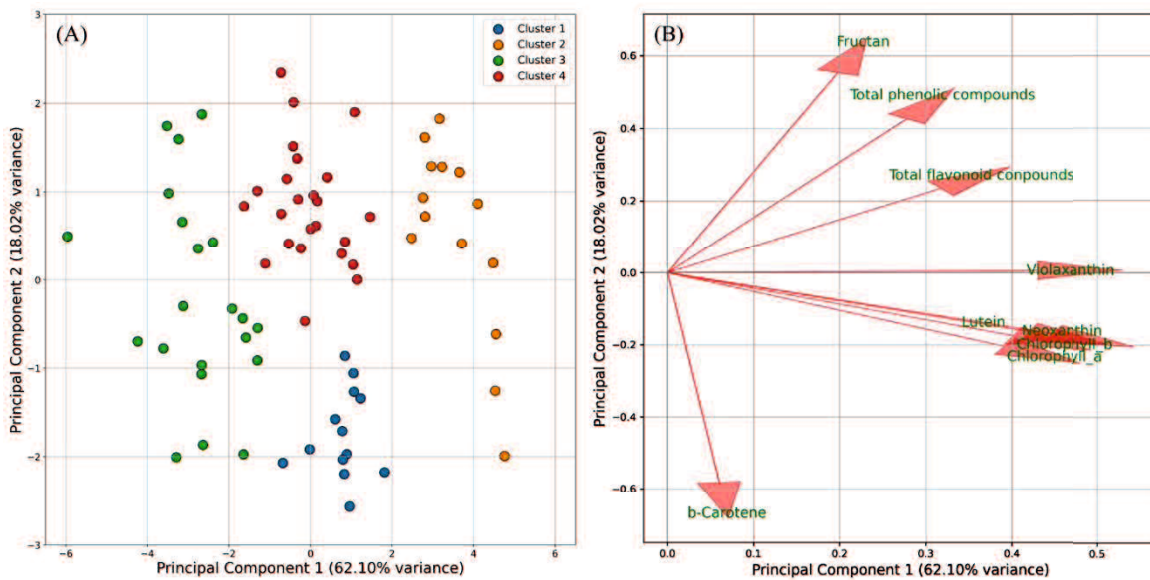


Figure 18. Principal component analysis (PCA) score plot with K-means clustering (A) and PCA loading plot (B) of the dataset from May sowing and July, August, and September harvests. (A) Samples are color-coded on K-means clustering, with four clusters identified. (B) Arrows represent the direction and magnitude of each variable's influence, with longer arrows indicating stronger contributions.

Table 4. Sample distribution by varieties or lines and growth conditions based on K-means clustering of a dataset from May sowing and July, August, and September harvests. The table summarizes the assignment of samples to four distinct clusters (cluster 1 to cluster 4), identified through K-means clustering.

Cluster	Features	Growth conditions	KAMI	NATS	NAKA	YAMI	YAM2	YAM3	YAM4	YAM5
cluster1	β -carotene_UP	May_Jul ^y			1	3	1	2	1	3
		May_Aug				2				
		May_Sep								
cluster2	Pigment cmpds_UP ^z	May_Jul								
		May_Aug								
		May_Sep				3	3	3	2	3
cluster3	Pigment cmpds_DOWN	May_Jul	3	3	2		2		2	
		May_Aug	3	3	2					
		May_Sep		1						
cluster4	Functional cmpds_UP	May_Jul						1		
		May_Aug			1	1	3	3	3	3
		May_Sep	3	2	3				1	

^y: Indicates the sowing month and the harvesting month.

^z: cmpds stands for compounds.

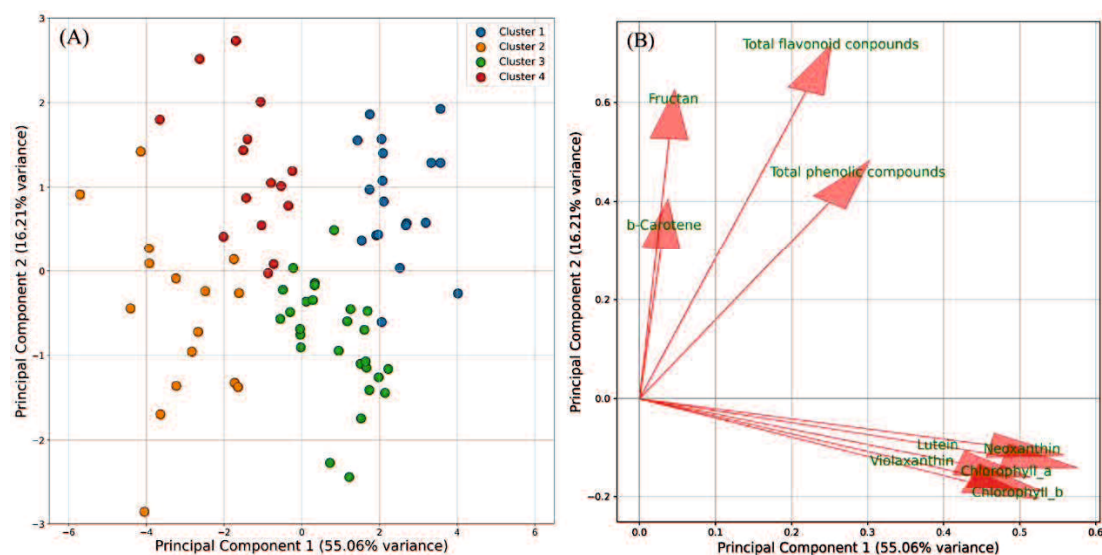


Figure 19. Principal component analysis (PCA) score plot with K-means clustering (A) and PCA loading plot (B) of a dataset from the May, June, and July sowing with September harvest. (A) Samples are color-coded on K-means clustering, with four clusters identified. (B) Arrows represent the direction and magnitude of each variable's influence, with longer arrows indicating stronger contributions.

Table 5. Sample distribution by varieties or lines and growth conditions based on the K-means clustering of a dataset from May, June, and July sowing and September harvest. The table summarizes the assignment of samples to four distinct clusters (Cluster 1 to Cluster 4) identified through K-means clustering.

Cluster	Features	Growth conditions	KAMI	NATS	NAKA	YSG1	YAM1	YAM2	YAM3	YAM4	YAM5
cluster1	Pigment cmpds_UP ^y Functional cmpds_UP	May_Sep ^z					3	3	2	2	2
		Jun_Sep					2				1
		Jul_Sep				3					1
cluster2	Pigment cmpds_DOWN Functional cmpds_DOWN	May_Sep		2	1						
		Jun_Sep	3	2							1
		Jul_Sep	3	3	1						
cluster3	Pigment cmpds_UP Functional cmpds_DOWN	May_Sep							1		1
		Jun_Sep			1	2	1	1	3	3	
		Jul_Sep			1		3	3	3	3	2
cluster4	Pigment cmpds_DOWN Functional cmpds_UP	May_Sep	3	1	2					1	
		Jun_Sep		1	2	1		2			1
		Jul_Sep			1						

^y: cmpds stands for compounds.

^z: Indicates the sowing month and the harvesting month.

Estimating the Metabolites Involved in Leaf Tipburn

The leaf tipburn rate across 153 samples from 9 varieties ranged from 0.00% to 1.23% under six different growth conditions, with no significant differences observed between varieties (Figure 20, Table 6). Based on these findings, we selected the top 5% of samples with the highest leaf tipburn rates (eight samples: leaf tipburn group) and the bottom 5% with the lowest rates (eight samples: control group) for further comparative analysis using the 267 metabolites identified from these samples.

To gain deeper insights into the contributions of specific metabolites in the leaf tipburn and control groups, we performed PLS-DA and evaluated the results using VIP scores. The analysis revealed that the leaf tipburn and control groups could be differentiated into two clusters based on two primary

components (Figure 21A). Component 1 contributed 11.4%, and Component 2 contributed 17.2%, with a cumulative contribution of 28.6%, though this remains relatively low. The VIP scores highlighted the importance of metabolites, particularly sulfur compounds such as cystathionine, gamma-glutamyl-propenyl-cysteine sulfoxide (gamma-Glu-PRENCISO), and cysteine, as well as flavonoids, in differentiating the groups. Notably, cystathionine and cysteine were found at higher concentrations in the control group (and lower in the leaf tipburn group), while gamma-Glu-PRENCISO was elevated in the leaf tipburn group (and lower in the control group) (Figure 21B). We then conducted a Student's *t*-test on the 267 metabolites between the leaf tipburn and control groups, followed by FDR correction for *p*-values. No metabolites showed significant differences between the two groups at a significance level of $q = 0.05$. As a result, we selected metabolites with significant uncorrected *p*-values and a \log_2 FC [Leaf tipburn/control] of ≥ 0.58 or ≤ -0.58 , equivalent to a 1.5-fold change. This selection identified 11 metabolites (8 increased, 3 decreased) (Figure 22). Many of these metabolites were also highlighted by high VIP scores from the PLS-DA analysis.

Finally, we applied a random forest regression model using the full dataset, with the leaf tipburn rate as the target variable and the 267 metabolites as input features. SHAP analysis was used to interpret the model's output. The top 20 metabolites ranked by average SHAP values were primarily associated with flavonoids and organosulfur compounds (Figure 23). Among these, gamma-Glu-PRENCISO stood out as a key metabolite, overlapping with

those identified by high VIP scores from the PLS-DA analysis and significant changes in the Student's *t*-test, exhibiting a 1.5-fold change. Gamma-Glu-PRENCISO is an intermediate of PRENCISO, a precursor of pungency-related compounds. In the leaf tipburn group, organosulfur compounds tended to proceed toward the alliin synthesis pathway rather than the sulfur-assimilation- or antioxidant-related pathways. This metabolic shift may lead to a deficiency in metabolites essential for stress responses, potentially resulting in inadequate adaptation to stress in the leaf tipburn group.

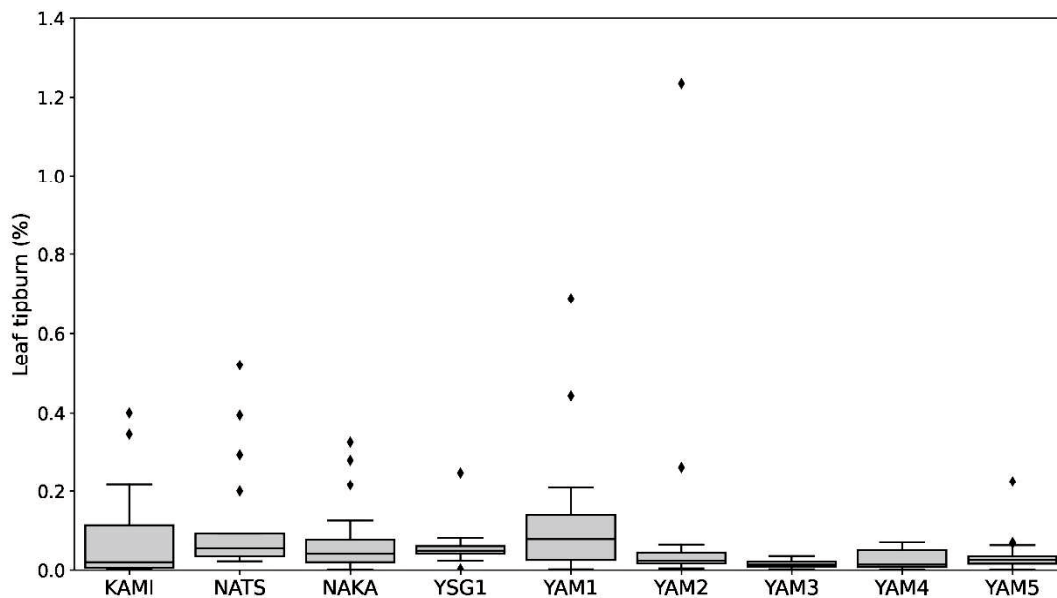


Figure 20. Boxplot of leaf tipburn by varieties and lines under all growing conditions. The box represents the interquartile range, the horizontal line within the box indicates the median, and dots represent outliers.

Table 6. Results of ANOVA for leaf tipburn rates under different varieties and growth conditions.

Factor	Source of Variation	df	Sum of Squares	Mean Square	F-value	p-value
Variety	Between groups	5	0.51	0.01	0.499	0.776
	Residuals (Error)	146	2.981	0.02	-	-
Growth condition	Between groups	8	0.245	0.031	1.572	0.138
	Residuals (Error)	143	2.787	0.019	-	-

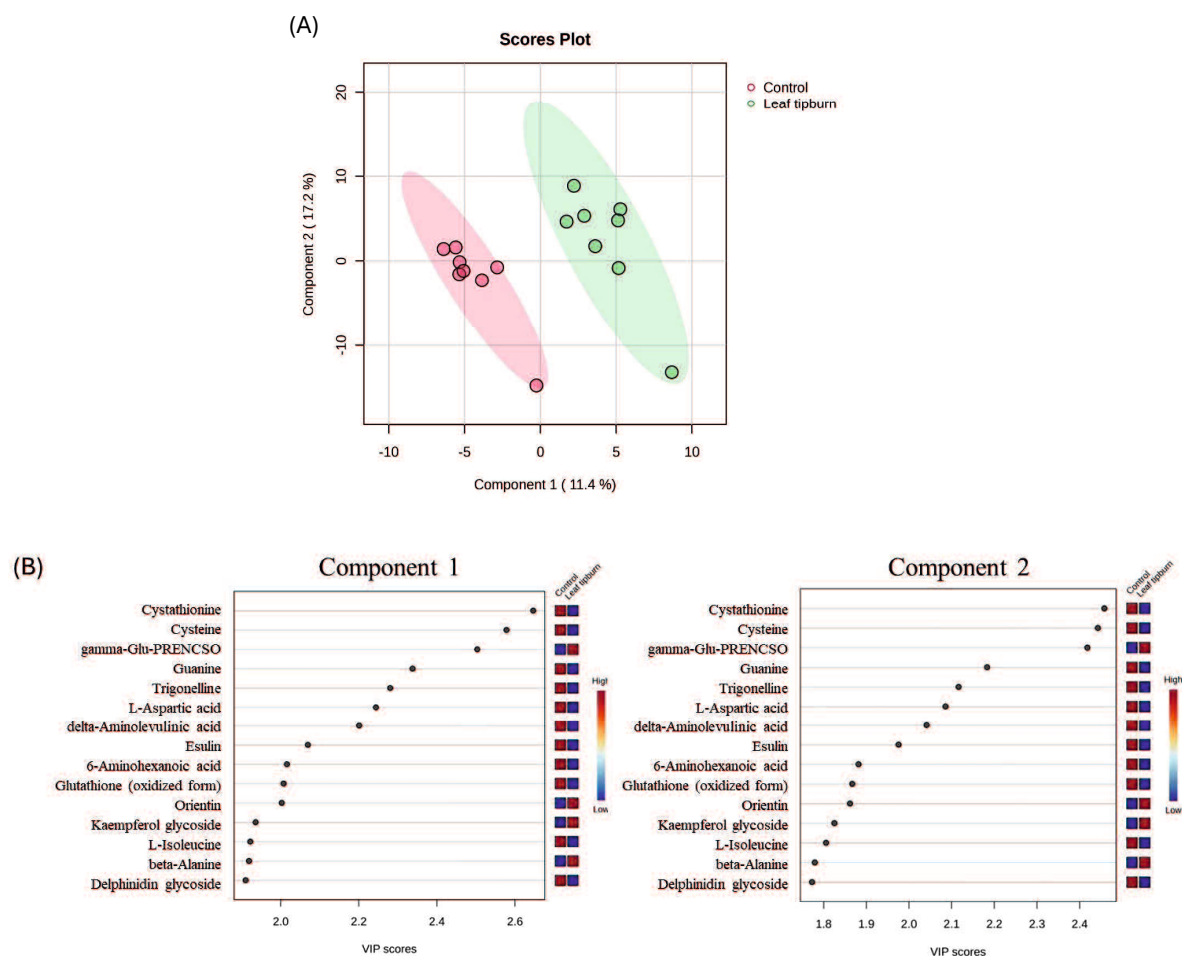


Figure 21. (A) Partial least squares discriminant analysis (PLS-DA) scores plot and (B) VIP (variable importance in projection) score plot of the metabolite profiles for the samples with the highest and lowest leaf tipburn rates. The contributions of the metabolites to Component 1 and Component 2 axes are color coded, based on the contribution scale according to the VIP score.

gamma-Glu-PRENCISO: gamma-glutamyl-propenyl cysteine sulfoxide.

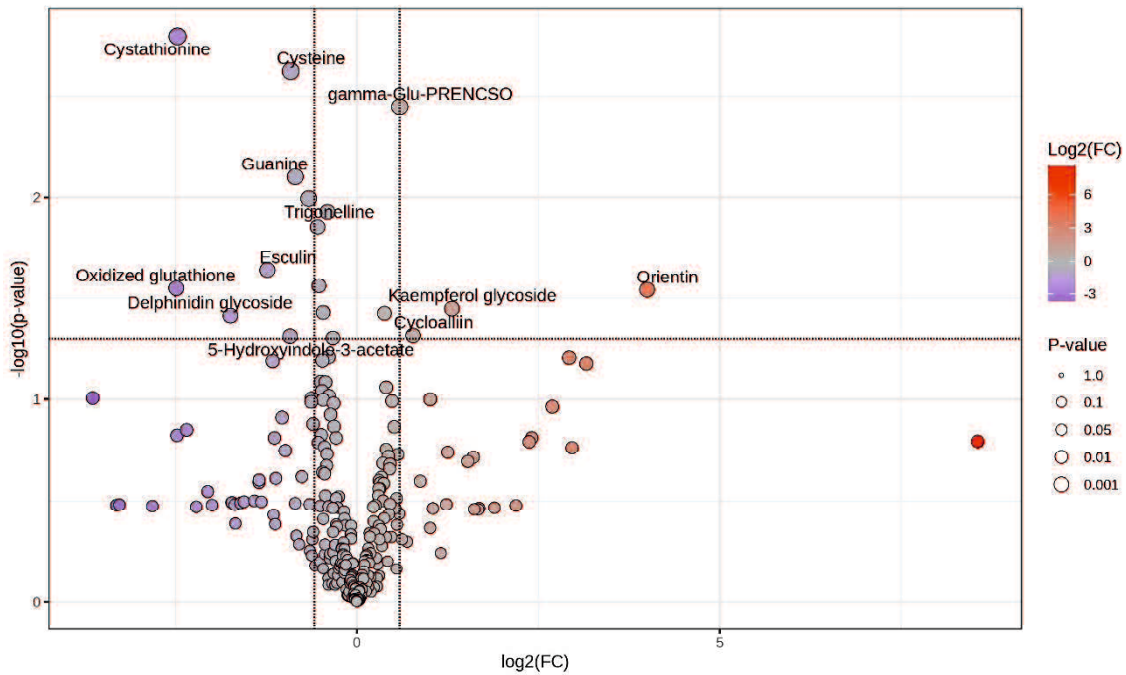


Figure 22. Volcano plot of the metabolite profiles for the highest and lowest leaf tipburn rates. The x-axis shows the \log_2 FC-fold changes (leaf tipburn group/control group). The y-axis represents the $-\log_{10}$ FC-transformed p-values. Each point corresponds to a metabolite, with its position indicating both the magnitude of change and the statistical significance. Points on the right side (positive \log_2 FC-fold change) indicate metabolites elevated in the leaf tipburn group, while points on the left side (negative \log_2 FC-fold change) indicate metabolites elevated in the control group. Metabolites with significant p-values ($p < 0.05$) are highlighted, with circle size corresponding to the significance level and color representing the \log_2 FC-fold change magnitude (red—higher in the leaf tipburn group; purple—higher in the control group).

gamma-Glu-PRENCISO: gamma-glutamyl-propenyl cysteine sulfoxide

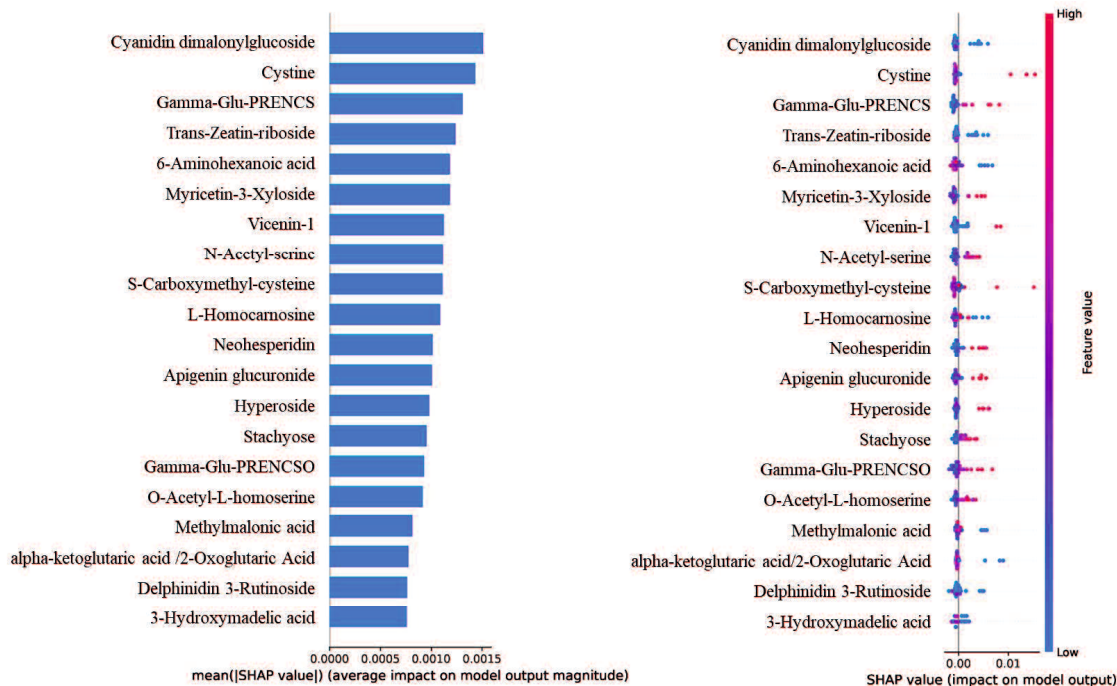


Figure 23. Shapley additive explanations (SHAP) analysis of metabolite profile influence on the leaf tipburn rate. (A) The bar plot of the SHAP mean value; (B) the summary plot of the top 20 most influential features. The feature ranking on the y-axis represents the order of importance for each feature in the prediction model. SHAP values on the x-axis indicate the predictive power of the model. Each row is plotted with dots representing the influence on individual validation data points. Red dots (high values) indicate a stronger prediction of high leaf tipburn rate, while blue dots (low values) indicate a stronger prediction of low leaf tipburn rate. In the summary plot, red dots indicate high metabolite concentrations, while blue dots indicate low concentrations. Dots on the positive side of the x-axis represent metabolites that contribute to an increase in leaf tipburn rate. Example interpretation: on the positive side of the x-axis, red dots indicate that higher concentrations of gamma-Glu-PRENCISO are associated with an increased leaf tipburn rate.

gamma-Glu-PRENCISO—gamma-glutamyl-propenyl cysteine sulfoxide; gamma-Glu-PRENCs—gamma-glutamyl-propenyl cysteine.

Variations in Organosulfur Compounds and Plant Hormones

Based on the analysis results related to leaf tipburn, several organosulfur compounds associated with the pungency of bunching onion were identified. A heat map was created to compare metabolites related to

organosulfur compounds and stress response hormones—ethylene, abscisic acid (ABA), and jasmonic acid (JA)—between the leaf tipburn group and the control group. In the control group, most organosulfur compounds showed an increase, with notable increases in cysteine and cystathionine. Additionally, there was a confirmed decrease in the accumulation of propenyl cysteine sulfoxide (PRENCSO) and gamma-Glu-PRENCSO, which are the main precursors of pungency. Conversely, in the leaf tipburn group, there was a general decrease in organosulfur compounds, while the accumulation of PRENCSO and gamma-Glu-PRENCSO increased. Regarding plant hormones, the precursor to ethylene—1-aminocyclopropane-1-carboxylic acid—increased in the control group, along with ABA and JA. These findings suggest that leaf tipburn is not caused by ethylene synthesis. Furthermore, since JA did not increase in the leaf tipburn group, it is unlikely that leaf tipburn is due to biotic stress, such as disease or herbivore damage (Figure 24A, 24B).

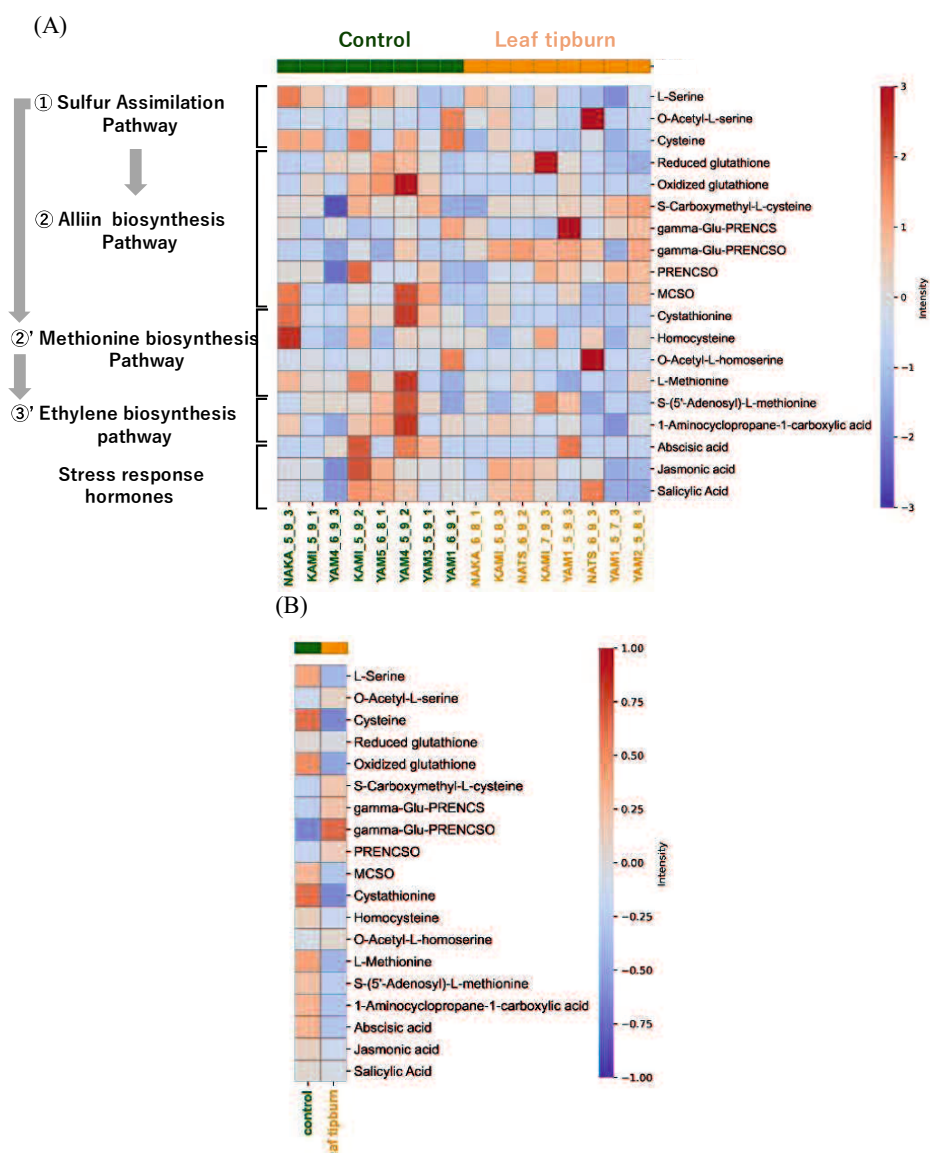


Figure 24. Comparison of the leaf tipburn group and control group based on organosulfur compounds and stress response hormones. (A) Heat map comparing the metabolite profiles between the leaf tipburn group (top 5% rate of leaf tipburn) and the control group (bottom 5% rate of leaf tipburn). Each column represents an individual sample. (B) Heat map shows the average values of each metabolite for the two groups. Each column represents an individual sample, and the rows indicate specific metabolites categorized into sulfur assimilation, alliin biosynthesis, methionine biosynthesis, ethylene biosynthesis pathways, and stress response hormones. gamma-Glu-PRENCs—gamma-glutamyl-propenyl cysteine; gamma-Glu-PRENCsO—gamma-glutamyl-propenyl cysteine sulfoxide; PRENCsO—propenyl cysteine sulfoxide; MCSO—methyl cysteine sulfoxide.

Discussion

Clarification of Differences in Pigment Compounds and Functional Components Among Varieties and Lines Based on Growing Conditions

We examined the effects of various growing conditions across nine varieties. For plants sown in May and harvested in July, August, and September, β -carotene levels increased in the July harvest (Figure 18A, Table 4). In the August harvest, β -carotene decreased, while functional components such as phenolic compounds, flavonoids, and fructans increased. By the September harvest, both functional components and pigment compounds showed increases. For plants sown in May, June, and July and harvested in September, the earliest sowing time (resulting in the longest growing period) led to a higher accumulation of both pigment compounds and functional components. In contrast, no significant differences were observed in the accumulation of these compounds between the June and July sowing dates (Figure 19A, Table 5). In summary, these results indicate that β -carotene content was the highest for May sowing and July harvest, while pigment compounds and functional components accumulated more with May sowing and September harvest. The observed changes in carotenoid content and composition are closely linked to environmental conditions, with light playing a critical role in regulating carotenoid biosynthesis in chloroplasts (Hermanns et al., 2020). For instance, in cucumbers, it has been reported that β -carotene accumulation increases under extended daylight conditions in photoperiod-sensitive varieties (Obel et al., 2022). This suggests that the

higher β -carotene levels in plants sown in May and harvested in July may be associated with the longer daylight hours during this period. In contrast, a study on bunching onion cultivation in Poland reported the highest chlorophyll levels after a 60-day growing period (Kołota et al., 2012). However, in the present study, chlorophyll content was highest after a 90-day period. The extended growing time and the high temperatures, coupled with intense light during July and August, likely contributed to chlorophyll degradation, making its accumulation more challenging (Efeoglu and Terzioglu, 2009; Sato et al., 2015). Regarding varietal characteristics, KAMI, NATS, and NAKA were grouped together based on lower pigment compound content, while YAM1-YAM5 and YSG1 exhibited higher pigment compound levels (Figure 16). In terms of functional components, a difference was observed between NATS and YSG1; however, no significant differences were found among the other varieties (Figure 17). These findings clarify the varietal characteristics under different growing conditions in summer.

Estimation of the Metabolites Involved in Leaf Tipburn

Leaf tipburn is generally attributed to calcium deficiency. It has been reported that Ca^{2+} , which moves along with water, tends to concentrate in mature leaves with active photosynthesis and transpiration, making young leaves more susceptible to Ca^{2+} deficiency (Maruo and Johkan, 2016). In the case of Chinese chives (*A. tuberosum*), it has been suggested that dehydration is the cause, particularly in the lower leaves with high stomatal density at the

leaf tips (Ooshima et al., 2015). In this experiment, leaf tipburn was also observed in the lower leaves, suggesting a potential link with water stress. The cultivation experiment was conducted using heat-tolerant variety under various growth conditions. However, ANOVA analysis revealed no significant differences in leaf tipburn rates either between cultivars or among growth conditions ($p > 0.05$, see Table 6). Nonetheless, variations in the incidence of leaf tipburn among individual plants suggest that multiple factors contribute to its occurrence.

To explore the underlying mechanisms, we conducted metabolome profiling of plants with high and low rates of leaf tipburn and analyzed the relationship between metabolites and leaf tipburn. The results from VIP scores based on PLS-DA (Figure 14B), volcano plots (Figure 15), and SHAP values (Figure 16) suggest a potential association between leaf tipburn and both flavonoids and organosulfur compounds. Flavonoids are one of the defensive antioxidant substances that play a critical role in plant stress responses (Hernández et al., 2009). They contribute to alleviating oxidative stress and protecting cell membranes, potentially influencing the occurrence of leaf tipburn through metabolic changes under stress conditions. Organosulfur compounds are involved in various stress responses, including the scavenging of reactive oxygen species (ROS) by glutathione, the synthesis of ethylene from methionine, and signal transduction via hydrogen sulfide (H₂S). Notably, H₂S plays a key role in inducing stomatal closure, promoting nitric oxide production, and enhancing ABA synthesis (Xuan et al., 2020; Jin et al., 2011; Wollers et al., 2008). Comparative analyses of organosulfur

compounds between the control and leaf tipburn groups revealed significant differences in key metabolic pathways. In the control group, metabolites associated with sulfur assimilation, glutathione, and methionine biosynthesis were increased, while gamma-Glu-PRENCISO, a precursor of pungency, was decreased (Figure 17). Gamma-Glu-PRENCISO is converted into PRENCISO, a precursor of pungency, by the action of gamma-glutamyl transferase (GGT), which cleaves the gamma-Glu group (Tolin et al., 2013). GGT plays a critical role in the synthesis of glutathione, which is involved in scavenging reactive oxygen species, by transferring gamma-Glu groups to specific amino acids or peptides. In Arabidopsis, GGT has been reported to be essential for mitigating oxidative stress (Ohkama-Ohtsu et al., 2007). Oxidative stress is caused by various factors, including environmental (abiotic) stress (Gechev and Petrov, 2020), and the ability to appropriately respond to such stress has been suggested to influence the occurrence of leaf tipburn. These findings indicate that stress-tolerant metabolic processes were more active in the control group, whereas these processes were diminished in the leaf tipburn group.

Regarding plant hormones, no significant differences in salicylic acid or jasmonic acid (JA), which are typically involved in plant defense responses, were observed between the two groups. However, the lack of increased levels of these hormones in the leaf tipburn group suggests insufficient activation of stress-related biological pathways (Chung et al., 2022; Miura and Tada, 2014). Moreover, reductions in the ethylene precursor 1-aminocyclopropane-1-carboxylic acid and the ABA in the leaf tipburn group imply a diminished hormonal response to water stress, potentially impairing the plants' ability to

adapt to adverse environmental conditions. These findings suggest that, in the control group, organosulfur compounds were efficiently processed through metabolic pathways, enabling preparations for stress adaptation and mitigation. In the leaf tipburn group, however, organosulfur compounds may have been diverted toward the synthesis of pungency precursors, resulting in a metabolic bias that effectively compromised the plants' response to water stress. These insights underscore the critical role of sulfur metabolism in regulating hormonal responses and highlight potential mechanisms contributing to leaf tipburn.

These results suggest that enhancing flavonoid accumulation and activating GGT to reduce gamma-Glu-PRENCISO could be critical strategies for mitigating oxidative stress and suppressing leaf tipburn. Our findings highlight the dual role of flavonoids as antioxidants and signaling molecules that can modulate plant responses to environmental stress and leaf tipburn symptoms, providing a biochemical foundation for developing stress-tolerant varieties. The activation of GGT to decrease gamma-Glu-PRENCISO levels could also serve as a metabolic intervention to reduce the buildup of reactive oxygen species, thereby preventing cellular damage and suppressing leaf tipburn. This insight could be applied in practical breeding programs to develop stress-resistant cultivars by targeting metabolic pathways associated with sulfur metabolism and flavonoid biosynthesis. Furthermore, future studies could explore the feasibility of using gamma-Glu-PRENCISO and flavonoids as biomarkers to monitor stress levels and predict leaf tipburn incidence in agricultural practices. Additionally, future research could

explore the genetic and environmental factors influencing these metabolic pathways, as well as their interactions with other stress response mechanisms, to develop comprehensive strategies for improving crop resilience.

Chapter 4: Metabolome Profiling and Predictive Modeling of Dark Green Trait in Heat-Tolerant Bunching Onion Varieties

Introduction

The bunching onion (*Allium fistulosum* L.), also known as the Welsh onion, green onion, spring onion, or scallion, is widely distributed from Siberia to tropical Asia, particularly in East Asia, where numerous varieties have adapted to diverse local environmental conditions (Yamasaki and Tsukazaki, 2022; Kayat et al., 2021). It is consumed year-round, with its green color and distinctive flavor being essential components of various dishes (Kim et al., 2023; Singh and Ramakrishna, 2017; Wako et al., 2015). The intensity of leaf color is a crucial trait directly linked to market value, nutritional content, and visual appeal. Furthermore, due to the impact of recent climate changes on the growth of bunching onions during summer, seed companies are developing varieties that combine heat tolerance with the dark green trait (Yamasaki and Tsukazaki, 2022; Padula et al., 2022).

The dark green color is not solely attributed to individual pigments but rather arises from the interactions among various pigment compounds (Cheng et al., 2018). Pheophytin, a compound formed under acidic or high-temperature conditions through chlorophyll degradation in tea leaves, is characterized by its brownish hue (Li et al., 2018). It is suggested that in bunching onions, the accumulation of pheophytin under high-temperature

conditions during summer may contribute to changes in leaf coloration. Furthermore, the accumulation of anthocyanins and phenolic compounds, increases in sugars and proline, and the reinforcement of the cuticle layer as part of the plant's environmental response are also considered important factors influencing the formation of dark green coloration (Naing and Kim, 2021; Sharma et al., 2019b; Ghosh et al., 2022; Sami et al., 2016; Tafesse et al., 2022).

Therefore, to understand the mechanism behind the dark green coloration in bunching onions, it is necessary not only to measure pigment compounds but also to conduct metabolomic analysis targeting primary and secondary metabolites. Metabolomics enables a comprehensive analysis of biochemical states and stress-related compounds in plant cells, making it highly effective in identifying stress metabolism byproducts and compounds associated with adaptive responses (Abdelrahman et al., 2019; Carrera et al., 2021). In the *Allium* genus, metabolomics has been widely applied to analyze the effects of stress, cultivation conditions, drying methods, pathogen infection, and the introduction of alien chromosomes, contributing significantly to the identification of pigment compounds and metabolites (Shulaev et al., 2008; Saviano et al., 2019; Farag et al., 2017; Medina-Melchor et al., 2022; Abdelrahman et al., 2019).

Beyond understanding the factors contributing to the dark green trait, developing efficient evaluation methods is essential. Conventional chemical analyses are time-consuming and costly, highlighting the need for simpler approaches to estimating pigment compound contents. Spectral reflectance

(400–700 nm) is a readily measurable property, and machine learning models utilizing these data have been shown to efficiently estimate pigment compound contents in various crops (Shah et al., 2019; Singhal et al., 2019). These predictive models not only simplify the analysis of dark green coloration but also serve as valuable tools for plant monitoring and real-time diagnostics in agricultural practices.

In this study, we aimed to clarify the relationship between metabolome profiles and dark green coloration in bunching onion leaves and to evaluate the accuracy of predictive models for pigment compound estimation. To achieve this, qualitative and quantitative analyses of pheophytin *a* were conducted with high precision using an HPLC fluorescence detector, along with the quantitative analyses of chlorophyll *a*, chlorophyll *b*, lutein, and β -carotene, as well as the evaluation of their optical properties. Additionally, widely targeted metabolite profiling based on targeted liquid chromatography–triple quadrupole mass spectrometry was performed. Finally, regression models based on spectral reflectance were developed to establish prediction equations for accurately estimating pigment compound contents. This study not only lays the foundation for improving the quality of bunching onions and developing stress-tolerant varieties but also opens avenues for future research focused on integrating genomic, transcriptomic, and metabolomic approaches to uncover the genetic basis of pigment accumulation and stress responses.

Materials and Methods

Materials and Growth Conditions

In this study, we examined two F_1 cultivars from Nakahara Seed Product Co., Ltd.—‘Natsuhiko’ (NATS) and ‘Kaminari’ (KAMI); two purebred varieties from Yamaguchi Prefecture—‘YSG1go’ (YSG1) and ‘08S20-2’ (08S2); and three F_1 hybrid lines bred in Yamaguchi Prefecture (hereafter referred to as YB- F_1)—‘Yamahiko’ (YAMA), ‘Yamakou03’ (YAM3), and ‘2331’ (2331) (Figure 25). These plant materials were sown on June 14, 2023, and harvested on August 21, 2023, in the greenhouse of the Yamaguchi Prefectural Agriculture and Forestry General Technology Center (34°N, 131°E). The crops were planted in 6 rows on a 90 cm wide ridge, with an inter-row spacing of 12 cm and a seeding density of 120 seeds per square meter. A total of 1.0 kg of nitrogen per area (kg/a) was applied during the experiment, divided into two applications: an initial 0.5 kg/a as basal fertilizer and an additional 0.5 kg/a as topdressing at the two-leaf stage.

The watering conditions were as follows: On the sowing day, 48 L/m² of water was applied, with soil water tension maintained at 1.5 pF. During the germination phase (0–4 days), irrigation was conducted at a rate of 24 L/m² per application, keeping the pF value between 1.5 and 1.6. In the cotyledon stage (4–11 days), water was supplied every 2–3 days at 6 L/m², maintaining a pF range of 1.6–1.8. At the one-leaf stage (11–18 days), irrigation was performed every 2–3 days with 10 L/m² of water, keeping the pF value

between 1.7 and 2.0. During the two-leaf stage (18–28 days), watering was increased to 12 L/m² daily, maintaining a pF range of 1.6–1.8. At the three-leaf stage (28–38 days), 6 L/m² of water was supplied every three days to maintain a pF value of 2.0–2.3. During the four-leaf stage (38–49 days), irrigation was carried out almost daily at a rate of 12 L/m², with the pF value maintained between 1.8 and 2.0. At the five-leaf stage (49–59 days), watering was conducted every three days at 5 L/m², keeping the pF level within 2.0–2.5. From the six-leaf stage (59 days onward), irrigation was adjusted as needed to maintain appropriate soil conditions. After harvest, five plants were randomly selected from each variety and grouped into a single unit to ensure sufficient material for analysis. For example, in the case of YSG1, five such groups were prepared (YSG1-1 to YSG1-5), resulting in five biological replicates (n = 5). The number of biological replicates for each sample was as follows: NATS, n = 5; KAMI, n = 5; YSG1, n = 4; 08S2, n = 3; YAMA, n = 5; YAM3, n = 5; and 2331, n = 5. For all samples, outer and older leaves were removed, and the two youngest central leaves were selected for optical property measurements and chemical analyses.

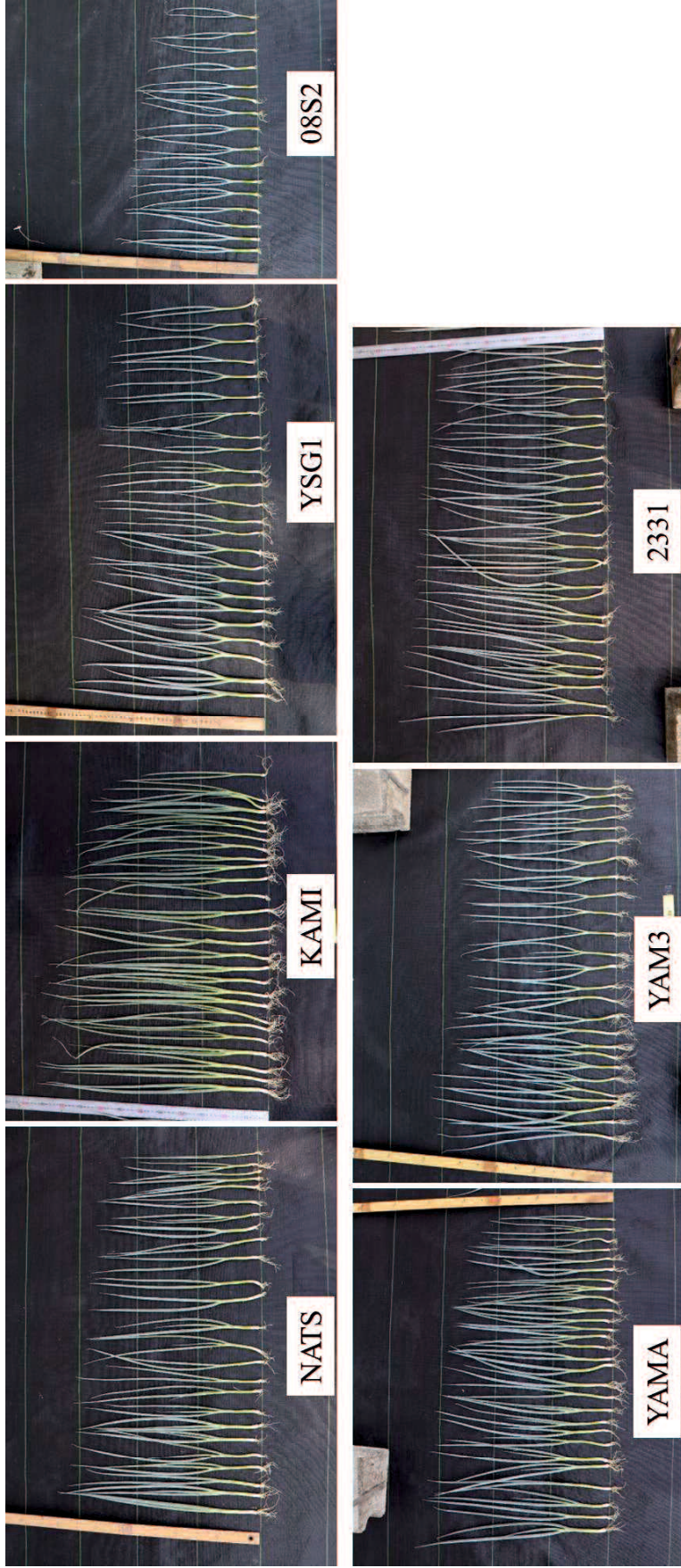


Figure 25. Plants of experimental materials: varieties and lines of bunching onion used in this study.

Optical Properties Measurement

As indicators of optical properties, the SPAD value and spectral reflectance (400–700 nm at 20 nm intervals) were measured. The SPAD value was measured by using a chlorophyll meter (SPAD-502Plus, KONICA MINOLTA, INC., Tokyo, Japan), while spectral reflectance was determined by using a spectrophotometer (NF555, Nippon Denshoku Industries Co., Ltd., Tokyo, Japan) (Markwell et al., 1995). For optical property measurements, three plants were randomly selected from each biological replicate of each variety. The final value for each parameter was calculated by averaging the measurements taken from the central part of the first and second leaves.

Powdering of Samples

The samples were frozen at $-80\text{ }^{\circ}\text{C}$ after their optical properties were measured. The frozen samples were then freeze-dried for three days by using a TAITEC VD-250R freeze dryer equipped with a vacuum pump (TAITEC, Saitama, Japan). The freeze-dried samples were ground by using a small blender.

Pigment Compound Measurement

The method for acetone extraction was developed with reference to Dissanayake et al. (Dissanayake et al., 2008). A precise amount of 20 mg of dried leaves was weighed and placed into a 15 mL tube, followed by the addition of 2.5 mL of chilled acetone. The mixture was vortexed for 2 minutes

and subsequently subjected to ultrasonic treatment for 20 minutes under cool conditions. After centrifugation at 5,000 rpm for 5 minutes at 10°C, the supernatant was collected. The remaining residue was then extracted again by adding another 2.5 mL of chilled acetone, repeating the same procedure to obtain the supernatant. All collected supernatants were filtered through a 0.45 µm filter (Advantec, Tokyo, Japan) and used as sample solutions for the measurement of pheophytin *a* and pigment compounds (chlorophyll *a*, chlorophyll *b*, lutein, and β-carotene). The sample solutions were kept in a freezer at -20 °C and analyzed within three days.

The method for measuring pheophytin *a* content was developed with reference to Almela et al. (Almela et al., 2000). Pheophytin *a* were measured by using an HPLC instrument (Alliance e2695, Waters Corporation, MA, USA) equipped with a fluorescence detector (Waters 2475, Waters Corporation, MA, USA). The sample solution was separated using a LiChroCART 250-4.0 Lichrospher 100 RP-18 (5 µm) column (KANTO CHEMICAL, Tokyo, Japan) with gradient elution consisting of two solvents: (A) 80% methanol solution (HPLC-grade) and (B) isopropanol (HPLC-grade). The gradient elution program was as follows: (i) the initial condition was 100% A; (ii) this was followed by a 20-minute linear gradient to 40% A and 60% B; (iii) finally, 40% A and 60% B were held for 30 minutes. The flow rate was maintained at 1.0 mL/min, with a column temperature of 30°C and an injection volume of 10 µL. Fluorescence detection was performed with excitation at 410 nm and emission at 660 nm. The pheophytin *a* standard was prepared by acidifying a chlorophyll *a* solution (dissolved in acetone) with a

few drops of 0.1 N hydrochloric acid, followed by neutralization with an equivalent amount of 0.1 N sodium hydroxide.

The method for measuring pigment compound contents was developed with reference to Dissanayake et al. (Dissanayake et al., 2008), as previously cited for the acetone extraction method. Chlorophyll *a*, chlorophyll *b*, lutein, and β -carotene were measured by using an HPLC instrument (HPLC L-7000 series, HITACHI, Tokyo, Japan) equipped with a UV–Vis detector (HITACHI L7420, HITACHI, Tokyo, Japan) set to 435 nm for the detection of pigment compounds. The sample solution was separated using a LiChroCART 250-4.0 Lichrospher 100 RP-18 (5 μ m) column (KANTO CHEMICAL, Tokyo, Japan) with gradient elution consisting of two solvents: (A) 80% methanol solution, prepared by mixing 400 mL of HPLC-grade methanol, 50 mL of ultrapure water, and 50 mL of 100 μ M HEPES buffer (pH 7.5), and (B) an ethyl acetate. The gradient elution program was as follows: (i) the initial condition was 100% A; (ii) this was followed by a 20-minute linear gradient to 50% A and 50% B; (iii) finally, 50% A and 50% B were held for 30 minutes. The flow rate was maintained at 1.0 mL/min, with a column temperature of 30 °C and an injection volume of 50 μ L.

Metabolome Analysis

Sample preparation was automated using a liquid-handling system (Microlab STAR Plus, Hamilton Company, Reno, NV, USA) for dispensing, plate transfer, solvent evaporation (Ultravap Mistral, Porvair PLC, Norfolk,

UK), dissolution, and filtration, following the method described by Sawada et al. (Sawada et al., 2017). A precisely weighed 4 mg portion of the powder was placed in a 2 mL tube along with a 5 mm zirconia ball (NIKKATO CORPORATION, Osaka, Japan). One milliliter of extraction solvent, consisting of 80% methanol and 0.1% formic acid, supplemented with 8.4 nmol/L lidocaine and 210 nmol/L 10-camphorsulfonic acid as internal standards, was then added to the tube, resulting in a final concentration of 4 mg/mL. Metabolite extraction was performed using a multi-bead shaker (Shake Master NEO, Biomedical Science, Tokyo, Japan) at 1,000 rpm for 2 minutes. Following centrifugation at $9,100 \times g$ for 1 minute, the supernatant was diluted fourfold with the extraction solvent, resulting in a final concentration of 1 mg/mL. Twenty-five microliters of each diluted sample was transferred to a 96-well plate, dried under a nitrogen stream, redissolved in 250 μ L of ultrapure water (LC-MS grade), and filtered using a 0.45 μ m pore size filter plate (Multiscreen HTS 384-Well HV, Merck, Rahway, NJ, USA). A 1 μ L aliquot of the extract, adjusted to a final concentration of 100 ng/ μ L, was analyzed using LC-QqQ-MS for widely targeted metabolomics (UHPLC-Nexera MP/LCMS-8050, SHIMADZU, Tokyo, Japan). The setting parameters and MRM transitions for LC-QqQ-MS analysis are summarized in Chapter 3, Table 2 and Chapter 3, Table 3 with reference to previous studies (Sawada et al., 2009; Uchida et al., 2020).

Data Analysis

The data on SPAD values and total pigment compound contents (chlorophyll *a*, chlorophyll *b*, pheophytin *a*, lutein, and β -carotene) were

analyzed by using one-way analysis of variance and Tukey's multiple comparison test. A significance level of $p < 0.05$ was applied. Principal component analysis (PCA) was performed using spectral reflectance and pigment compounds to classify the varieties. The dataset was created using the average values of 3 to 5 replicates for each sample and standardized with the StandardScaler function from the scikit-learn Python library. PCA (with components=2) was then conducted using the PCA function implemented in the same library. Following PCA, hierarchical clustering was performed using the Ward method to group the varieties based on their PCA scores. A random forest regression model was employed to predict each pigment compound using spectral reflectance from 400 nm to 700 nm at 20 nm intervals as input features. The dataset was split into training and test sets using an 80–20 ratio. Furthermore, to account for multicollinearity among input features, dimensionality reduction was performed using PCA. The number of components was varied while evaluating the coefficient of determination (R^2), and the optimal number of components was set to four, as it yielded the highest R^2 . The model was implemented with the Scikit-learn library using default hyperparameters: `n_estimators=100`, `max_depth=None`, `min_samples_split=2`, `min_samples_leaf=1`, `max_features='sqrt'`, and `bootstrap=True`. To ensure reproducibility, a fixed random seed (`random_state=42`) was applied throughout the analysis. All analyses and visualizations were conducted using Python 3.9.7, Pandas 1.3.4, Scikit-learn 0.24.2, and Matplotlib 3.4.3.

Classification of Green Color Patterns Using Metabolomics

A total of 452 metabolite intensities were obtained from the metabolome analysis. Missing values were imputed with a fixed value of 10, and the signal intensities for all samples ($n = 3$) were averaged. Metabolites with signal-to-noise ratios (S/N, defined as the ratio of the average signal intensity to that of the extraction solvent control) less than 5 across all samples were excluded. Additionally, metabolites with relative standard deviations (RSD) greater than 0.3 across all samples, as well as those with RSD values of 0, were also excluded. As a result of these filtering steps, a final dataset containing 186 metabolites was obtained. The data matrix was then normalized to the median and auto-scaled. The processed data were used for comparative analysis. Initially, partial least squares discriminant analysis (PLS-DA) was performed on all 186 metabolites, and VIP scores were calculated to assess the overall trends in metabolomic data among the green color types. Hierarchical clustering was applied to both samples and metabolites using Ward's method, with Euclidean distance as the similarity metric. Preprocessing steps, including missing value imputation, S/N ratio filtering, RSD calculations, and normalization of intensities to internal standards, were performed using Python 3.9.7 and Pandas 1.3.4. Data normalization and subsequent analyses were conducted using MetaboAnalyst 6.0.

Results

Optical Properties Measurement

The SPAD values and spectral reflectance measurements for all samples are presented in Table 7. First, the average SPAD values of each variety and line were compared. The purebred variety 08S2 displayed the highest SPAD value, significantly exceeding those of the other varieties and lines. Similarly, the purebred variety YSG1 and the YB-F₁ lines YAM3 and 2331 showed relatively high SPAD values. In contrast, the F₁ cultivars NATS and KAMI showed significantly lower SPAD values compared to the others (Figure 26). These results suggest that the purebred varieties have darker green coloration, the F₁ cultivars have lighter green coloration, and the YB-F₁ lines exhibit intermediate characteristics.

Table 7. SPAD values and spectral reflectance measurements across all samples (Sown on 14 June, 2023 and harvested on 10 September, 2023).

Variety	No	SPAD	Spectral reflectance (%)																
			400 nm	420 nm	440 nm	460 nm	480 nm	500 nm	520 nm	540 nm	560 nm	580 nm	600 nm	620 nm	640 nm	660 nm	680 nm	700 nm	
NATS	1	36.63	16.39	16.45	16.21	15.83	15.35	15.42	19.35	24.30	24.40	18.76	16.49	15.78	14.21	12.90	12.46	12.52	
	2	34.30	16.76	16.80	16.55	16.16	15.73	15.89	19.70	24.63	25.03	19.29	17.00	16.34	14.76	13.39	12.84	13.09	
	3	35.53	14.27	14.30	14.10	13.78	13.41	13.64	17.55	22.51	22.91	17.31	15.03	14.35	12.85	11.64	11.18	11.29	
	4	30.67	14.05	14.13	14.01	13.76	13.41	13.73	18.38	24.11	24.57	18.44	15.89	15.04	13.24	11.74	11.20	11.32	
	5	34.67	15.79	15.87	15.69	15.36	14.94	15.13	19.50	24.92	25.12	19.19	16.74	15.93	14.27	12.93	12.47	12.52	
KAMI	1	31.27	10.30	10.53	10.65	10.64	10.39	10.68	15.69	21.50	21.69	16.15	13.25	11.75	10.10	9.28	8.73	8.78	
	2	31.63	11.37	11.57	11.63	11.57	11.28	11.56	16.56	22.27	22.19	16.72	13.92	12.47	10.79	9.86	9.26	9.40	
	3	33.33	10.89	11.21	11.39	11.43	11.18	11.43	16.51	22.38	22.49	16.97	14.07	12.55	10.92	10.14	9.69	9.59	
	4	31.47	12.12	12.41	12.51	12.48	12.17	12.36	17.35	23.20	23.38	17.66	14.72	13.20	11.47	10.55	10.02	10.01	
	5	31.48	11.52	11.92	12.17	12.27	12.03	12.31	17.86	24.10	24.16	18.71	15.64	13.91	12.33	11.79	11.53	11.08	
YSG1	1	47.90	17.62	17.94	17.84	17.54	17.08	16.76	18.87	21.69	21.33	17.64	16.05	15.41	14.31	13.46	13.02	13.29	
	2	45.78	15.89	16.15	16.05	15.81	15.48	15.37	17.50	20.30	20.18	16.51	14.96	14.40	13.35	12.52	12.08	12.37	
	3	48.55	17.34	17.79	17.80	17.57	17.08	16.59	18.49	21.10	20.67	17.27	15.75	15.11	14.16	13.51	13.15	13.33	
	4	45.78	17.98	18.77	19.06	19.00	18.33	17.41	20.32	23.78	22.73	19.56	17.47	16.13	15.43	15.73	16.00	15.06	
08S2	1	54.50	19.31	19.50	19.25	18.84	18.45	18.31	19.92	22.13	21.88	18.73	17.41	16.89	15.97	15.23	15.01	15.00	
	2	55.32	22.54	22.88	22.65	22.18	21.60	21.10	22.46	24.65	24.34	20.93	19.59	19.17	18.22	17.40	17.25	17.14	
	3	55.38	23.31	23.64	23.38	22.89	22.33	21.87	23.09	25.17	24.97	21.52	20.34	20.14	19.23	18.29	18.13	18.11	
YAMA	1	37.35	16.18	16.56	16.60	16.44	16.08	15.97	19.00	22.91	22.96	18.34	16.30	15.48	14.14	13.17	12.66	12.91	
	2	36.22	17.95	18.34	18.34	18.08	17.49	17.11	20.70	25.26	25.04	20.06	17.62	16.42	14.92	14.03	13.60	13.58	
	3	39.22	15.76	16.10	16.09	15.89	15.42	15.17	18.39	22.50	22.41	17.76	15.63	14.73	13.43	12.59	12.16	12.26	
YAM3	4	38.45	16.09	16.43	16.43	16.25	15.85	15.76	19.14	23.44	23.54	18.69	16.46	15.48	14.03	13.03	12.52	12.71	
	5	37.92	17.21	17.53	17.50	17.25	16.73	16.55	20.65	25.54	25.21	20.43	17.97	16.76	15.50	14.97	14.67	14.52	
2331	1	43.13	19.89	20.06	19.77	19.27	18.67	18.36	20.75	24.16	24.05	19.48	17.72	17.24	16.00	14.91	14.56	14.64	
	2	43.72	19.51	19.76	19.55	19.09	18.42	17.92	20.47	24.06	23.91	19.40	17.53	16.94	15.79	14.92	14.68	14.58	
	3	47.28	18.01	18.05	17.70	17.19	16.68	16.50	18.48	21.38	21.43	17.29	15.78	15.49	14.49	13.57	13.25	13.40	
	4	44.07	19.05	19.15	18.83	18.31	17.72	17.44	19.76	23.15	23.17	18.52	16.86	16.60	15.47	14.40	14.04	14.22	
	5	45.15	19.59	19.63	19.24	18.66	18.05	17.79	20.01	23.40	23.59	18.79	17.21	17.09	15.92	14.69	14.14	14.65	
2331	1	46.83	18.07	18.22	17.95	17.50	16.97	16.66	18.62	21.37	21.14	17.43	15.78	15.11	14.10	13.41	13.03	13.20	
	2	45.97	13.20	13.46	13.43	13.23	12.84	12.61	14.92	17.91	17.72	14.09	12.51	11.94	11.03	10.45	10.06	10.29	
	3	44.27	13.87	14.12	14.07	13.84	13.42	13.19	15.60	18.81	18.76	14.87	13.09	12.40	11.42	10.84	10.47	10.61	
	4	44.23	15.49	15.59	15.37	15.02	14.63	14.60	17.11	20.35	20.26	16.26	14.56	13.97	12.92	12.16	11.77	11.95	
	5	47.00	14.81	15.04	14.93	14.66	14.26	14.04	16.11	18.92	18.81	15.24	13.69	13.15	12.25	11.65	11.31	11.48	

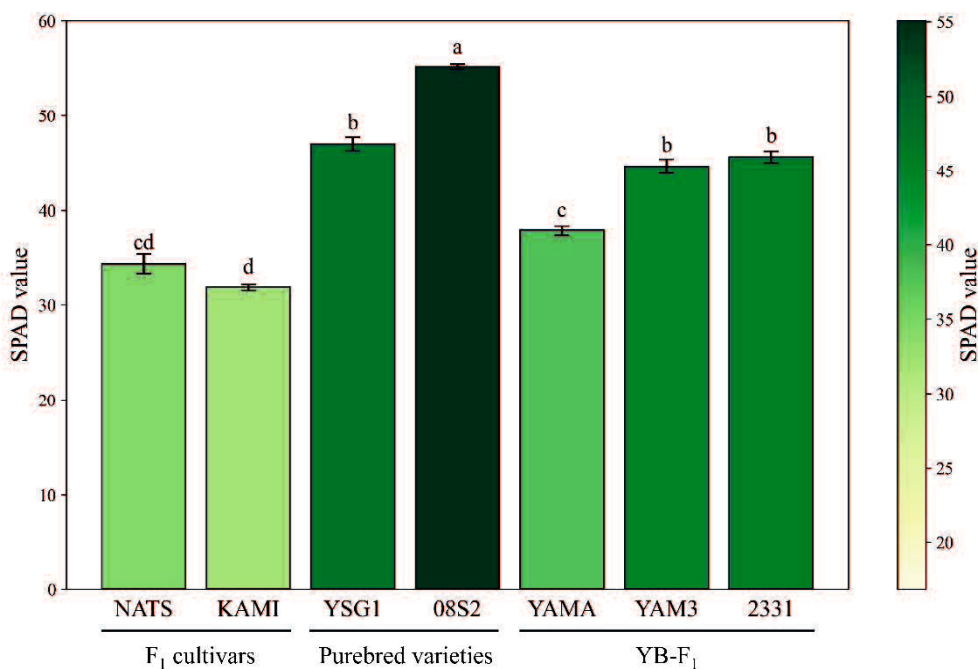


Figure 26. Bar chart of SPAD values across varieties and lines. Bars represent the mean \pm standard error. Different letters indicate significant differences at $p < 0.05$. NATS: ‘Natsuhiko’, KAMI: ‘Kaminari’, YSG1: ‘YSG1go’, 08S2: ‘08S20-2’, YAMA: ‘Yamahiko’, YAM3: ‘Yamakou03’, 2331: ‘2331’, Purebred varieties: Purebred varieties from Yamaguchi Prefecture, YB-F₁: F₁ hybrid lines bred in Yamaguchi prefecture

Qualitative and Quantitative Determination of Pheophytin *a* and Pigment Compound

HPLC analysis using a fluorescence detector identified three peaks from the standard sample of pheophytin *a* (Figure 27A). Similarly, three peaks were also detected from chlorophyll *a*, which was used to prepare pheophytin *a*, suggesting that these peaks were influenced by components derived from chlorophyll *a* (Figure 28). Therefore, the largest peak at 43.06 minutes was identified as the peak for pheophytin *a*. A corresponding peak with the same retention time was also detected in the actual sample (YSG1) (Figure 27B). Based on this retention time, pheophytin *a* levels were quantified across all

samples, with YSG1 exhibiting the highest levels (Figure 29). A comparison among different groups revealed that the F₁ cultivars generally had lower pheophytin *a* levels, the purebred varieties showed higher levels, and the YB-F₁ lines displayed intermediate levels (Figure 29). Next, the results for chlorophyll *a*, chlorophyll *b*, lutein, and β -carotene are provided as Figure 30. These four pigment compounds, along with pheophytin *a*, were visualized as a stacked bar chart, and the total amount of the five pigment compounds was statistically analyzed using Tukey's multiple comparison test. The purebred varieties 08S2 and YSG1, along with the YB-F₁ line 2331, exhibited the highest total pigment levels in this order, significantly surpassing those of other varieties and lines. In contrast, the F₁ cultivars NATS and KAMI, as well as the YB-F₁ line YAMA, exhibited lower values, while the YB-F₁ line YAM3 showed intermediate levels (Figure 31). Additionally, an analysis of the correlation coefficients between SPAD values and each pigment compound revealed a high correlation with chlorophyll *a*, whereas the correlations with other pigment compounds were moderate (Table 8).

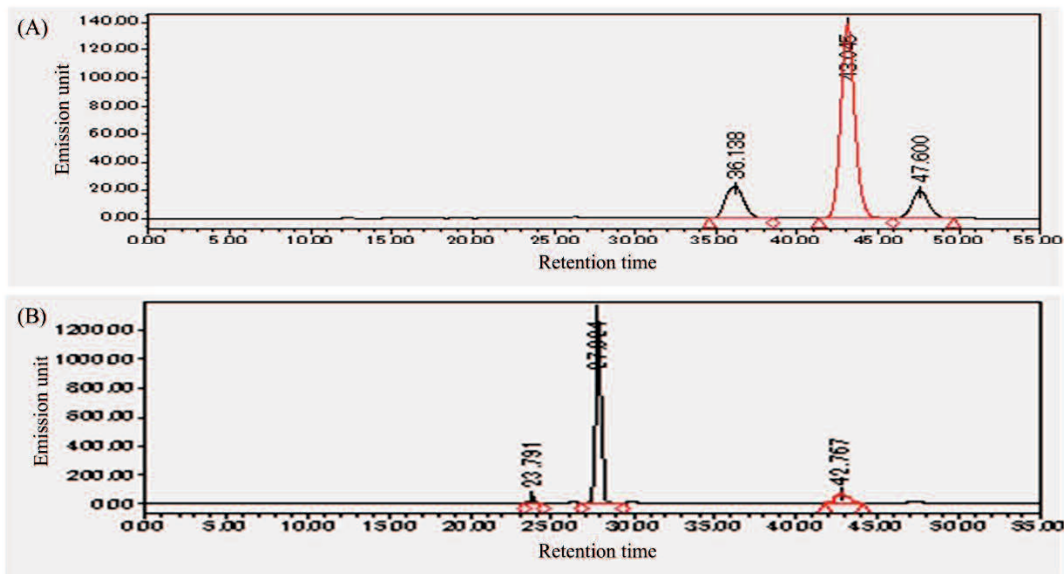


Figure 27. Chromatograms of pheophytin *a* (A) and YSG1 (B) obtained using HPLC with a fluorescence detector. The x-axis represents the retention time, and the y-axis represents the emission units.

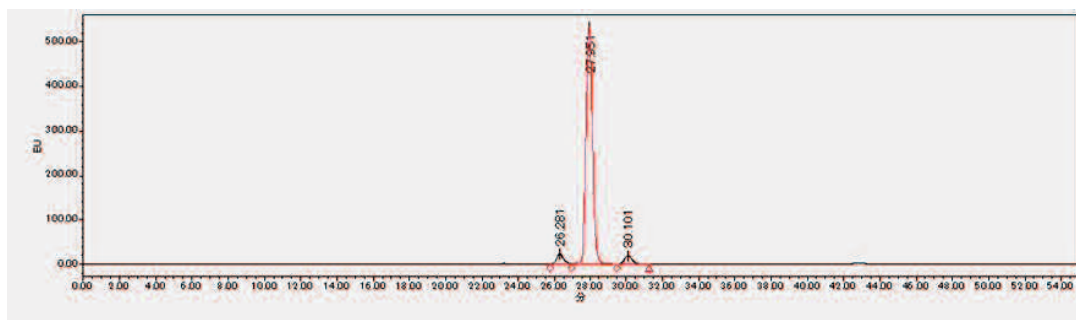


Figure 28. Chromatograms of chlorophyll *a* obtained using HPLC with a fluorescence detector.

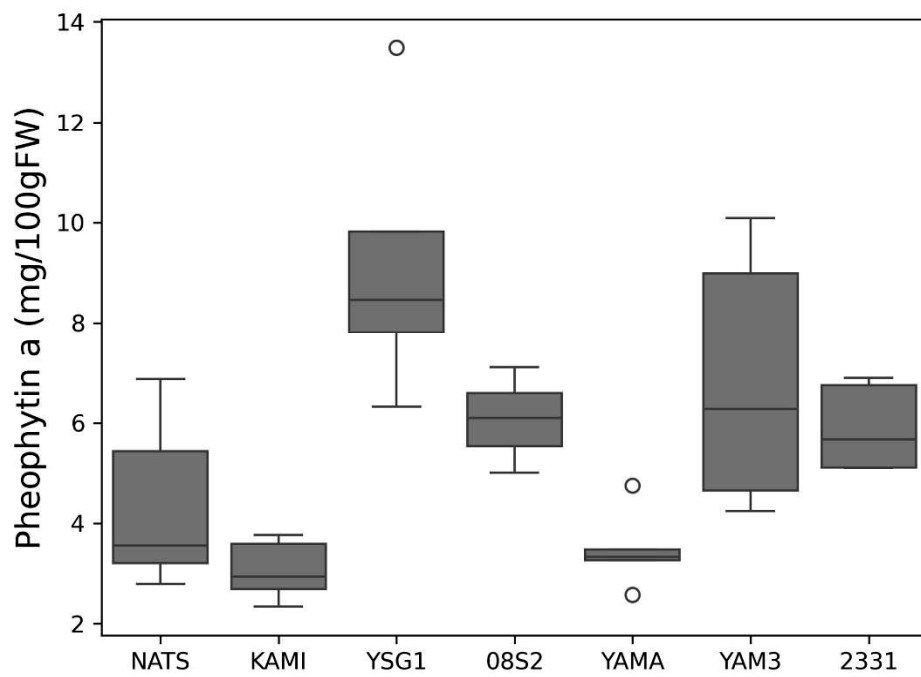


Figure 29. Boxplot of pheophytin *a* across varieties and lines. The box represents the interquartile range, the horizontal line within the box indicates the median, and dots represent outliers.

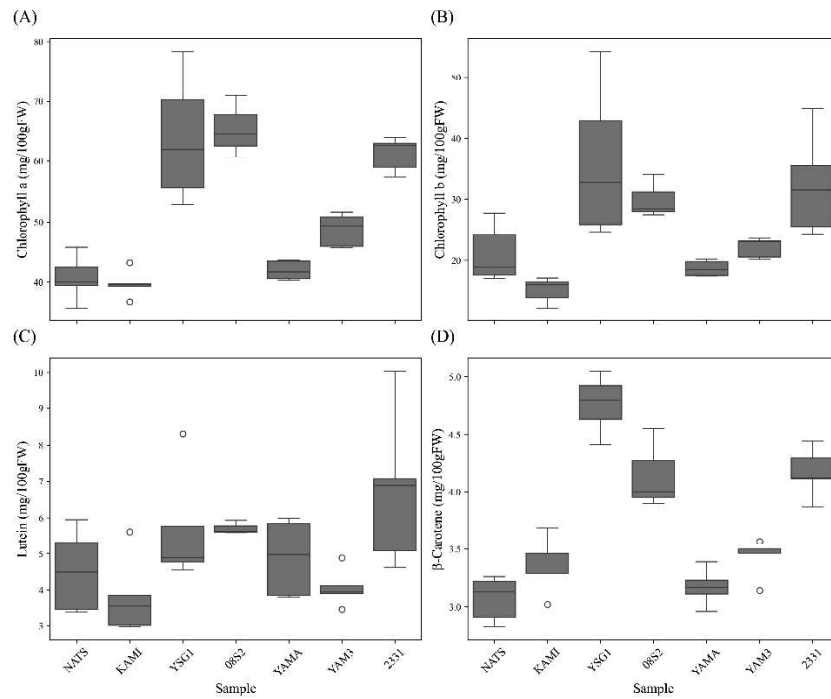


Figure 30. Boxplot of pigment compounds, including chlorophyll *a* (A), chlorophyll *b* (B), lutein (C), and β -carotene (D).

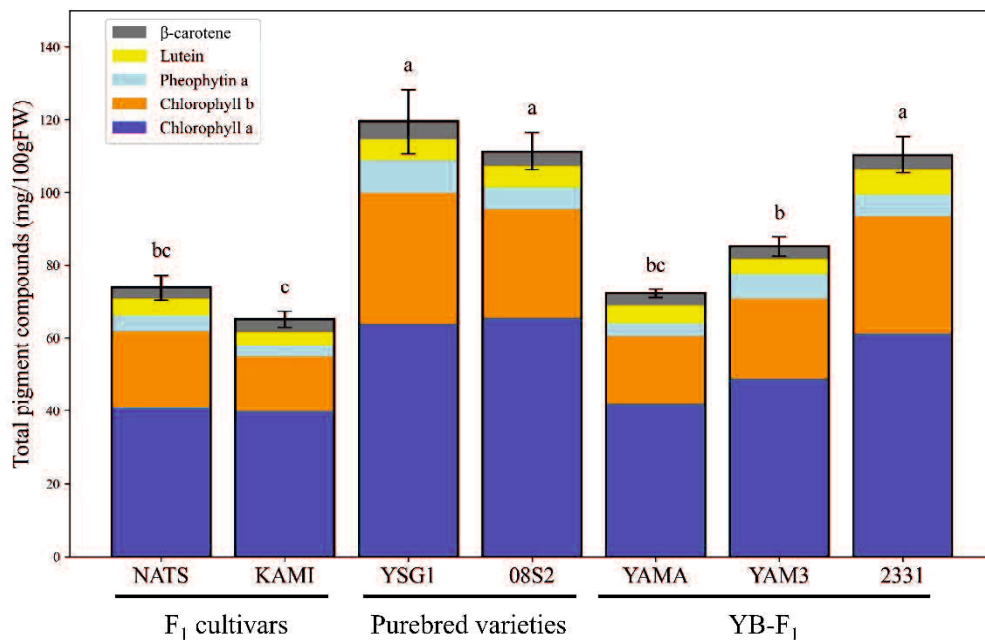


Figure 31. Stacked bar chart of total pigment compounds across varieties and lines. Different letters indicate significant differences at $p < 0.05$.

Table 8. Correlation coefficients (*r*) between SPAD values and each pigment compound.

Pigment compound	Correlation coefficient (<i>r</i>)
Chlorophyll <i>a</i>	0.850
Chlorophyll <i>b</i>	0.609
Pheophtin <i>a</i>	0.572
Lutein	0.405
β-carotene	0.690

PCA Analysis Using Spectral Reflectance of Each Variety and Line

PCA was performed using pigment compound data for each variety and line. The principal component scores for each variety and line were plotted, and the results showed that the data were distributed around the center, with no clear separation observed (Figure 32A, 32B). Next, PCA was conducted using the spectral reflectance data (400–700 nm) for each variety and line. The results showed that the data were projected onto Principal Component 1 (PC1) and Principal Component 2 (PC2), which together explained 99.6% of the total variance. The contribution rates of PC1 and PC2 were 85.5% and 14.1%, respectively (Figure 33A). Examination of the principal component loadings for PC1 and PC2 revealed that PC1 was composed of spectral reflectance, excluding the range of 540–580 nm. The positive side of PC1 indicated increases in reflectance in the violet, blue, yellow, and red regions,

while the negative side indicated decreases in reflectance in these regions. PC2, on the other hand, was composed of spectral reflectance in the range of 540–580 nm, with increases in green spectral reflectance on the positive side and decreases on the negative side (Figure 33A). These findings suggest that PC1 differentiates dull green (grayish-green) coloration based on increases in reflectance at purple, blue, yellow, and red wavelengths, while PC2 distinguishes bright green and dark green based on variations in green spectral reflectance. Using the average PCA scores for each variety and line, the data were grouped into four clusters (Figure 33B). The F₁ cultivar KAMI was classified into Cluster 1 (green), the purebred variety 08S2 into Cluster 4 (gray green), and the YB-F₁ line 2331 into Cluster 2 (dark green). The remaining varieties and lines were grouped into Cluster 3, which exhibited intermediate characteristics based on PC1 and PC2. The average spectral reflectance curves in the visible light range for these green groups revealed that all groups exhibited the highest reflectance within the 540–560 nm range (Figure 34). Examining each group in detail, 08S2 displayed notably high reflectance across all wavelengths. KAMI showed slightly lower reflectance than 08S2 in the 540–560 nm range, but it exhibited the lowest reflectance in other wavelength regions. 2331 exhibited the lowest reflectance in the 540–560 nm range; however, its reflectance at other wavelengths was intermediate between those of 08S2 and KAMI.

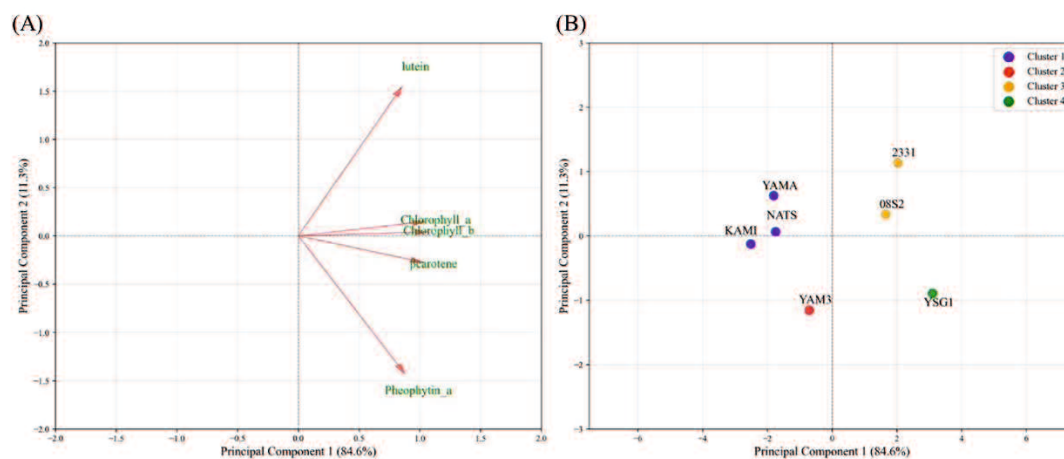


Figure 32. Principal component analysis (PCA) loading plot (A) and PCA score plot with hierarchical clustering (B) of the dataset based on five pigment compounds.

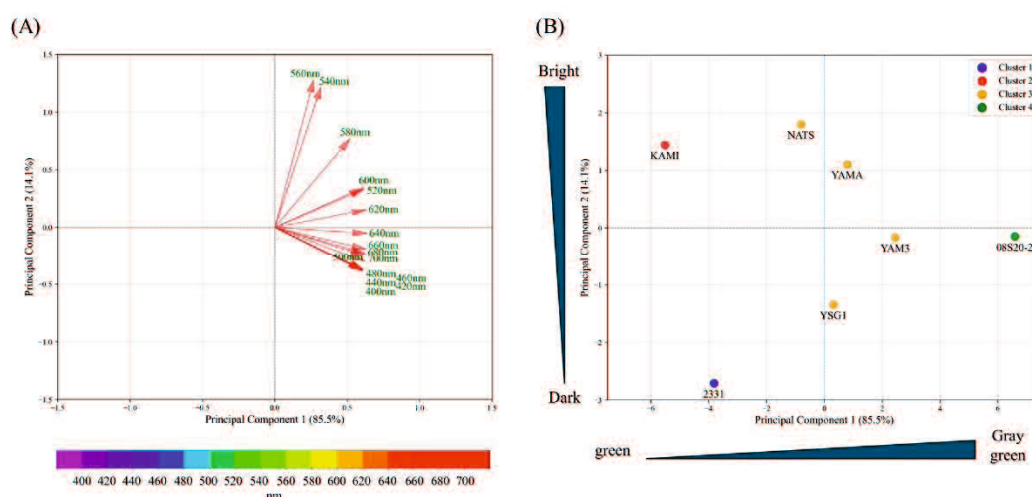


Figure 33. PCA loading plot (A) and PCA score plot with hierarchical clustering (B) of the dataset based on spectral reflectance. (A) Arrows represent the direction and magnitude of each variable's influence, with longer arrows indicating stronger contributions. The color bar at the bottom represents the visible light spectrum. (B) The trend indicators on the left and bottom of the figure represent conceptual images of each principal component based on PCA loadings.

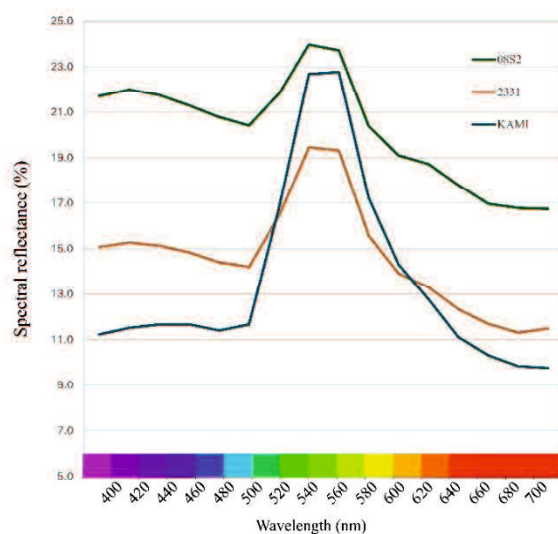


Figure 34. Average spectral reflectance curves (400–700 nm) for different green groups. The color bar at the bottom represents the visible light spectrum.

Development of Prediction Models for Pigment Compounds Using Spectral Reflectance

The measured values of each pigment compound obtained in this study were used as response variables, and the spectral reflectance data (400–700 nm) were used as explanatory variables to construct prediction models. The spectral reflectance data (16 points from 400–700 nm) were subjected to PCA to reduce dimensionality and avoid multicollinearity issues, resulting in four principal components (PCs). These four PCs were used as independent variables, and random forest regression was applied to construct prediction models. Given the limited sample size, Leave-One-Out Cross-Validation (LOOCV) was employed to assess the generalization performance of the models. As a result, the prediction model for chlorophyll *a* achieved coefficients of determination (R^2) and root mean square errors (RMSE) of 0.96 (RMSE = 2.28) in calibration, 0.88 (RMSE = 2.91) in testing, and 0.78 (RMSE = 5.28) in LOOCV, demonstrating a highly accurate regression model.

Additionally, the scatter plot of predicted versus observed values confirmed that the data points were closely distributed along the ideal line (Table 9, Figure 35). On the other hand, the prediction model for β -carotene exhibited a high R^2 of 0.92 (RMSE = 0.19) in calibration but showed an R^2 of -0.10 (RMSE = 0.38) in the test phase, while LOOCV yielded an R^2 of 0.60 (RMSE = 0.38), indicating moderate accuracy. These findings suggest a potential relationship between β -carotene and spectral reflectance. For the other pigment compounds, the R^2 values were low, confirming that the prediction accuracy was insufficient (Table 9).

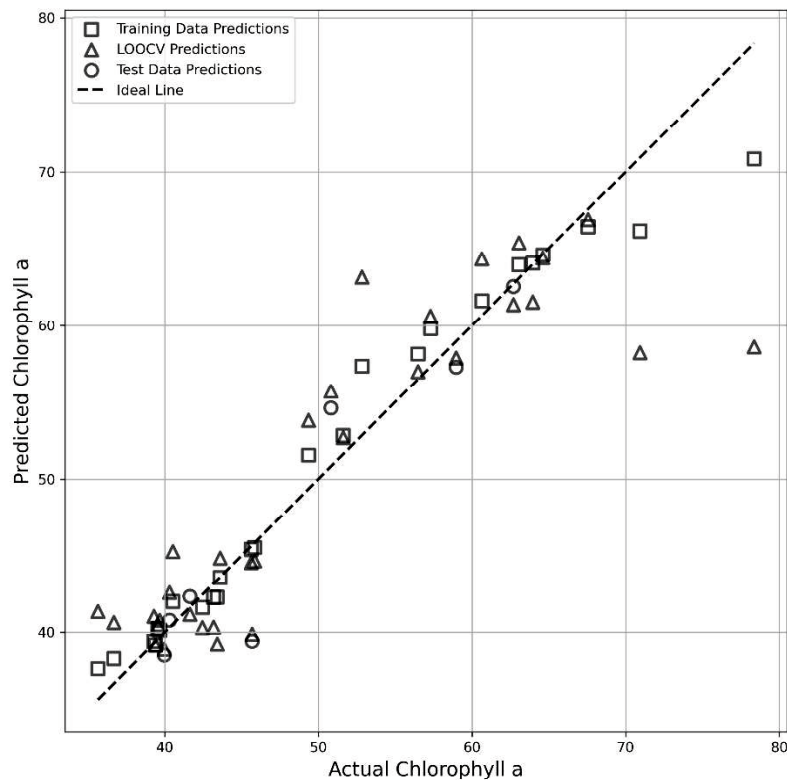


Figure 35. Graphical representation of measured vs. predicted values during the calibration, crossvalidation, and testing steps for the models based on Random Forest for chlorophyll *a*.

Table 9. Quality parameters for the prediction of each pigment compound.

Pigment compound	Quality parameter	Calibration	Test	Leave-One-Out Cross-Validation
Chlorophyll <i>a</i>	R ²	0.96	0.88	0.78
	RMSE	2.28	2.91	5.28
Chlorophyll <i>b</i>	R ²	0.79	-1.07	0.38
	RMSE	4.50	6.70	7.08
Pheophytin <i>a</i>	R ²	0.86	0.47	0.17
	RMSE	0.96	1.58	2.26
Lutein	R ²	0.88	-0.57	-0.15
	RMSE	0.47	2.12	1.63
β -carotene	R ²	0.92	-0.10	0.60
	RMSE	0.19	0.38	0.38

R²: Coefficient of determination, RMSE: Root mean square error.

Metabolome Analysis of Three Green Color Patterns

Based on the PCA results, samples were categorized into three distinct green color groups: green (KAMI, n = 3), dark green (2331, n = 5), and gray green (08S2, n = 5). Metabolome analysis was performed after filtering the dataset from a total of 452 metabolites to 186 through data preprocessing. PLS-DA analysis revealed a clear separation among the three groups, with CP1 and CP2 contributing 21.5% and 13.8% of the variance, respectively. CP1 effectively distinguished samples into the green, dark green, and gray green groups (Figure 36A). Key contributors to this separation included amino acids such as alanine/sarcosine, norvaline/valine, and 5-aminovaleric acid. The green group exhibited higher amino acid accumulation compared to the other groups. Additionally, the dark green group showed elevated levels of quercetin derivatives and cyanidin derivatives. However, among the top 15 VIP scores, no specific metabolites were uniquely increased in the gray green group (Figure 36B). Next, clustering of metabolites was performed, and a

heatmap was created, revealing distinct accumulation patterns of metabolites across the three green color patterns (green, dark green, and gray green) (Figure 37). In the green group, metabolite accumulation was primarily associated with carbohydrates, including D-glucose6-phosphate/D-fructose-6-phosphate, D-glucose-1-phosphate/D-galactose-1-phosphate, 1-kestose, and raffinose. In the dark green group, anthocyanins (e.g., cyanidin-3-glucoside) and their precursor, shikimic acid, were notably accumulated. In the gray green group, amino acids such as Gln, Asp, along with nicotinic acid mononucleotide, nicotinamide mononucleotide, phenylpropanoids, and sinapinic acid, were highly accumulated. These results indicate that each green color pattern activates different metabolic pathways. Specifically, sugar metabolism was emphasized in the green group, pyridine nucleotide cycle and polyphenol metabolism were highlighted in the gray green group, and anthocyanin metabolism was prominent in the dark green group.

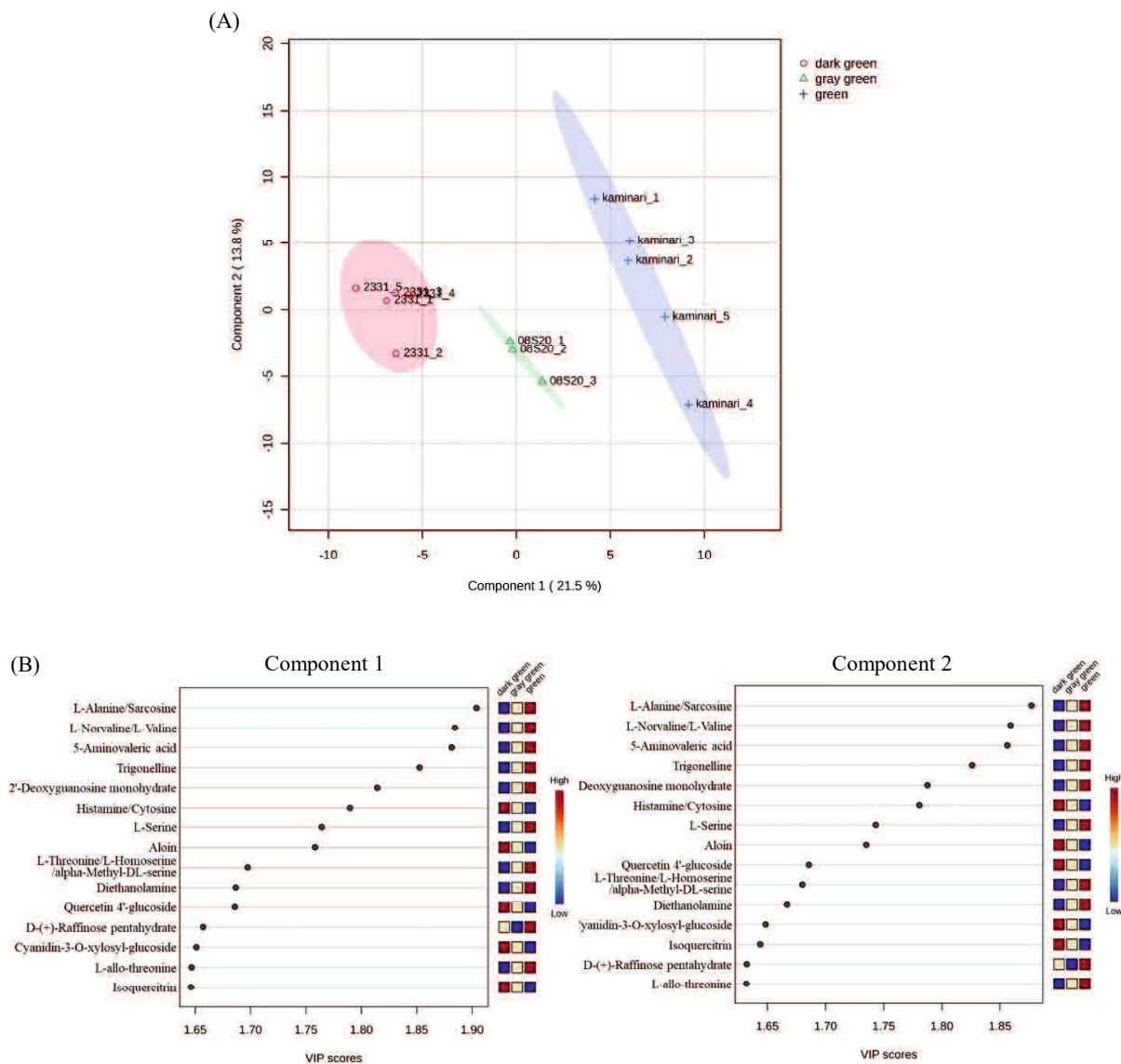


Figure 36. (A) Partial Least Squares–Discriminant Analysis (PLS–DA) score plot and (B) VIP (Variable Importance in Projection) score plot, illustrating metabolite profiles based on different green groups. The contributions of metabolites to the first and second principal component axes are color-coded according to the contribution scale derived from the VIP scores.

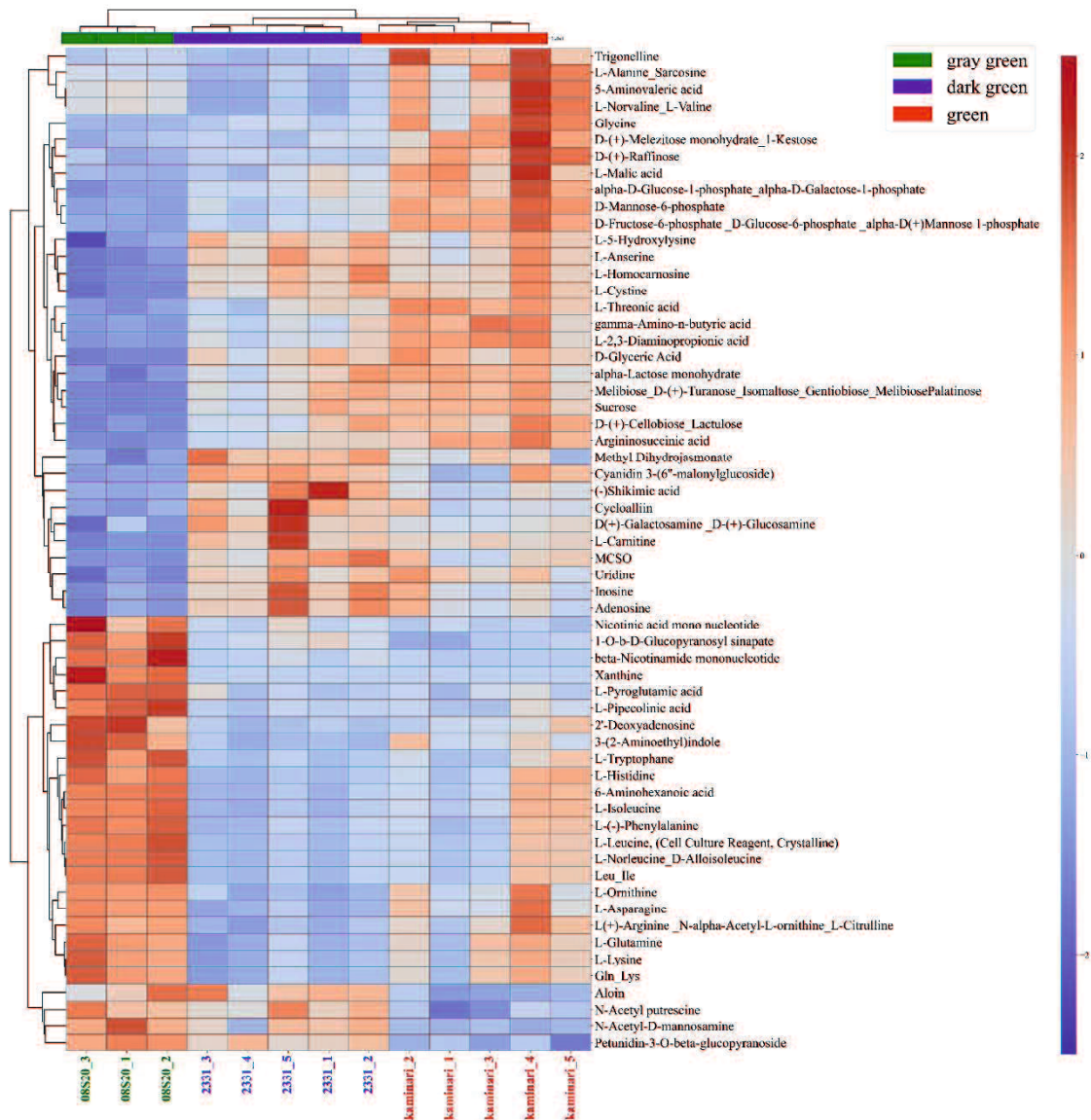


Figure 37. Dendrogram clustering and heatmap for the different green groups based on metabolome analysis.

Discussion

Comparison of SPAD Values and Pigment Analysis in Dark Green Color Evaluation

This study provides valuable insights into the relationship between SPAD values, pigment compound content, and green coloration patterns in heat-tolerant bunching onions. The comparison of SPAD values among the varieties and lines revealed distinct differences (Figure 26). The F₁ cultivars NATS and KAMI exhibited lower values, while the purebred varieties YSG1 and 08S2 showed higher values, with the YB-F₁ lines displayed intermediate values. While the quantification of five pigment compounds generally aligned with these trends, inconsistencies were observed. For example, YSG1 and 2331 had significantly lower SPAD values than 08S2, yet there were no notable differences in the total pigment compound contents. Conversely, 'YMA3' showed SPAD values comparable to those of YSG1 and 2331 but had significantly lower total pigment levels. The correlation analysis between SPAD values and individual pigment compounds revealed a strong relationship with chlorophyll *a*, but only moderate correlations with pheophytin *a*, β -carotene, and lutein (Table 8). This suggests that while SPAD values effectively reflect chlorophyll *a* content, they are insufficient for assessing the more complex dark green coloration, which results from the interplay of multiple pigments. The limitations of SPAD meters arise from their reliance on transmittance measurements at specific wavelengths (650 nm and 940 nm), without accounting for other wavelengths critical to pigment

interactions (Süß et al., 2015). In sweet pepper (*Capsicum annuum* L.), it has been reported that considering parameters such as chroma and hue is necessary for a more accurate measurement of color (Madeira et al., 2003).

To classify varieties and lines based on the five pigment compounds, PCA was conducted. However, the principal component scores for each variety and line did not show clear differences (Figure 32A, 32B). Subsequently, PCA was performed again using spectral reflectance in the visible light range. PC1 was associated with spectral reflectance at 400–700 nm, excluding the 540–560 nm range (Figure 33A). This component was interpreted as representing "dullness", indicating variations in overall leaf brightness. In contrast, PC2 was specifically associated with the 540–560 nm range, where higher spectral reflectance corresponds to lighter green, and lower reflectance indicates darker green (Shull, 1929). Based on this, PC2 was interpreted as representing "brightness". A plot of the principal component scores (PC1 × PC2) for each variety and line showed that KAMI, 08S2, and 2331 were classified into distinct clusters, corresponding to green, gray green, and dark green, respectively (Figure 33A, 33B).

Finally, metabolome analysis was conducted using these green color patterns. PLS-DA enabled clear classification into three green groups (Figure 36A), and heatmaps identified metabolites that were specifically accumulated in each group (Figure 37). In the green group, 1-kestose, raffinose, trigonelline, and gamma-aminobutyric acid were accumulated. These metabolites have been shown to function as osmolytes in the *Allium* genus and *Arabidopsis* (Liu et al., 2022; ElSayed et al., 2014; Abdelrahman et al.,

2015a; Li et al., 2022; Hasan et al., 2021). Heat stress suppresses chlorophyll synthesis. To adapt to such temperature fluctuations, osmolytes are accumulated, exerting protective effects (Sharma et al., 2019a). In *maize*, it has been reported that under drought stress conditions, drought-tolerant lines accumulate more osmolytes compared to sensitive lines, thereby suppressing the reduction of chlorophyll *a* and contributing to the maintenance of green color (Moharramnejad et al., 2019). Based on these findings, it is considered that the green group adapts to environmental stress by accumulating osmolytes and maintaining chlorophyll content.

In the gray green group, NAD intermediates such as nicotinic acid mononucleotide and β -nicotinamide mononucleotide, along with the amino acids Gln and Asp, were accumulated, indicating high activity of the pyridine nucleotide cycle. NAD and NADH in this cycle function as cofactors in redox reactions and are believed to be directly involved in oxidative stress responses (Møller, 2001). Additionally, the accumulation of sinapic acid, a phenolic compound, was observed. Sinapic acid, being an antioxidant and possessing the ability to effectively absorb ultraviolet radiation (Dean et al., 2014), is presumed to enhance photoprotective functions and contribute to environmental stress responses. Furthermore, spectral reflectance data confirmed that the gray green group exhibited higher overall reflectance compared to other groups (Figure 34). In wheat and sorghum, it has been reported that wax-coated genotypes show an increase in reflectance in the visible light range (Camarillo-Castillo et al., 2021; Carvalho et al., 2020). Based on this, it is suggested that in the gray green group, the synthesis and

accumulation of waxes in the cuticle layer may enhance light reflectance and protective functions against environmental stress. However, since waxes are lipids, they could not be clearly detected in the LC/MS-based metabolome analysis conducted in this study. Therefore, future research should employ lipidomic analysis to further elucidate the characteristics and functional roles of waxes.

Finally, in the dark green group it was confirmed that cyanidin glycosides and their precursor, shikimic acid, accumulated (Figure 37). The typical UV-Vis spectrum of anthocyanins exhibits two major absorption clusters: one in the wavelength range of 260–280 nm and the other in the range of 490–550 nm (Saha et al., 2020). Metabolome analysis revealed that the dark green group 2331 accumulated more cyanidin than other groups (Figure 37). Furthermore, the reflectance spectrum of 2331 showed a decrease in reflectance at 540–560 nm and an increase in reflectance at 640–700 nm (red wavelength region) compared to KAMI. These results are consistent with the absorption characteristics of cyanidin, suggesting that the presence of cyanidin contributes to the dark green appearance of the leaves. Additionally, in Zikui Tea (*Camellia sinensis* cv. *Zikui*), it has been reported that the interaction between anthocyanins and chlorophyll results in a dark green appearance rather than a pure purple color, which aligns with the findings of this study (Jin et al., 2024). Anthocyanins have been reported to accumulate in response to environmental stress, mitigating its effects by scavenging excess reactive oxygen species (Naing and Kim, 2021). Similarly, in the case of 2331, it is considered that the accumulation of cyanidin in response to

environmental stress may have influenced the development of a darker green color. This study identified three distinct green color patterns: "green", which adapts to stress responses through osmotic adjustment; "gray green", which indicates the accumulation of redox-related and phenolic compounds; and "dark green," which is associated with anthocyanin accumulation. These differences are closely related to drought stress responses and hold great potential for agricultural applications. Future research should further elucidate the effects of drought stress and utilize these findings to develop drought-tolerant cultivars.

Construction of Prediction Models for Pigment Compounds Using Machine Learning

The validation results of the model using LOOCV showed that the R^2 for chlorophyll *a* was 0.78, indicating high predictive accuracy. On the other hand, the R^2 value for β -carotene was 0.60, revealing some challenges in predictive accuracy (Table 9). For other pigment compounds, it was not possible to construct high-accuracy models (Table 9). Victor and Pozzobon (Victor and Camarena-Bernard, 2023) reported that measuring absorbance at 1 nm intervals within a wavelength range of 340–800 nm using a spectrophotometer enabled highly accurate prediction of chlorophyll *a*, chlorophyll *b*, β -carotene, and lutein. These findings suggest that utilizing broader wavelength ranges, high-resolution spectral data, and their derivatives could lead to the development of more accurate predictive models.

Furthermore, the concentrations of carotenoids and chlorophyll provide essential information about the level of stress experienced by plants and their ability to tolerate it (Strzałka et al., 2003). Therefore, highly accurate regression models for pigment compounds not only hold significance for developing selection markers for dark green traits but also suggest their potential as stress indicators. In this study, we constructed a method to rapidly and simply estimate chlorophyll *a* by utilizing spectral reflectance data. Moving forward, improving the accuracy for other pigment compounds is expected to further enhance practical applicability in agricultural fields and enable the use of these models as indicators for monitoring environmental stress and optimizing cultivation management. This study highlights the potential of combining physiological measurements, metabolomic analyses, and machine learning to improve our understanding of green coloration patterns and stress responses in bunching onions.

Building on these findings, several promising avenues for future research and applications can be pursued. Future work should focus on increasing sample size and incorporating high-resolution spectral reflectance data, such as absorbance measured at 1 nm intervals across a broader wavelength range. This approach, as suggested by Victor and Pozzobon (Victor and Camarena-Bernard, 2023), could refine prediction models by capturing subtle absorption characteristics and interactions among pigments, leading to more accurate and robust estimations of pigment compounds. To further understand the biochemical and genetic regulation of green coloration patterns, future studies could integrate genomics, transcriptomics, and

metabolomics. This would provide deeper insights into the molecular mechanisms driving pigment biosynthesis, and drought stress responses. Investigating how varying environmental conditions, such as different drought intensities, light spectra, and temperature fluctuations, affect pigment metabolism and green coloration will enhance the applicability of these findings to diverse agricultural settings. These directions underscore the importance of integrating advanced technologies with applied agricultural research to develop innovative strategies for crop improvement under challenging environmental conditions.

Chapter 5: GENERAL DISCUSSION

In this study, we analyzed metabolite and gene expression levels associated with dark green coloration and environmental stress responses in bunching onions by integrating wide targeted metabolome analysis, quantification of pigment compounds, and spectral reflectance measurements. As a result, we identified key metabolites and pigment compounds related to leaf tipburn incidence and dark green coloration and further identified genes involved in ABA accumulation. Therefore, this discussion will comprehensively examine the findings from each chapter.

(1) Role of Sulfur Compounds in Abiotic Stress

Drought and heat are major abiotic stresses that reduce crop productivity and weaken global food security, especially given the current and growing impacts of climate change and increases in the occurrence and severity of both stress factors. Plants have developed dynamic responses at the morphological, physiological, and biochemical levels, allowing them to escape and/or adapt to unfavorable environmental conditions (Lamaoui et al., 2018). In recent years, it has become increasingly clear that sulfur compounds play a crucial role in plant stress responses. Sulfur exists as biologically active molecules—such as amino acids (cysteine and methionine), glutathione, and hydrogen sulfide—and is involved in oxidative stress responses and

signal transduction (Bekturova and Sagi, 2024). The results in Chapter 3 revealed that individuals with a higher incidence of leaf tipburn actively progressed in alliin biosynthesis, while those with a lower incidence accumulated sulfur compounds outside the alliin pathway. This suggests that differences in the incidence of leaf tipburn may influence the branching of the sulfur metabolism. Sulfur compounds are thought to contribute to oxidative stress reduction by being converted into glutathione. Additionally, hydrogen sulfide has been reported to activate signal transduction related to ABA biosynthesis and stomatal closure, as well as to induce the synthesis of heat shock proteins, thereby improving heat tolerance (Li et al., 2024b). Therefore, sulfur compounds play a crucial role in abiotic stress responses. In Chapter 2, FF+1A was reported to exhibit high *ABAI* expression and significant ABA accumulation under drought stress conditions. However, as *ABAI* is not located on the first chromosomes of either shallots or bunching onions, it is presumed that alternative regulatory factors promoting *ABAI* expression exist on the first chromosome of shallot. In wheat, exogenous hydrogen sulfide has been shown to upregulate *ABAI* and other enzymes involved in ABA biosynthesis (Ma et al., 2016). Thus, it is possible that a gene located on the first chromosome of shallot promotes the production of hydrogen sulfide, which in turn enhances *ABAI* expression and increases ABA accumulation. In the next studies, it will be necessary to investigate the dynamics of sulfur compounds under drought stress conditions and clarify their relationship with ABA.

(2) Breeding value for ‘2331’ with Both Dark Green Leaf Color and Abiotic Stress Tolerance

Recent breeding objectives include increasing yield, enhancing environmental stress tolerance, improving resistance to pests and diseases, and refining quality. Among these, because bunching onions are cultivated year-round, strengthening environmental stress tolerance is particularly important, especially during the summer, when they are exposed to harsh conditions such as high temperatures and drought. Furthermore, leaf color is a key quality indicator that significantly influences the market value of bunching onions. In general, varieties with darker green leaves tend to be regarded as higher quality. Dark green leaves not only enhance visual appeal but also serve as an indicator of nutritional value, making them an important trait for both consumers and producers. In Chapter 3, it was revealed that, in addition to organic sulfur compounds, the anthocyanin cyanidin was abundantly accumulated in samples with lower leaf tipburn incidence. This suggests that cyanidin may contribute to suppressing leaf tipburn by enhancing antioxidant activity and stress tolerance. In *Arabidopsis thaliana*, it has been reported that the excessive accumulation of flavonoids alleviates drought and oxidative stress, with anthocyanins exhibiting particularly strong antioxidant activity (Nakabayashi et al., 2014). This finding is consistent with the results of Chapter 3 and suggests that cyanidin plays a crucial role in plant adaptation to environmental conditions. Furthermore, Chapter 4 reported that the dark green group ‘2331’ accumulates high levels of cyanidin, which significantly contributes to its dark green leaf coloration. These findings

indicate that the dark green group '2331' not only exhibits strong resistance to leaf tipburn but also has an excellent dark green appearance. These characteristics indicate that this line holds significant potential for future breeding programs and stable production, as it can adapt to evolving cultivation environments and meet market demands.

(3) Application of Visible Light Spectral Reflectance for Pigment Compound Content Prediction and Environmental Stress Assessment

Visible and near-infrared spectroscopy is a widely used spectral analysis technique for inspecting the quality and safety of plants (Farber et al., 2019). Plants develop various physiological defense mechanisms to adapt to adverse abiotic environmental conditions. These mechanisms influence the absorption and reflectance properties of light through changes in pigment composition and leaf structure (Lichtenthaler et al., 1998). Therefore, by utilizing Vis-NIR spectroscopy, these changes associated with plant stress responses can be detected non-destructively, facilitating early diagnosis and the implementation of appropriate protective measures (Sanaeifar et al., 2022). In Chapter 4, in addition to the classification of dark green coloration, the construction of predictive models for pigment compound contents using visible light spectral reflectance was attempted. While an estimation model for chlorophyll *a* content was developed with high accuracy, achieving an R^2 value of 0.78 in leave-one-out cross-validation, the β -carotene estimation model, with an R^2 value of 0.60, has not yet reached sufficient precision.

However, it shows considerable potential for improvement. Since β -carotene is a vital pigment involved in photosynthesis and antioxidant activity, accurately estimating its content could greatly contribute to understanding the physiological state and stress responses of plants. The results in Chapter 3 confirmed a moderate correlation between β -carotene content and abscisic acid content. ABA is a key hormone in plant defense responses to environmental stresses such as drought and salt damage, and fluctuations in its content are closely related to plant stress tolerance. In *Arabidopsis thaliana*, it has been reported that ABA content increases with the accumulation of β -carotene (Sun et al., 2023). This suggests that β -carotene content may also be useful for predicting ABA levels. The effectiveness of growth monitoring using chlorophyll and carotenoid content as indicators in the leaves of wheat and tea (*Camellia sinensis* L.) has been reported (Shah et al., 2019; Wang et al., 2019b). By incorporating ABA into this analysis, it will be possible to gain a more comprehensive understanding of the effects of environmental stress and achieve more advanced cultivation management.

(4) Future Research Challenges

This study has provided insights into the metabolites involved in abiotic stress tolerance and dark green pigment accumulation in bunching onions. However, the behavior and interactions of these related metabolites remain unclear. Moving forward, it is necessary to further elucidate the biochemical mechanisms underlying stress responses and pigment formation

in bunching onions by measuring volatile sulfur compounds and lipid-related metabolites using gas chromatography–mass spectrometry and liquid chromatography–mass spectrometry. Additionally, focusing on ‘2331,’ which was identified in this study as exhibiting a high accumulation of cyanidin associated with a low incidence of leaf tipburn and dark green coloration, we aim to investigate leaf tipburn rates under various growth conditions. By evaluating its abiotic stress tolerance, we intend to further explore its potential as a cultivar and advance our research. For enhancing the efficiency of future breeding programs and promoting the dissemination of heat-tolerant varieties, the development of DNA markers for the efficient selection of these associated compounds is expected to be beneficial.

In relation to pigment compound estimation models, we aim to improve accuracy by increasing the number of samples, optimizing the data sampling methods used in machine learning, and expanding the measurement range of reflectance to the ultraviolet and near-infrared regions while enhancing the resolution to 1 nm. Moreover, in addition to β -carotene and ABA, we plan to estimate zeaxanthin and violaxanthin, which are involved in the xanthophyll cycle, and apply these estimations for simplified monitoring of the growth conditions of bunching onions and environmental stress. This approach will enable a more precise understanding of pigment synthesis dynamics in response to light stress and temperature fluctuations in the cultivation environment of bunching onions, thereby improving stress tolerance. By leveraging these data to optimize cultivation conditions, this research is expected to contribute to the stabilization of yield and quality.

Moving forward, the knowledge gained from this research is expected to contribute to the development of environmentally adaptive varieties and the optimization of cultivation management techniques, ultimately ensuring stable agricultural production and a secure food supply.

LITERATURE CITED

- ABBEY, L., JOYCE, D. C., AKED, J. & SMITH, B. 2002. Genotype, sulphur nutrition and soil type effects on growth and dry-matter production of spring onion. *The Journal of Horticultural Science and Biotechnology*, 77, 340-345.
- ABDELRAHMAN, M., HIRATA, S., SAWADA, Y., HIRAI, M. Y., SATO, S., HIRAKAWA, H., MINE, Y., TANAKA, K. & SHIGYO, M. 2019. Widely targeted metabolome and transcriptome landscapes of *Allium fistulosum*–*A. cepa* chromosome addition lines revealed a flavonoid hot spot on chromosome 5A. *Scientific Reports*, 9, 3541.
- ABDELRAHMAN, M., NISHIYAMA, R., TRAN, C. D., KUSANO, M., NAKABAYASHI, R., OKAZAKI, Y., MATSUDA, F., CHÁVEZ MONTES, R. A., MOSTOFA, M. G., LI, W., WATANABE, Y., FUKUSHIMA, A., TANAKA, M., SEKI, M., SAITO, K., HERRERA-ESTRELLA, L. & TRAN, L.-S. P. 2021. Defective cytokinin signaling reprograms lipid and flavonoid gene-to-metabolite networks to mitigate high salinity in *Arabidopsis*. *Proceedings of the National Academy of Sciences*, 118, e2105021118.
- ABDELRAHMAN, M., SAWADA, Y., NAKABAYASHI, R., SATO, S., HIRAKAWA, H., EL-SAYED, M., HIRAI, M. Y., SAITO, K., YAMAUCHI, N. & SHIGYO, M. 2015a. Integrating transcriptome and target metabolome variability in doubled haploids of *Allium cepa* for abiotic stress protection. *Molecular Breeding*, 35, 195.
- ABDELRAHMAN, M., SAWADA, Y., NAKABAYASHI, R., SATO, S., HIRAKAWA, H., EL-SAYED, M., HIRAI, M. Y., SAITO, K., YAMAUCHI, N. & SHIGYO, M. 2015b. Integrating transcriptome and target metabolome variability in doubled haploids of *Allium cepa* for abiotic stress protection. *Molecular Breeding*, 35.
- AHMAD, M. N., BÜKER, P., KHALID, S., VAN DEN BERG, L., SHAH, H. U., WAHID, A., EMBERSON, L., POWER, S. A. & ASHMORE, M. 2013. Effects of ozone on crops in north-west Pakistan. *Environmental Pollution*, 174, 244-249.
- ALLIUMTDB. 2017. *Keyword Search* [Online]. Japan: Kazusa DNA Red. Inst., YAMAGUCHI UNIVERSITY. Available: <http://alliumtdb.kazusa.or.jp/index.html> [Accessed 2, May 2024].
- ALMELA, L., FERNÁNDEZ-LÓPEZ, J. A. & ROCA, M. A. J. 2000. High-performance

- liquid chromatographic screening of chlorophyll derivatives produced during fruit storage. *Journal of Chromatography A*, 870, 483-489.
- AUDRAN, C., BOREL, C., FREY, A., SOTTA, B., MEYER, C., SIMONNEAU, T. & MARION-POLL, A. 1998. Expression Studies of the Zeaxanthin Epoxidase Gene in *Nicotiana plumbaginifolia*. *Plant Physiology*, 118, 1021-1028.
- AWAN, S. A., KHAN, I., RIZWAN, M., ZHANG, X., BRESTIC, M., KHAN, A., EL - SHEIKH, M. A., ALYEMENI, M. N., ALI, S. & HUANG, L. 2021. Exogenous abscisic acid and jasmonic acid restrain polyethylene glycol - induced drought by improving the growth and antioxidative enzyme activities in pearl millet. *Physiologia Plantarum*, 172, 809-819.
- BEKTUROVA, A. & SAGI, M. 2024. The Crucial Role of Sulfite in Enhancing Plant Stress Response. *BULLETIN of the LN Gumilyov Eurasian National University. BIOSCIENCE Series*, 147, 137-148.
- BHARATH, P., GAHIR, S. & RAGHAVENDRA, A. S. 2021. Abscisic Acid-Induced Stomatal Closure: An Important Component of Plant Defense Against Abiotic and Biotic Stress. *Frontiers in Plant Science*, 12.
- CAMARILLO-CASTILLO, F., HUGGINS, T. D., MONDAL, S., REYNOLDS, M. P., TILLEY, M. & HAYS, D. B. 2021. High-resolution spectral information enables phenotyping of leaf epicuticular wax in wheat. *Plant Methods*, 17, 58.
- CARRERA, F. P., NOCEDA, C., MARIDUEÑA-ZAVALA, M. G. & CEVALLOS-CEVALLOS, J. M. 2021. Metabolomics, a Powerful Tool for Understanding Plant Abiotic Stress. *Agronomy*, 11, 824.
- CARVALHO, H. D. R., HEILMAN, J. L., MCINNES, K. J., ROONEY, W. L. & LEWIS, K. L. 2020. Epicuticular wax and its effect on canopy temperature and water use of Sorghum. *Agricultural and Forest Meteorology*, 284, 107893.
- CHENG, G.-X., LI, R.-J., WANG, M., HUANG, L.-J., KHAN, A., ALI, M. & GONG, Z.-H. 2018. Variation in leaf color and combine effect of pigments on physiology and resistance to whitefly of pepper (*Capsicum annuum* L.). *Scientia Horticulturae*, 229, 215-225.
- CHEVRE, A. M., EBER, F., THIS, P., BARRET, P., TANGUY, X., BRUN, H., DELSENY, M. & RENARD, M. 1996. Characterization of *Brassica nigra* chromosomes and of blackleg resistance in *B. napus*-*B. nigra* addition lines. *Plant Breeding*, 115, 113-118.
- CHUNG, K., DEMIANSKI, A. J., HARRISON, G. A., LAURIE-BERRY, N.,

- MITSUDA, N. & KUNKEL, B. N. 2022. Jasmonate Hypersensitive 3 negatively regulates both jasmonate and ethylene-mediated responses in *Arabidopsis*. *Journal of Experimental Botany*, 73, 5067-5083.
- CURRAH, L. 2002. Onions in the tropics: cultivars and country reports. *Allium crop science: recent advances*. CABI Publishing Wallingford UK.
- DEAN, J. C., KUSAKA, R., WALSH, P. S., ALLAIS, F. & ZWIER, T. S. 2014. Plant Sunscreens in the UV-B: Ultraviolet Spectroscopy of Jet-Cooled Sinapoyl Malate, Sinapic Acid, and Sinapate Ester Derivatives. *Journal of the American Chemical Society*, 136, 14780-14795.
- DISSANAYAKE, P. K., YAMAUCHI, N. & SHIGYO, M. 2008. Chlorophyll degradation and resulting catabolite formation in stored Japanese bunching onion (*Allium fistulosum* L.). *Journal of the Science of Food and Agriculture*, 88, 1981-1986.
- DOLATABADIAN, A., MODARRES SANAVY, S. A. M. & ASILAN, K. S. 2010. Effect of Ascorbic Acid Foliar Application on Yield, Yield Component and several Morphological Traits of Grain Corn under Water Deficit Stress Conditions. *Notulae Scientia Biologicae*, 2, 45-50.
- EFEUGLU, B. & TERZIOGLU, S. 2009. Photosynthetic responses of two wheat varieties to high temperature. *EurAsia J BioSci*, 3, 97-106.
- EGEA, I., ESTRADA, Y., FLORES, F. B. & BOLARIN, M. C. 2022. Improving production and fruit quality of tomato under abiotic stress: Genes for the future of tomato breeding for a sustainable agriculture. *Environmental and Experimental Botany*, 204, 105086.
- ELSAYED, A. I., RAFUDEEN, M. S. & GOLLDACK, D. 2014. Physiological aspects of raffinose family oligosaccharides in plants: protection against abiotic stress. *Plant Biology*, 16, 1-8.
- ENDANG, S., TASHIRO, Y., SHIGYO, M. & ISSHIKI, S. 1997. Morphological and cytological characteristics of haploid shallot (*Allium cepa* L. *Aggregatum* group). *Bulletin of the Faculty of Agriculture-Saga University (Japan)*.
- FARAG, M. A., ALI, S. E., HODAYA, R. H., EL-SEEDI, H. R., SULTANI, H. N., LAUB, A., EISSA, T. F., ABOU-ZAID, F. O. F. & WESSJOHANN, L. A. 2017. Phytochemical Profiles and Antimicrobial Activities of *Allium cepa* Red cv. and *A. sativum* Subjected to Different Drying Methods: A Comparative MS-Based Metabolomics. *Molecules*, 22, 761.
- FARBER, C., MAHNKE, M., SANCHEZ, L. & KUROUSKI, D. 2019. Advanced spectroscopic techniques for plant disease diagnostics. A review. *TrAC Trends in*

- Analytical Chemistry*, 118, 43-49.
- FOLIN, O. & DENIS, W. 1915. A COLORIMETRIC METHOD FOR THE DETERMINATION OF PHENOLS (AND PHENOL DERIVATIVES) IN URINE. *Journal of Biological Chemistry*, 22, 305-308.
- FOOD AND AGRICULTURE ORGANIZATION OF THE UNITED NATIONS. 2022. *FAOSTAT: Value of Agricultural Production* [Online]. FAOSTAT. Available: <https://www.fao.org/faostat/en/#data/QV> [Accessed 29, December 2024].
- FORD-LLOYD, B. V. & ARMSTRONG, S. J. 1993. Welsh onion: *Allium fistulosum* L. *Genetic improvement of vegetable crops*. Elsevier.
- FRIESEN, N., SMIRNOV, S. V., SHMAKOV, A. I., HERDEN, T., OYUNTSETSEG, B. & HURKA, H. 2020. *Allium* species of section Rhizomatosa, early members of the Central Asian steppe vegetation. *Flora*, 263, 151536.
- FU, S., SUN, C., YANG, M., FEI, Y., TAN, F., YAN, B., REN, Z. & TANG, Z. 2013. Genetic and Epigenetic Variations Induced by Wheat-Rye 2R and 5R Monosomic Addition Lines. *PLOS ONE*, 8, e54057.
- GAAFAR, A. A., ALI, S. I., EL-SHAWADFY, M. A., SALAMA, Z. A., SEKARA, A., ULRICHS, C. & ABDELHAMID, M. T. 2020. Ascorbic Acid Induces the Increase of Secondary Metabolites, Antioxidant Activity, Growth, and Productivity of the Common Bean under Water Stress Conditions. *Plants*, 9, 627.
- GALMARINI, C. R. 2018. Economic and Academic Importance. In: SHIGYO, M., KHAR, A. & ABDELRAHMAN, M. (eds.) *The Allium Genomes*. Cham: Springer International Publishing.
- GECHEV, T. & PETROV, V. 2020. Reactive Oxygen Species and Abiotic Stress in Plants. *International Journal of Molecular Sciences*, 21, 7433.
- GHOSH, U. K., ISLAM, M. N., SIDDIQUI, M. N., CAO, X. & KHAN, M. A. R. 2022. Proline, a multifaceted signalling molecule in plant responses to abiotic stress: understanding the physiological mechanisms. *Plant Biology*, 24, 227-239.
- HAFEZ, E. & GHARIB, H. 2016. Effect of exogenous application of ascorbic acid on physiological and biochemical characteristics of wheat under water stress. *International Journal of plant production*, 10, 579-596.
- HAMIDON, M. H. & AHAMED, T. 2022. Detection of Tip-Burn Stress on Lettuce Grown in an Indoor Environment Using Deep Learning Algorithms. *Sensors*, 22, 7251.
- HANG, T. T. M., SHIGYO, M., YAGUCHI, S., YAMAUCHI, N. & TASHIRO, Y. 2004. Effect of single alien chromosome from shallot (*Allium cepa* L. Aggregatum

- group) on carbohydrate production in leaf blade of bunching onion (*A. fistulosum* L.). *Genes & Genetic Systems*, 79, 345-350.
- HAO, F., LIU, X., ZHOU, B., TIAN, Z., ZHOU, L., ZONG, H., QI, J., HE, J., ZHANG, Y., ZENG, P., LI, Q., WANG, K., XIA, K., GUO, X., LI, L., SHAO, W., ZHANG, B., LI, S., YANG, H., HUI, L., CHEN, W., PENG, L., LIU, F., RONG, Z.-Q., PENG, Y., ZHU, W., MCCALLUM, J. A., LI, Z., XU, X., YANG, H., MACKNIGHT, R. C., WANG, W. & CAI, J. 2023. Chromosome-level genomes of three key *Allium* crops and their trait evolution. *Nature Genetics*, 55, 1976-1986.
- HASAN, M. M., ALABDALLAH, N. M., ALHARBI, B. M., WASEEM, M., YAO, G., LIU, X.-D., ABD EL-GAWAD, H. G., EL-YAZIED, A. A., IBRAHIM, M. F. M., JAHAN, M. S. & FANG, X.-W. 2021. GABA: A Key Player in Drought Stress Resistance in Plants. *International Journal of Molecular Sciences*, 22, 10136.
- HERMANN, A. S., ZHOU, X., XU, Q., TADMOR, Y. & LI, L. 2020. Carotenoid Pigment Accumulation in Horticultural Plants. *Horticultural Plant Journal*, 6, 343-360.
- HERNÁNDEZ, I., ALEGRE, L., VAN BREUSEGEM, F. & MUNNÉ-BOSCH, S. 2009. How relevant are flavonoids as antioxidants in plants? *Trends in Plant Science*, 14, 125-132.
- HIRAI, M. Y., YANO, M., GOODENOWE, D. B., KANAYA, S., KIMURA, T., AWAZUHARA, M., ARITA, M., FUJIWARA, T. & SAITO, K. 2004. Integration of transcriptomics and metabolomics for understanding of global responses to nutritional stresses in *Arabidopsis thaliana*. *Proceedings of the National Academy of Sciences*, 101, 10205-10210.
- HU, T., ZHU, S., TAN, L., QI, W., HE, S. & WANG, G. 2016. Overexpression of *OsLEA4* enhances drought, high salt and heavy metal stress tolerance in transgenic rice (*Oryza sativa* L.). *Environmental and Experimental Botany*, 123, 68-77.
- HUAN, L., JIN-QIANG, W. & QING, L. 2020. Photosynthesis product allocation and yield in sweet potato with spraying exogenous hormones under drought stress. *J Plant Physiol*, 253, 153265.
- HUTCHINGS, J. B. 2011. *Food colour and appearance*, Springer Science & Business Media.
- INDEN, H. & ASAHIRA, T. 1990. Japanese bunching onion (*Allium fistulosum* L.). *Onions and allied Crops. Volume III. Biochemistry, Food Sciences, and Minor*

- Crops*, 159-179.
- INDEN, H., ASAHIRA, T. AND OKUI H., . Analysis of factors influencing leaf tip drying of Japanese bunching onion in summer (in Japanese), Abstr. Hortic. Sci. Spring Meet., 1987. 272.
- JEYAKUMAR, P. & BALAMOCHAN, T. 2007. *Micronutrients for horticultural crops*, Tamil Nadu Agricultural University, Coimbatore.
- JIA, H., WANG, X., SHI, Y., WU, X., WANG, Y., LIU, J., FANG, Z., LI, C. & DONG, K. 2020. Overexpression of *Medicago sativa* *LEA4-4* can improve the salt, drought, and oxidation resistance of transgenic *Arabidopsis*. *PLOS ONE*, 15, e0234085.
- JIN, J., CHEN, Y., CAI, J., LV, L., ZENG, X., LI, J., ASGHAR, S. & LI, Y. 2024. Establishment of an efficient regeneration system of ‘ZiKui’ tea with hypocotyl as explants. *Scientific Reports*, 14, 11603.
- JIN, Z., SHEN, J., QIAO, Z., YANG, G., WANG, R. & PEI, Y. 2011. Hydrogen sulfide improves drought resistance in *Arabidopsis thaliana*. *Biochemical and Biophysical Research Communications*, 414, 481-486.
- KAUR, G., KUMAR, S., NAYYAR, H. & UPADHYAYA, H. 2008. Cold stress injury during the pod - filling phase in chickpea (*Cicer arietinum* L.): Effects on quantitative and qualitative components of seeds. *Journal of agronomy and crop science*, 194, 457-464.
- KAYAT, F., MOHAMMED, A. & IBRAHIM, A. M. 2021. Spring Onion (*Allium fistulosum* L.) breeding strategies. *Advances in Plant Breeding Strategies: Vegetable Crops*. Springer.
- KHANDAGALE, K., KRISHNA, R., ROYLAWAR, P., ADE, A. B., BENKE, A., SHINDE, B., SINGH, M., GAWANDE, S. J. & RAI, A. 2020. Omics approaches in *Allium* research: Progress and way ahead. *PeerJ*, 8, e9824.
- KIM, S.-H., YOON, J., HAN, J., SEO, Y., KANG, B.-H., LEE, J. & OCHAR, K. 2023. Green Onion (*Allium fistulosum*): An Aromatic Vegetable Crop Esteemed for Food, Nutritional and Therapeutic Significance. *Foods*, 12, 4503.
- KOŁOTA, E., ADAMCZEWSKA-SOWIŃSKA, K. & UKLAŃSKA-PUSZ, C. 2012. Yield and nutritional value of Japanese bunching onion (*Allium fistulosum* L.) depending on the growing season and plant maturation stage. *Journal of Elementology*, 17, 587-596.
- KOPSELL, D. A., SAMS, C. E., DEYTON, D. E., ABNEY, K. R., KOPSELL, D. E. & ROBERTSON, L. 2010. Characterization of Nutritionally Important Carotenoids

- in Bunching Onion. *HortScience*, 45, 463-465.
- KUMAZAWA, S. K., H. 1965. *Negi. Sosai-Engei Kakuron*. Tokyo, Japan: Yokendo Press.
- KURONUMA, T., WATANABE, Y., ANDO, M. & WATANABE, H. 2019. Relevance of tipburn incidence to the competence for Ca acquirement and Ca distributivity in lisianthus [*Eustoma grandiflorum* (Raf.) Shinn.] cultivars. *Scientia Horticulturae*, 246, 805-811.
- KUSHIRO, T., OKAMOTO, M., NAKABAYASHI, K., YAMAGISHI, K., KITAMURA, S., ASAMI, T., HIRAI, N., KOSHIBA, T., KAMIYA, Y. & NAMBARA, E. 2004. The *Arabidopsis* cytochrome P450 CYP707A encodes ABA 8' -hydroxylases: key enzymes in ABA catabolism. *The EMBO Journal*, 23, 1647-1656.
- LAMAOU, M., JEMO, M., DATLA, R. & BEKKAOU, F. 2018. Heat and Drought Stresses in Crops and Approaches for Their Mitigation. *Front Chem*, 6, 26.
- LI, S., YANG, X., HUANG, H., QIAO, R., JENKS, M. A., ZHAO, H. & Lü, S. 2022. Arabidopsis ACYL-ACTIVATING ENZYME 9 (AAE9) encoding an isobutyl-CoA synthetase is a key factor connecting branched-chain amino acid catabolism with iso-branched wax biosynthesis. *New Phytologist*, 233, 2458-2470.
- LI, X., ZHANG, W., NIU, D. & LIU, X. 2024a. Effects of abiotic stress on chlorophyll metabolism. *Plant Science*, 112030.
- LI, X., ZHOU, R., XU, K., XU, J., JIN, J., FANG, H. & HE, Y. 2018. Rapid Determination of Chlorophyll and Pheophytin in Green Tea Using Fourier Transform Infrared Spectroscopy. *Molecules*, 23, 1010.
- LI, Z.-G., FANG, J.-R. & BAI, S.-J. 2024b. Hydrogen sulfide signaling in plant response to temperature stress. *Frontiers in Plant Science*, 15.
- LIAO, N., HU, Z., MIAO, J., HU, X., LYU, X., FANG, H., ZHOU, Y. M., MAHMOUD, A., DENG, G., MENG, Y. Q., ZHANG, K., MA, Y. Y., XIA, Y., ZHAO, M., YANG, H., ZHAO, Y., KANG, L., WANG, Y., YANG, J. H., ZHOU, Y. H., ZHANG, M. F. & YU, J. Q. 2022. Chromosome-level genome assembly of bunching onion illuminates genome evolution and flavor formation in *Allium* crops. *Nat Commun*, 13, 6690.
- LICHTENTHALER, H., WENZEL, O., BUSCHMANN, C. & GITELSON, A. 1998. Plant stress detection by reflectance and fluorescence. *Annals of the New York Academy of Sciences*, 851, 271-285.
- LITING, W., LINA, W., YANG, Y., PENGFEI, W., TIANCAI, G. & GUOZHANG, K.

2015. Abscisic acid enhances tolerance of wheat seedlings to drought and regulates transcript levels of genes encoding ascorbate-glutathione biosynthesis. *Frontiers in Plant Science*, 6.
- LIU, R., JIAO, T., ZHANG, Z., YAO, Z., LI, Z., WANG, S., XIN, H., LI, Y., WANG, A. & ZHU, J. 2022. Ectopic Expression of the *Allium cepa* 1-SST gene in cotton improves drought tolerance and yield under drought stress in the field. *Frontiers in Plant Science*, 12, 783134.
- LIU, X., GAO, S., LIU, Y., CAO, B., CHEN, Z. & XU, K. 2021. Alterations in leaf photosynthetic electron transport in Welsh onion (*Allium fistulosum* L.) under different light intensity and soil water conditions. *Plant Biology*, 23, 83-90.
- MA, C., WANG, Y., WANG, Y., WANG, L., CHEN, S. & LI, H. 2011. Identification of a sugar beet *BvM14-MADS box* gene through differential gene expression analysis of monosomic addition line M14. *Journal of Plant Physiology*, 168, 1980-1986.
- MA, D., DING, H., WANG, C., QIN, H., HAN, Q., HOU, J., LU, H., XIE, Y. & GUO, T. 2016. Alleviation of Drought Stress by Hydrogen Sulfide Is Partially Related to the Abscisic Acid Signaling Pathway in Wheat. *PLOS ONE*, 11, e0163082.
- MADEIRA, A. C., FERREIRA, A., DE VARENNES, A. & VIEIRA, M. I. 2003. SPAD Meter Versus Tristimulus Colorimeter to Estimate Chlorophyll Content and Leaf Color in Sweet Pepper. *Communications in Soil Science and Plant Analysis*, 34, 2461-2470.
- MANTRI, N., PATADE, V., PENNA, S., FORD, R. & PANG, E. 2012. Abiotic stress responses in plants: present and future. *Abiotic stress responses in plants: metabolism, productivity and sustainability*, 1-19.
- MARKWELL, J., OSTERMAN, J. C. & MITCHELL, J. L. 1995. Calibration of the Minolta SPAD-502 leaf chlorophyll meter. *Photosynthesis Research*, 46, 467-472.
- MARUO, T. & JOHKAN, M. 2016. Chapter 12 - Tipburn. In: KOZAI, T., NIU, G. & TAKAGAKI, M. (eds.) *Plant Factory*. San Diego: Academic Press.
- MASCELLANI BERGO, A., LEISS, K. & HAVLIK, J. 2024. Twenty Years of (1)H NMR Plant Metabolomics: A Way Forward toward Assessment of Plant Metabolites for Constitutive and Inducible Defenses to Biotic Stress. *J Agric Food Chem*, 72, 8332-8346.
- MCCALLUM, J., BALDWIN, S., SHIGYO, M., DENG, Y., VAN HEUSDEN, S., PITHER-JOYCE, M. & KENEL, F. 2012. AlliumMap-A comparative genomics resource for cultivated *Allium* vegetables. *BMC Genomics*, 13, 168.

- MEDINA-MELCHOR, D. L., ZAPATA-SARMIENTO, D. H., BECERRA-MARTÍNEZ, E., RODRÍGUEZ-MONROY, M., VALLEJO, L. G. Z. & SEPÚLVEDA-JIMÉNEZ, G. 2022. Changes in the metabolomic profiling of *Allium cepa* L. (onion) plants infected with *Stemphylium vesicarium*. *European Journal of Plant Pathology*, 162, 557-573.
- MIURA, K. & TADA, Y. 2014. Regulation of water, salinity, and cold stress responses by salicylic acid. *Frontiers in Plant Science*, 5.
- MOHARRAMNEJAD, S., SOFALIAN, O., VALIZADEH, M., ASGHARI, A., SHIRI, M. & ASHRAF, M. 2019. Response of maize to field drought stress: Oxidative defense system, Osmolytes' accumulation and photosynthetic pigments. *Pakistan Journal of Botany*, 51.
- MØLLER, I. M. 2001. Plant mitochondria and oxidative stress: electron transport, NADPH turnover, and metabolism of reactive oxygen species. *Annual review of plant biology*, 52, 561-591.
- MULTANI, D. S., KHUSH, G. S., DELOS REYES, B. G. & BRAR, D. S. 2003. Alien genes introgression and development of monosomic alien addition lines from *Oryza latifolia* Desv. to rice, *Oryza sativa* L. *Theoretical and Applied Genetics*, 107, 395-405.
- NAING, A. H. & KIM, C. K. 2021. Abiotic stress - induced anthocyanins in plants: Their role in tolerance to abiotic stresses. *Physiologia Plantarum*, 172, 1711-1723.
- NAKABAYASHI, R., YONEKURA-SAKAKIBARA, K., URANO, K., SUZUKI, M., YAMADA, Y., NISHIZAWA, T., MATSUDA, F., KOJIMA, M., SAKAKIBARA, H., SHINOZAKI, K., MICHAEL, A. J., TOHGE, T., YAMAZAKI, M. & SAITO, K. 2014. Enhancement of oxidative and drought tolerance in *Arabidopsis* by overaccumulation of antioxidant flavonoids. *The Plant Journal*, 77, 367-379.
- NILSSON, T. 2000. Postharvest handling and storage of vegetables. *Fruit and Vegetable Quality*. CRC Press.
- OBEL, H. O., CHENG, C., TIAN, Z., NJOGU, M. K., LI, J., DU, S., LOU, Q., ZHOU, J., YU, X., OGWENO, J. O. & CHEN, J. 2022. Transcriptomic and Physiological Analyses Reveal Potential Genes Involved in Photoperiod-Regulated β -Carotene Accumulation Mechanisms in the Endocarp of Cucumber (*Cucumis sativus* L.) Fruit. *International Journal of Molecular Sciences*, 23, 12650.

- OHKAMA - OHTSU, N., RADWAN, S., PETERSON, A., ZHAO, P., BADR, A. F., XIANG, C. & OLIVER, D. J. 2007. Characterization of the extracellular γ - glutamyl transpeptidases, GGT1 and GGT2, in Arabidopsis. *The Plant Journal*, 49, 865-877.
- OOSHIMA, K., YUKO, N., YOSHINORI, S., RYUJI, S. & TOMOMI, M. 2015. Elucidation of the cause for Chinese chive leaf tip-burn. *Bull. Tochigi Agr. Exp. Stn.*, No73, 11-20.
- PADULA, G., XIA, X. & HOŁUBOWICZ, R. 2022. Welsh Onion (*Allium fistulosum* L.) Seed Physiology, Breeding, Production and Trade. *Plants*, 11, 343.
- PALENCIA, P., MARTINEZ, F., RIBEIRO, E., PESTANA, M., GAMA, F., SAAVEDRA, T., DE VARENNES, A. & CORREIA, P. J. 2010. Relationship between tipburn and leaf mineral composition in strawberry. *Scientia Horticulturae*, 126, 242-246.
- PERCHERON, F. Dosage colorimétrique du fructose et des fructofuranosides par l'acide thiobarbiturique. *Compte Rendu*, 1962. 2521-2522.
- POSPÍŠIL, P. & PRASAD, A. 2014. Formation of singlet oxygen and protection against its oxidative damage in Photosystem II under abiotic stress. *Journal of Photochemistry and Photobiology B: Biology*, 137, 39-48.
- RAI, G. K., KHANDAY, D. M., CHOUDHARY, S. M., KUMAR, P., KUMARI, S., MARTÍNEZ-ANDÚJAR, C., MARTÍNEZ-MELGAREJO, P. A., RAI, P. K. & PÉREZ-ALFOCEA, F. 2024. Unlocking nature's stress buster: Abscisic acid's crucial role in defending plants against abiotic stress. *Plant Stress*, 11, 100359.
- RAMEL, F., BIRTIC, S., CUINÉ, S., TRIANTAPHYLIDÈS, C., RAVANAT, J.-L. & HAVAUX, M. 2012. Chemical Quenching of Singlet Oxygen by Carotenoids in Plants. *Plant Physiology*, 158, 1267-1278.
- REAMON-RAMOS, S. M. & WRICKE, G. 1992. A full set of monosomic addition lines in *Beta vulgaris* from *Beta webbiana*: morphology and isozyme markers. *Theoretical and Applied Genetics*, 84, 411-418.
- RIAZ, M., MAHMOOD, R., KHAN, S. N., HAIDER, M. S. & RAMZAN, S. 2020. Onion tip burn: Significance, and response to amount and form of nitrogen. *Scientia Horticulturae*, 261, 108773.
- ROSEN, C. J. 1990. Leaf Tipburn in Cauliflower as Affected by Cultivar, Calcium Sprays, and Nitrogen Nutrition. *HortScience HortSci*, 25, 660-663.
- SAHA, S., SINGH, J., PAUL, A., SARKAR, R., KHAN, Z. & BANERJEE, K. 2020.

- Anthocyanin profiling using UV-vis spectroscopy and liquid chromatography mass spectrometry. *Journal of AOAC International*, 103, 23-39.
- SAMI, F., YUSUF, M., FAIZAN, M., FARAZ, A. & HAYAT, S. 2016. Role of sugars under abiotic stress. *Plant Physiol Biochem*, 109, 54-61.
- SANAEIFAR, A., ZHANG, W., CHEN, H., ZHANG, D., LI, X. & HE, Y. 2022. Study on effects of airborne Pb pollution on quality indicators and accumulation in tea plants using Vis-NIR spectroscopy coupled with radial basis function neural network. *Ecotoxicology and Environmental Safety*, 229, 113056.
- SATO, R., ITO, H. & TANAKA, A. 2015. Chlorophyll b degradation by chlorophyll b reductase under high-light conditions. *Photosynthesis research*, 126, 249-259.
- SAURE, M. C. 1998. Causes of the tipburn disorder in leaves of vegetables. *Scientia Horticulturae*, 76, 131-147.
- SAVIANO, G., PARIS, D., MELCK, D., FANTASMA, F., MOTTA, A. & IORIZZI, M. 2019. Metabolite variation in three edible Italian *Allium cepa* L. by NMR-based metabolomics: a comparative study in fresh and stored bulbs. *Metabolomics*, 15, 105.
- SAWADA, Y., AKIYAMA, K., SAKATA, A., KUWAHARA, A., OTSUKI, H., SAKURAI, T., SAITO, K. & HIRAI, M. Y. 2009. Widely targeted metabolomics based on large-scale MS/MS data for elucidating metabolite accumulation patterns in plants. *Plant and Cell Physiology*, 50, 37-47.
- SAWADA, Y., TSUKAYA, H., LI, Y., SATO, M., KAWADE, K. & HIRAI, M. Y. 2017. A novel method for single-grain-based metabolic profiling of Arabidopsis seed. *Metabolomics*, 13, 1-8.
- SCHWARZ, N., ARMBRUSTER, U., IVEN, T., BRÜCKLE, L., MELZER, M., FEUSSNER, I. & JAHNS, P. 2015. Tissue-Specific Accumulation and Regulation of Zeaxanthin Epoxidase in Arabidopsis Reflect the Multiple Functions of the Enzyme in Plastids. *Plant and Cell Physiology*, 56, 346-357.
- SH, S. M. 2014. Role of ascorbic acid and α tocopherol in alleviating salinity stress on flax plant (*Linum usitatissimum* L.). *Journal of Stress Physiology & Biochemistry*, 10, 93-111.
- SHAH, S. H., ANGEL, Y., HOUBORG, R., ALI, S. & MCCABE, M. F. 2019. A Random Forest Machine Learning Approach for the Retrieval of Leaf Chlorophyll Content in Wheat. *Remote Sensing*, 11, 920.
- SHANNON, M. & GRIEVE, C. 1998. Tolerance of vegetable crops to salinity. *Scientia horticulturae*, 78, 5-38.
- SHARMA, A., SHAHZAD, B., KUMAR, V., KOHLI, S. K., SIDHU, G. P. S., BALI, A.

- S., HANDA, N., KAPOOR, D., BHARDWAJ, R. & ZHENG, B. 2019a. Phytohormones Regulate Accumulation of Osmolytes Under Abiotic Stress. *Biomolecules*, 9, 285.
- SHARMA, A., SHAHZAD, B., REHMAN, A., BHARDWAJ, R., LANDI, M. & ZHENG, B. 2019b. Response of Phenylpropanoid Pathway and the Role of Polyphenols in Plants under Abiotic Stress. *Molecules*, 24.
- SHIGYO, M., TASHIRO, Y., ISSHIKI, S. & MIYAZAKI, S. 1996. Establishment of a series of alien monosomic addition lines of Japanese bunching onion (*Allium fistulosum* L.) with extra chromosomes from shallot (*A. cepa* L. Aggregatum group). *Genes & Genetic Systems*, 71, 363-371.
- SHULAEV, V., CORTES, D., MILLER, G. & MITTLER, R. 2008. Metabolomics for plant stress response. *Physiologia Plantarum*, 132, 199-208.
- SHULL, C. A. 1929. A spectrophotometric study of reflection of light from leaf surfaces. *Botanical Gazette*, 87, 583-607.
- ŞİMŞEK, Ö., ISAK, M. A., DÖNMEZ, D., DALDA ŞEKERCI, A., İZGÜ, T. & KAÇAR, Y. A. 2024. Advanced Biotechnological Interventions in Mitigating Drought Stress in Plants. *Plants*, 13, 717.
- SINGH, B. & RAMAKRISHNA, Y. 2017. Welsh onion (*Allium fistulosum* L.): A promising spicing-culinary herb of Mizoram. *Indian Journal of Hill Farming*, 30, 201-208.
- SINGHAL, G., BANSOD, B., MATHEW, L., GOSWAMI, J., CHOUDHURY, B. U. & RAJU, P. L. N. 2019. Chlorophyll estimation using multi-spectral unmanned aerial system based on machine learning techniques. *Remote Sensing Applications: Society and Environment*, 15.
- SIRKO, A., WAWRZYŃSKA, A., BRZYWCZY, J. & SIENKO, M. 2021. Control of ABA Signaling and Crosstalk with Other Hormones by the Selective Degradation of Pathway Components. *International Journal of Molecular Sciences*, 22, 4638.
- STRZAŁKA, K., KOSTECKA-GUGAŁA, A. & LATOWSKI, D. 2003. Carotenoids and Environmental Stress in Plants: Significance of Carotenoid-Mediated Modulation of Membrane Physical Properties. *Russian Journal of Plant Physiology*, 50, 168-173.
- SU, T., LI, P., WANG, H., WANG, W., ZHAO, X., YU, Y., ZHANG, D., YU, S. & ZHANG, F. 2019. Natural variation in a calreticulin gene causes reduced resistance to Ca²⁺ deficiency - induced tipburn in Chinese cabbage (*Brassica*

- rapa ssp. pekinensis*). *Plant, Cell & Environment*, 42, 3044-3060.
- SUN, M., XU, Q.-Y., ZHU, Z.-P., LIU, P.-Z., YU, J.-X., GUO, Y.-X., TANG, S., YU, Z.-F. & XIONG, A.-S. 2023. AgMYB5, an MYB transcription factor from celery, enhanced β -carotene synthesis and promoted drought tolerance in transgenic *Arabidopsis*. *BMC Plant Biology*, 23, 151.
- Süß, A., DANNER, M., OBSTER, C., LOCHERER, M., HANK, T., RICHTER, K. & CONSORTIUM, E. 2015. Measuring leaf chlorophyll content with the Konica Minolta SPAD-502Plus.
- TAFESSE, E. G., WARKENTIN, T. D., SHIRTLIFFE, S., NOBLE, S. & BUECKERT, R. 2022. Leaf Pigments, Surface Wax and Spectral Vegetation Indices for Heat Stress Resistance in Pea. *Agronomy*, 12, 739.
- TAIR. 1999. Phoenix Bioinformatics Corporation. Available: <https://www.arabidopsis.org/> [Accessed 2, May 2024].
- THOMPSON, A. J., JACKSON, A. C., PARKER, R. A., MORPETH, D. R., BURBIDGE, A. & TAYLOR, I. B. 2000. Abscisic acid biosynthesis in tomato: regulation of zeaxanthin epoxidase and 9-*cis*-epoxycarotenoid dioxygenase mRNAs by light/dark cycles, water stress and abscisic acid. *Plant Molecular Biology*, 42, 833-845.
- TOLIN, S., ARRIGONI, G., TRENTIN, A. R., VELJOVIC-JOVANOVIC, S., PIVATO, M., ZECHMAN, B. & MASI, A. 2013. Biochemical and quantitative proteomics investigations in *Arabidopsis ggt1* mutant leaves reveal a role for the gamma-glutamyl cycle in plant's adaptation to environment. *PROTEOMICS*, 13, 2031-2045.
- UCHIDA, K., SAWADA, Y., OCHIAI, K., SATO, M., INABA, J. & HIRAI, M. Y. 2020. Identification of a Unique Type of Isoflavone O-Methyltransferase, GmIOMT1, Based on Multi-Omics Analysis of Soybean under Biotic Stress. *Plant and Cell Physiology*, 61, 1974-1985.
- UNO, Y., OKUBO, H., ITOH, H. & KOYAMA, R. 2016. Reduction of leaf lettuce tipburn using an indicator cultivar. *Scientia Horticulturae*, 210, 14-18.
- VICTOR, P. & CAMARENA-BERNARD, C. 2023. Lutein, violaxanthin, and zeaxanthin spectrophotometric quantification: A machine learning approach. *Journal of Applied Phycology*, 35, 73-84.
- VU, H. Q., EL-SAYED, M. A., ITO, S., YAMAUCHI, N. & SHIGYO, M. 2012. Discovery of a new source of resistance to *Fusarium oxysporum*, cause of Fusarium wilt in *Allium fistulosum*, located on chromosome 2 of *Allium cepa* Aggregatum group. *Genome*, 55, 797-807.

- VU, Q. H., HANG, T. T. M., YAGUCHI, S., ONO, Y., PHAM, T. M. P., YAMAUCHI, N. & SHIGYO, M. 2013. Assessment of biochemical and antioxidant diversities in a shallot germplasm collection from Vietnam and its surrounding countries. *Genetic resources and crop evolution*, 60, 1297-1312.
- WAKO, T., YAMASHITA, K.-I., TSUKAZAKI, H., OHARA, T., KOJIMA, A., YAGUCHI, S., SHIMAZAKI, S., MIDORIKAWA, N., SAKAI, T. & YAMAUCHI, N. 2015. Screening and incorporation of rust resistance from *Allium cepa* into bunching onion (*Allium fistulosum*) via alien chromosome addition. *Genome*, 58, 135-142.
- WANG, W., WANG, J., WEI, Q., LI, B., ZHONG, X., HU, T., HU, H. & BAO, C. 2019a. Transcriptome-Wide Identification and Characterization of Circular RNAs in Leaves of Chinese Cabbage (*Brassica rapa* L. ssp. *pekinensis*) in Response to Calcium Deficiency-Induced Tip-burn. *Scientific Reports*, 9, 14544.
- WANG, Y., HU, X., JIN, G., HOU, Z., NING, J. & ZHANG, Z. 2019b. Rapid prediction of chlorophylls and carotenoids content in tea leaves under different levels of nitrogen application based on hyperspectral imaging. *Journal of the Science of Food and Agriculture*, 99, 1997-2004.
- WEI, L., WANG, L., YANG, Y., WANG, P., GUO, T. & KANG, G. 2015. Abscisic acid enhances tolerance of wheat seedlings to drought and regulates transcript levels of genes encoding ascorbate-glutathione biosynthesis. *Frontiers in plant science*, 6, 458.
- WOLLERS, S., HEIDENREICH, T., ZAREPOUR, M., ZACHMANN, D., KRAFT, C., ZHAO, Y., MENDEL, R. R. & BITTNER, F. 2008. Binding of Sulfurated Molybdenum Cofactor to the C-terminal Domain of ABA3 from *Arabidopsis thaliana* Provides Insight into the Mechanism of Molybdenum Cofactor Sulfuration*. *Journal of Biological Chemistry*, 283, 9642-9650.
- XUAN, L., LI, J., WANG, X. & WANG, C. 2020. Crosstalk between Hydrogen Sulfide and Other Signal Molecules Regulates Plant Growth and Development. *International Journal of Molecular Sciences*, 21, 4593.
- YAGUCHI, S., ATARASHI, M., IWAI, M., MASUZAKI, S.-I., YAMAUCHI, N. & SHIGYO, M. 2008. Production of Alien Addition Lines in Polyploid Bunching Onion (*Allium fistulosum*) Carrying 1A Chromosome(s) of Shallot (*Allium cepa*) and Their Application to Breeding for a New Vitamin C-Rich Vegetable. *Journal of the American Society for Horticultural Science J. Amer. Soc. Hort. Sci.*, 133, 367-373.
- YAMAMOTO, K. 2004. LIA for Win32 (LIA32) release 0.377 e (English version)

- User's manual. [http://www. agr. nagoya-u. ac. jp/~ shinkan/LIA32/index-e. html](http://www.agr.nagoya-u.ac.jp/~shinkan/LIA32/index-e.html).
- YAMASAKI, A. & TSUKAZAKI, H. 2022. Edible Alliums Botany, Production and Uses. *In*: HAIM D. RABINOWITCH, B. T. (ed.) *CABI*. UK.
- YAO, P.-Q., CHEN, J.-H., MA, P.-F., XIE, L.-H., SHI, J. & CHENG, S.-P. 2024. Karyotype analysis of Chinese chive germplasms with different ploidy levels and their evolutionary relationships. *Genetic Resources and Crop Evolution*, 71, 1749-1758.
- YIU, J.-C., LIU, C.-W., KUO, C.-T., TSENG, M.-J., LAI, Y.-S. & LAI, W.-J. 2008. Changes in antioxidant properties and their relationship to paclobutrazol-induced flooding tolerance in Welsh onion. *Journal of the Science of Food and Agriculture*, 88, 1222-1230.
- ZHANG, L., GAO, M., HU, J., ZHANG, X., WANG, K. & ASHRAF, M. 2012. Modulation Role of abscisic acid (ABA) on growth, water relations and glycinebetaine metabolism in two maize (*Zea mays* L.) cultivars under drought stress. *Int J Mol Sci*, 13, 3189-3202.
- ZOLFAGHARI, B., YAZDINIPOUR, Z., SADEGHI, M., TROIANO, R. & LANZOTTI, V. 2016. Furostanol Saponins from the Bulbs of Welsh Onion, *Allium fistulosum* L. *Planta Medica*, 82, 1584-1590.

SUMMARY

Abiotic stresses, which have been increasing due to global warming and drought caused by climate change, have made the development of heat- and drought-tolerant varieties of bunching onion (*Allium fistulosum* L., genomes FF) a critical challenge. Leaf tipburn, a physiological disorder caused by abiotic stresses, significantly reduces the commercial value of the bunching onion. On the other hand, a dark green color is considered a trait that enhances commercial value and is also in demand from producers. In this study, the characteristics of heat- and drought-tolerant bunching onion varieties were elucidated to facilitate their breeding. For this purpose, a series of bunching onion–shallot addition lines (FF+1A to FF+8A), each containing a single alien chromosome derived from a stress-tolerant shallot (*A. cepa* L. *Aggregatum* group, AA), and heat-tolerant varieties were used. Functional analyses were conducted to investigate adaptive responses to abiotic stress and changes in metabolites, as well as their relationship to the expression of various agronomic traits.

(1) Effects of Drought Stress on Abscisic Acid Content and Its Related Transcripts in *Allium fistulosum*—*A. cepa* Monosomic Addition Lines

A series of bunching onion–shallot addition lines were subjected to drought treatment, and the contents of abscisic acid (ABA), a key hormone related to drought stress, and its precursor, β -carotene, were measured. Additionally, gene expression analyses were conducted on genes involved in

ABA biosynthesis, catabolism, and signaling responses to examine the effects of adding alien chromosomes on the drought-stress response in the bunching onion. As a result, in FF+1A under drought treatment, the contents of β -carotene and ABA were significantly higher at the 5% level than those in FF under the same conditions. Multiple genes involved in ABA biosynthesis were also markedly upregulated. In contrast, the gene expression profile of FF+6A, which had ABA and β -carotene contents comparable to those of FF, differed significantly from that of FF+1A. Notably, *zeaxanthin epoxidase (ABA1)* exhibited high expression in FF+1A, while showing low expression in FF+6A. *ABA1* is known to directly participate in the rate-limiting step of ABA biosynthesis. The introduction of the first chromosome from shallot into the bunching onion was suggested to enhance the expression of this gene, leading to an increase in ABA content. Consequently, stomatal closure may be promoted, potentially improving the drought tolerance of the plant.

(2) Metabolite Profiling and Association Analysis of Leaf Tipburn in Heat-Tolerant Bunching Onion Varieties

As plant materials, leaf blades from 8 heat-tolerant varieties and lines of bunching onion, obtained through six patterns of summer cultivation with different sowing and harvesting dates (6 experimental groups \times 8 varieties/lines \times 3 biological replicates = 144 samples) were used. For all samples, absolute quantification data of six pigment compounds and three functional components, relative quantification data of 267 metabolites, and leaf tipburn rates were obtained.

Statistical analyses using the absolute quantification data revealed that varieties and lines with notably darker leaf blade colors generally had higher contents of chlorophyll and carotenoids. In particular, 'Yamakou01,' 'Yamakou03,' and 'YSG1' accumulated higher amounts of these pigment compounds in their leaf blades, suggesting that these compounds are the main contributors to dark green leaf blade coloration. Additionally, machine learning was used to analyze the relationship between the relative quantification data of metabolites from all samples and the same phenotypic traits. As a result, gamma-Glu PRENCISO, an organosulfur compound, and several flavonoids were identified as metabolites associated with leaf tipburn. These metabolites are suggested to suppress leaf tipburn by utilizing the redox reactions of glutathione, which plays a crucial role in the synthesis of sulfur compounds, as well as their antioxidant activities.

(3) Metabolome Profiling and Predictive Modeling of Dark Green Trait in Heat-Tolerant Bunching Onions

Seven heat-tolerant varieties and lines of bunching onion were cultivated during the summer season to measure pigment compounds, metabolome, and spectral reflectance in the 400–700 nm range at 20 nm intervals. Based on these measurements, a system of classification of dark green types and predictive models for pigment compound contents were developed. Principal component analysis (PCA) of the spectral reflectance data revealed that the green coloration of heat-tolerant varieties could be categorized into three groups: "green" (high reflectance at 540–560 nm), "dark green" (low reflectance at 540–560 nm), and "gray green" (high

reflectance across all wavelengths). Metabolome analysis using representative varieties and lines from these three groups revealed an increase in cyanidin derivatives in the "dark green" group and an increase in sinapinic acid in the "gray green" group. Furthermore, using absolute pigment compound data and spectral reflectance values, a predictive model was constructed via random forest regression. For chlorophyll *a* content, the regression model achieved high accuracy with an R^2 value of 0.88 in the test dataset and 0.78 in leave-one-out cross-validation. This study elucidated the effects of adding shallot chromosomes on the drought stress response in the bunching onion, as well as the metabolites involved in leaf tipburn and dark green coloration. In addition, for the first time in the *Allium* genus, a novel method was successfully developed to construct a highly accurate regression model for predicting the total chlorophyll content using spectral reflectance data. By integrating genetic and physiological–ecological approaches, a method combining metabolite analysis with simplified pigment measurement was developed, providing foundational knowledge for the development of cultivation techniques for drought-tolerant bunching onions. In subsequent research, the insights gained from this research are expected to contribute to the development of bunching onion varieties suitable for cultivation under adverse environmental conditions.

JAPANESE SUMMARY

近年、気候変動による温暖化や局地的な少雨などの非生物的ストレスの増加に伴い、葉ネギ (*Allium fistulosum* L., ゲノム構成 FF) の耐乾性や耐暑性を高めることが重要な課題となっている。葉ネギでは、「葉先枯れ」と呼ばれる生理障害がとりわけ問題視されており、商品価値を著しく低下させる要因となっている。また、生産者からは濃緑色を持つ品種の開発が強く求められている。本研究では、耐暑性および耐乾性ネギの特性解明とその育種に向けて、環境ストレス耐性を有するシャロット (*A. cepa* L. Aggregatum group, AA) に由来する 8 種類の単一異種染色体をそれぞれ添加したネギ系統 (ネギ-シャロット添加系統) のシリーズ (FF+1A~FF+8A) および耐暑性品種を用い、非生物的ストレス誘発適応応答および代謝物変化に関わる機能解析を実施して各種農業形質の形質発現との関連性を考察した。

(1) 乾燥ストレスがネギ-シャロット添加系統のアブシシン酸含量およびその関連遺伝子転写量に及ぼす影響

ネギ-シャロット添加系統シリーズに乾燥処理を行い、乾燥ストレスと関連のあるアブシシン酸 (ABA) とその前駆体である β -カロテンの含量を測定した。さらに、ABA の合成・分解およびシグナル応答に関わる遺伝子の発現解析を行い、異種染色体添加がネギの乾燥ストレス応答に及ぼす影響を検証した。その結果、FF+1A では乾燥処理区下において

β -カロテンおよび ABA の含量が乾燥処理区の FF よりも 5%水準で有意に高く、ABA の合成に関わる複数の遺伝子が軒並み高発現していることが確認された。一方、ABA と β -カロテンの含量が FF と同等であった FF+6A における遺伝子発現の様相は FF+1A とは大きく異なり、特に前者で発現量が低かった *zeaxanthin epoxidase* (*ABA1*) のみが後者で高発現していた。*ABA1* は ABA 合成の律速段階に直接関与することが知られており、シャロットの第 1 染色体をネギに導入することで本遺伝子の発現が上方修正され、ABA 含量が増加することで気孔が閉鎖して植物体の乾燥性が高まる可能性が示唆された。

(2) 耐暑性ネギ品種における葉先枯れの代謝プロファイリングおよび関連解析

植物材料として、播種と収穫の時期が異なる 6 パターンの夏季栽培により得られた耐暑性ネギ 8 品種・系統の葉身部 (6 試験区 \times 8 品種・系統 \times 生物学的反復 3 個体=144 サンプル) をそれぞれ用いた。全サンプルにおいて、6 種類の色素化合物と 3 種類の機能性成分の絶対量データ、267 種類の代謝産物の相対量データおよび葉先枯れ率を取得した。絶対量データを用いた統計処理により、明らかに濃い葉身色をもつ品種・系統ではクロロフィルとカロテノイド類の含量が総じて高くなり、特に‘山交 01’、‘山交 03’および‘YSG1 号’は葉身部に上記色素化合物が多く蓄積しており、これらは葉身濃緑色に関与する主要化合物であることが示唆された。また、全サンプルの代謝産物相対量データを用いた機械学習により同表現型値との関連解析を行った。その結果、葉先枯れに関連する代謝物として有機硫黄化合物である γ -Glu

PRENCSO と複数のフラボノイド類が特定され、これらの代謝物が硫黄化合物の合成経路で重要な役割を持つグルタチオンの酸化還元反応ならびに抗酸化作用を利用して葉先枯れを抑制している可能性が示唆された。

(3) 耐暑性ネギにおける濃緑色形質のメタボロームプロファイリングと予測モデルの構築

耐暑性ネギ 7 品種・系統を用いて夏季に栽培を行い、色素化合物、メタボロームおよび 400~700nm の分光反射率 (20nm 間隔) を測定し、濃緑色の類型化と色素化合物量の推定モデルを構築した。分光反射率データを用いて主成分分析を行った結果、耐暑性品種の緑色は、540~560nm の反射率が高い「green」、540~560nm が低い「dark green」、その他の波長すべてが高い「gray green」の 3 つに分類された。これらの 3 つのグループを代表する品種・系統を用いてメタボローム解析を実施したところ、「dark green」ではシアニジン類が、また、「gray green」ではシナピン酸がそれぞれ増加していることが明らかになった。さらに、色素化合物絶対量と分光反射率の数値データを用いてランダムフォレスト回帰によるモデル構築を試みた結果、クロロフィル *a* 含量についてテストデータでは R^2 値が 0.88、Leave-One-Out Cross-Validation による R^2 値が 0.78 と高精度な数理モデルが得られた。

以上の研究により、シャロット染色体の添加が葉ネギの乾燥ストレス応答に与える影響、ならびに葉先枯れと濃緑色性に関与する代謝物がそれぞれ明らかになった。さらに、クロロフィル *a* 含量を高精度に推定する数理モデルを分光反射率データの利用により構築する手法をネギ

類で初めて開発することに成功した。一連の遺伝学および生理生態学に関わる基礎的研究を通じて、代謝産物解析や簡易的色素計測を巧みに組み合わせる手法を考案でき、非生物学的ストレスに強いネギの栽培技術開発に資する基盤的知見が得られた。今後、本研究で得られた知見を不良環境条件下での栽培に適した葉ネギ品種の開発へ応用することも期待される。

LIST OF PAPERS RELATED TO THE THESIS

NAKAJIMA, T.; YAGUCHI, S.; HIRATA, S.; ABDELRAHMAN, M.; WADA, T.; MEGA, R.; SHIGYO, M. Effects of Drought Stress on Abscisic Acid Content and Its Related Transcripts in *Allium fistulosum*—*A. cepa* Monosomic Addition Lines. *Genes* 2024, 15 (6), 754, doi:10.3390/genes15060754. (In press)

(In relation to Chapter 2)

NAKAJIMA, T.; YAMAMOTO, R.; MATSUSE K.; FUJI, M.; FUJII, K.; HIRATA, S.; ABDELRAHMAN, M.; SATO, M.; HIRAI, M.Y.; SSHIGYO, M. Metabolite Profiling and Association Analysis of Leaf Tipburn in Heat-Tolerant Bunching Onion Varieties. *Plants* 2025, 14 (2), 187, doi.org/10.3390/plants14020187. (In press)

(In relation to Chapter 3)

ACKNOWLEDGEMENT

I wish to express my sincerest thanks to Dr. Masayoshi Shigyo, my major supervisor (Professor of the Department of Life Science, Graduate School of Sciences and Technology for Innovation, Yamaguchi University) for his scientific guidance. He always provides me with invaluable suggestions for my scientific research. I greatly appreciated his encouragement for my study and advice for my daily life throughout the time I have studied in the Laboratory of Vegetable Crop Science, Yamaguchi University.

I would like to express my deep gratitude to Dr. Kenji Matsui (Professor of the Department of Life Science, Graduate School of Sciences and Technology for Innovation, Yamaguchi University) for his kind support and encouragement for my work.

I am very grateful to Dr. Jun'ichi Mano (Professor of the Science Research Center, Yamaguchi University) for his kind support and encouragement for my work.

I wish to thank Dr. Yasuomi Ibaraki (Professor of the Department of Life Science, Graduate School of Sciences and Technology for Innovation, Yamaguchi University) for his kind support and encouragement for my work.

I am very grateful to Dr. Ryosuke Mega (Associate Professor of the Department of Life Science, Graduate School of Sciences and Technology for

Innovation, Yamaguchi University) for his kind support and encouragement for my work.

We extend our appreciation to the following individuals and groups for their specific contributions:

- Dr. Kouei Fujii for providing valuable samples that were crucial for this study.
- RIKEN Center for Sustainable Resource Science for conducting the metabolome analysis that greatly contributed to this study.
- Dr. Naoki Yamauchi for their valuable advice on the measurement of pigment compounds.
- Mr. Yasumasa Matsuoka, Institute of Systems Biology and Radioisotope Analysis, Yamaguchi University, for his valuable advice and support for the analysis of pheophytin *a* using the Alliance e2695.
- Ms. Tomomi Wada for sharing essential data and resources that greatly facilitated our analysis.

This work was the result of using research equipment shared in MEXT Project for promoting public utilization of advanced research infrastructure (Program for supporting construction of core facilities) Grant Number JPMXS0440400024. Additionally, I acknowledge the financial support from JSPS KAKENHI (Grant No. 21H02188) and JST SPRING (Grant No. JPMJSP2111).

Finally, I also thank our laboratory members, my friends, and my family most sincerely for supporting me intellectually.